NTNU – Trondheim
Norwegian University of
Science and Technology

Development of an Oil Production Platform for Year-Round Operation in the Beaufort Sea

Roar Christian Håversen Lohne

Marine Technology
Submission date: June 2012
Supervisor: Kaj Antero Riska, IMT

Norwegian University of Science and Technology
Department of Marine Technology

Problem Text

Development of an oil production platform for year-round operation in the Beaufort Sea

Background:

There exists initiatives to start oil production in the Beaufort Sea. Drilling operations can be carried out during the open season but once the production starts, it must be a year-round operation. In shallow waters the production platform that are applied can be bottom founded but in deeper waters floating units must be used. Then the stationkeeping will be a challenge. Several solutions for stationkeeping have been considered; both mooring and dynamic positioning (DP) have been studied as well as DP assisted mooring. The present Master's thesis will analyse a production platform in terms of ice loading and stationkeeping in the Beaufort Sea.

Contents:

The target of the thesis is to analyse the ice loading on a production platform and based on the loading develop a stationkeeping system for the platform. Further, this is used to analyse the operability of the platform. As the platform type is not selected, the thesis will start by considering the options for platform type and selecting a suitable type. This selected platform is design to suit a given production. After the design of the platform, the ice conditions at the operation area are described and design conditions are determined. These ice conditions may include several different ice types. Ice loading in the design conditions is to be determined and especially the requirements for the stationkeeping system developed. Finally, the feasibility of the stationkeeping system is checked. It is foreseen that a year-round operation requires, apart from the stationkeeping system of the platform, also an ice management system. Thus the thesis must analyse also the fleet of ice management ships required.

The thesis should thus consist of at least:

1. Analysis of environmental conditions in the Beaufort Sea. Factors such as ice conditions, ice season and other important factors should be considered;
2. Functional requirements for the production platform;
3. Selection of platform type;
4. Calculations of ice loads on the selected platform;
5. Selection of stationkeeping system and estimates of restoring forces;
6. Comparison of the ice loading with the restoring forces from the stationkeeping system. Evaluation of the feasibility of the proposed platform and stationkeeping for year-round production; and
7. Requirements of ice management system.

The thesis supervisor will be Prof. (II) Kaj Riska.

Abstract

Due to high expectancy of hydrocarbon resources in the Beaufort Sea it is seen as an important area for energy in the future. As the focus now is shifting towards the deeper parts of the sea, there is a need for floating production platforms that are able to operate year-round in this area. In this Master's thesis the design of such a platform is performed, with respect to global ice loads acting on the platform and the capacity of the stationkeeping system. This is used to analyse the operability of the platform.

To be able to develop a floating production platform it is crucial to have information on ice conditions in the Beaufort Sea. Literature has been used to determine ice conditions in the seasonal transitional zone, where it is expected that the platform will operate. Factors such as level ice, first-year and multi-year ridge dimensions, floe size and ice island mass have been defined. These represent some of the most common ice conditions in the Beaufort Sea, and as such represent ice conditions a platform can expect to meet.

Functional specifications have been used to determine the most appropriate platform type. Several platform types were considered based on factors such as production and storage, ice loads, and ice interaction with risers and mooring lines. A circular FPSO was selected due to its insensitivity to ice drift direction. To reduce ice loading, the platform was designed as a downward sloping cone.

Ice loads on the platform have been calculated using several methods commonly applied in literature. Results show that managed ice yields lowest loads, followed by level ice. Higher loads are seen for ridges, both first-year and multi-year, and large ice floes.

A water depth of 500 m was assumed for the location of the platform. Since this can be considered as a moderate water depth, a conventional mooring

system was selected for stationkeeping. The system has 24 mooring lines connected to a buoy, which again connects to the turret on the platform. Internal mooring was seen as necessary to protect mooring lines from ice. Restoring coefficients have been determined using the inelastic catenary equations. Maximum allowable horizontal displacement is defined as 5 % of the water depth. Together with the restoring coefficients this was used to determine maximum allowable horizontal load on the platform. For the selected platform type and mooring system this was found to be 53.38 MN.

Lastly, the operability of the platform was judged by comparing various ice loads to the maximum allowable load given by the mooring system. Ice management is clearly needed when operating in any ice other than level ice. The requirements of the ice management system has been defined, and a general analysis of the primary and secondary objectives of the ice management system has been performed. It is proposed to use one icebreaker throughout the year, since the platform may encounter multi-year ice floes during the summer. As the ice season starts an additional ice breaker is introduced. In severe ice conditions it may be necessary with a third ice breaker. It is concluded that if proper ice management is ensured, the platform should be able to operate year-round.

Sammendrag

Hydrokarbon-ressursene i Beauforthavet blir sett på som en viktig kilde for energi for fremtiden. Så langt har produksjon foregått i de grunne områdene ved bruk av faste plattformer eller kunstige øyer. Nå er det økt interesse i de dypere områdene, noe som krever flytende produksjonsplattformer som kan operere året rundt. Denne oppgaven presenterer et innledende design for en flytende produksjonsplattform ved å analysere globale iskrefter og ankringssystem.

For å utvikle en flytende produksjonsplattform er det viktig å ha informasjon om isforholdene i Beauforthavet. Litteratur har blitt brukt for å finne typiske isforhold i området hvor det er ventet at platformen skal operere. Faktorer som istykkelse, førsteårs og andreårs isrygger, isflakstørrelse og masse til store isøyer har blitt funnet. Generelt er isforholdene i Beauforthavet ganske alvorlige.

Forskjellige plattformtyper har blitt gjennomgått, og faktorer som produksjon, lagring og egenskaper i is har blitt lagt til grunn for valg av

den mest hensiktsmessige plattformtypen. En sirkulær platform har blitt valgt, spesielt siden plattformen ikke er sensitiv for retning av isdrift. For å redusere iskrefter er plattformen formet som en nedoverbrytende kon.

Iskrefter på plattformen har blitt beregnet ved å bruke flere forskjellige metoder. Resultatene viser at iskrefter er lavest i is som er brutt av isbrytere, og deretter i jevn is. Iskreftene øker for isrygger og andre større istyper.

En vanndybde på 500 m er antatt for lokasjonen til plattformen. Dette kan klassifiseres som en moderat dybde og derfor har vanlig ankring blitt valgt for å holde lokasjonen. Systemet har 24 ankerliner som er festet til en bøye, som igjen festes til plattformen. Reaksjonskreftene fra ankersystemet har blitt funnet ved å bruke ligninger for uelastisk kjedelinje. Grensen for ankersystemet er satt ut i fra en maksimum horisontal forskyvning på 5 % av vanndybden. Høyeste tillatte kraft på plattformen er blitt funnet som 53.38 MN.

Til slutt har funksjonsdyktigheten til plattformen blitt gjennomgått ved å sammenligne de forskjellige iskreftene med høyeste tillatte horisontale kraft gitt av ankersystemet. Det er et klart behov for ishåndtering når plattformen opererer i alt annet enn jevn is. Krav for ishåndtering har også blitt definert. Det er foreslått å bruke en isbryter hele året. Dette fordi plattformen kan møte på flerårsis. Når issesongen starter blir det satt inn en ekstra isbryter, og hvis nødvendig en tredje. Konseptet med en flytende plattform som kan operere året rundt er realistisk, så lenge et effektivt ishånderingssystem blir opprettholdt.

Preface

This report is the result of my Master's Thesis in Marine Technology at the Norwegian University of Science and Technology (NTNU). The work was conducted during the spring semester of 2012.

The purpose of this thesis is to develop a production platform for year-round operation in the Beaufort Sea. This is an important topic as there is increased interest in the deeper parts of the Arctic Seas for hydrocarbon production.

Through my project thesis conducted during the autumn semester of 2011 I was introduced to Arctic Offshore Engineering. I find it to be an interesting topic, but also very challenging. After completing the Master's Thesis I feel that I have learnt a lot on ice loads on offshore structures and how presence of ice will govern the operability of these structures. However, Arctic Offshore Engineering is a topic that requires engineering experience to judge results and methods.

I would like to thank my supervisor, Professor Kaj Riska, for very helpful guidance and encouragement throughout the semester. I am grateful for his important contributions and time for discussions in spite of his tight schedule.

Trondheim, June 7, 2012

Roar Christian Håversen Lohne

Contents

Problem Text iii

Abstract v

Preface ix

Acronyms xix

Nomenclature xxi

1 Introduction 1
- 1.1 Experience with Floating Vessels in the Beaufort Sea 3
- 1.2 Outline of Thesis 5

2 The Beaufort Sea 7
- 2.1 Bathymetry 8
- 2.2 Winds 9
- 2.3 Waves 9
- 2.4 Currents 10
- 2.5 Ice Conditions 10
  - 2.5.1 Seasonal Transitional Zone 11
  - 2.5.2 Extreme Ice Features 14
  - 2.5.3 Ice Season 15
  - 2.5.4 Conclusion 16

3 Functional Specifications 21

4 Selection of Platform Type 25
- 4.1 Ice Loading and Structure Geometry 29
- 4.2 Ice Management 30
- 4.3 Platform Types 31
  - 4.3.1 Spar platform 32

4.3.2 FPSO . . . 35
4.3.3 Semi-submersible . . . 38
4.3.4 TLP . . . 39
4.4 Conclusion . . . 40

5 Ice Loads 43
5.1 Ice interaction with Sloping Structures . . . 46
5.2 Level Ice Loads . . . 47
5.2.1 Ralston . . . 47
5.2.2 Croasdale . . . 50
5.3 First-year Ridge Loads . . . 51
5.3.1 Dolgopolov . . . 52
5.3.2 Mellor . . . 53
5.4 Multi-year Ridge Loads . . . 54
5.4.1 Elastic Ridge Bending - Ralston . . . 54
5.4.2 Plastic Limit Method - Wang . . . 55
5.5 Limit Momentum . . . 57
5.6 Ice Loads in Managed Ice . . . 58
5.6.1 Scenario 1 . . . 58
5.6.2 Scenario 2 . . . 59
5.6.3 Scenario 3 . . . 61
5.7 Limit Force . . . 62
5.8 Input for Ice Load Calculations . . . 64
5.9 Results . . . 66
5.10 Conclusion . . . 66

6 Stationkeeping 73
6.1 Mooring . . . 73
6.1.1 Mooring System . . . 78
6.2 Dynamic Positioning . . . 81
6.3 Conclusion . . . 81

7 Operability 83
7.1 Ice Loads and Restoring Forces . . . 83
7.1.1 Ice Loads in Varying Ice Conditions . . . 85
7.2 Ice Management . . . 91
7.3 Operability of Platform . . . 96
7.4 Summary . . . 98

8 Conclusions and Further Work 101

References **103**

A Ice Forces from Ralston's Equations **I**

B Multi-year Ridge Model by Wang **VII**

C Matlab Program **XIII**
C.1 Verification of Code XVIII

List of Figures

1.1 Map of Beaufort Sea. 2
1.2 Picture of the Kulluk. 5

2.1 Map of Beaufort Sea. 7
2.2 Bathymetry of the Beaufort Sea. 8
2.3 Winter ice zones of the Beaufort Sea. 11
2.4 Extent of landfast ice in the Beaufort Sea. 12
2.5 Seasonal variation of ice drift speeds. 13
2.6 Cross-section of first-year ridge. 14
2.7 Idealized ridge model. 14
2.8 Probability of finding first-year ridges of a given sail height in the seasonal zone of the Beaufort Sea. 15
2.9 Size distribution of seasonal floes in the transitional zone in summer. 16
2.10 Mean number of multi-year ice floes in pack ice. 17
2.11 Annual ice growth for landfast and seasonal zones. 17

4.1 Typical maximum water depths of different offshore structures. 27
4.2 Breaking ice using downward and upward slopes. 29
4.3 Cell Spar platform. 33
4.4 Detachable Spar platform. 34
4.5 Figure of Arctic Spar. 35
4.6 Terra Nova FPSO. 36
4.7 Turret system of Terra Nova FPSO. 36
4.8 Sevan Voyageur, circular FPSO. 37
4.9 Semi-submersible Eirik Raude. 38
4.10 TLP. 40
4.11 Sketch of platform. 42

5.1 Failure modes of ice. 46
5.2 Ice interacting with structure. 47
5.3 Coefficients for Ralston's solution. 49

5.4 Initial and hinge cracks. 54
5.5 Deformation of Long Ridge Type I. 56
5.6 Ridge cross-section. 56
5.7 Scenario 1, managed ice. 59
5.8 Scenario 2, managed ice. 60
5.9 Scenario 3, managed ice. 61
5.10 Simplification of Scenario 3. 62
5.11 Values of average pack-ice forces. 64

6.1 Comparison of catenary and taut mooring. 74
6.2 Catenary mooring line. 74
6.3 Spread mooring. 76
6.4 Horizontal length of anchor line 1. 79

7.1 Horizontal ice loads compared to maximum allowable load. . 84
7.2 Level ice loads. 86
7.3 First-year ridge loads. 87
7.4 Multi-year ridge loads. 87
7.5 Ice loads in scenario 1, managed ice. 88
7.6 Ice loads in scenario 2 and 3, managed ice. 88
7.7 Maximum mass of ice feature versus ice drift speed. 91
7.8 Typical ice management. 92
7.9 Typical ice management patterns. 93
7.10 Ice management zones. 95
7.11 Operability of platform in terms of ice management. 97
7.12 Platform operating in level ice. 98

B.1 Ridge cross-section. VIII
B.2 Deformation of Long Ridge Type I. VIII

C.1 Flowchart of MATLAB program. XV

List of Tables

2.1 Ice data for Beaufort Sea. 18

4.1 Classification of platforms. 26

5.1 Input to ice load calculations. 65
5.2 Results from ice load calculations. 66

6.1 Mooring line characteristics. 78
6.2 Mooring system characteristics. 79
6.3 Mooring system characteristics when platform is displaced 25 m in negative x-direction. 81

7.1 Explanation of method numbers in Figure 7.1. 83
7.2 Explanation of ice management zones in Figure 7.10. 95

C.1 Input to level ice load calculations. XIX
C.2 Comparison of results. XIX
C.3 Input to level ice load calculations. XIX
C.4 Comparison of results. XX
C.5 Input to ridge breaking load calculations. XX
C.6 Comparison of results. XX
C.7 Input to ridge breaking load calculations. XXI
C.8 Comparison of results. XXI

Acronyms

API	American Petroleum Institute
MBS	Minimum Breaking Strength
MODU	Mobile Offshore Drilling Unit
FPSO	Floating Production, Storage and Offloading
FSO	Floating Storage and Offloading
TLP	Tension Leg Platform
OEB	Oil-Equivalent Barrels
GOEB	Billion Oil-Equivalent Barrels
BOPD	Barrels of Oil Per Day
ISO	International Organization for Standardization
GSZ	General Surveillance Zone
TAZ	Threat Assessment Zone
PMZ	Physical Management Zone
PDL	Planned Disconnection Limit
EDL	Emergency Disconnection Limit
EXZ	Exclusion Zone
EDZ	Emergency Disconnection Zone
QCDC	Quick Connect Dis-Connect

Nomenclature

C_{11}^M	Restoring coefficient in surge.
C_{22}^M	Restoring coefficient in sway.
C_{66}^M	Restoring coefficient in yaw.
D	Diameter of platform at waterline.
D_r	Diameter at height/depth of maximum rubble pile-up/ride-down.
E	Elastic modulus of ice.
F_1^M	Restoring force in surge from mooring system.
F_2^M	Restoring force in sway from mooring system.
F_6^M	Restoring moment in yaw from mooring system.
F_H	Horizontal ice force.
F_V	Vertical ice force.
T	Tension in anchor line.
T_H	Horizontal component of tension in anchor line.
T_V	Vertical component of tension in anchor line.
X	Horizontal distance between anchor and platform.
α	Angle of sloping sides of platform. Positive value is for upward breaking and negative value is for downward breaking.
ρ_a	Density of air.

ρ_i	Density of ice.
ρ_w	Density of sea water.
σ_c	Unconfined compressive strength of ice.
σ_f	Flexural strength of level ice.
σ_r	Flexural strength of ridge ice.
ξ	Ratio between horizontal and vertical force.
d	Water depth.
g	Acceleration of gravity.
h	Level ice thickness.
h_f	Thickness of managed ice floes.
h_r	Thickness of ridge.
l	Length of anchor line.
l_b	Length of anchor line laying on the seabed.
l_s	Length of anchor line suspended between the seabed and the platform.
x	Horizontal distance between anchor and the point where the line leaves the seabed.

Chapter 1

Introduction

The Arctic contains substantial amounts of the remaining hydrocarbon reserves. However, due to the remoteness and harsh Arctic climate, these areas have not been explored thoroughly and there are only a few examples of already producing fields in the Arctic. Since the world's energy demands have steadily increased, development in Arctic Engineering has progressed. These unused reserves are seen as important sources of energy for the future, and the task of extracting these sources in a safe manner is a fundamental issue. The Beaufort Sea is seen as one of the important areas and it is selected for further analysis. Figure 1.1 gives an overview of the area.

Previous offshore hydrocarbon production in the Beaufort Sea has been in shallow waters, using bottom founded structures. In areas with multi-year ice present IMVPA [20] suggests that maximum water depth for bottom-founded structures is 100 m. This argument is based on overturning moment due to ice loading and practical dimensions of the structure. Now, several companies such as Imperial Oil (ExxonMobil) and Chevron are exploring the deeper parts of the Beaufort Sea [14], [6]. This requires the development of floating platforms that can perform the tasks of drilling and production in a safe manner. While drilling can be performed in summer months with less ice, it is preferable to have year-round production. This raises concerns for stationkeeping in ice that must be able to sustain a safe, year-round production.

One of the main challenges when designing a platform for operation in ice, besides the infrastructure and remoteness of field, is the highly varying ice properties. Ice is not homogeneous, and it is very dynamic. This makes it

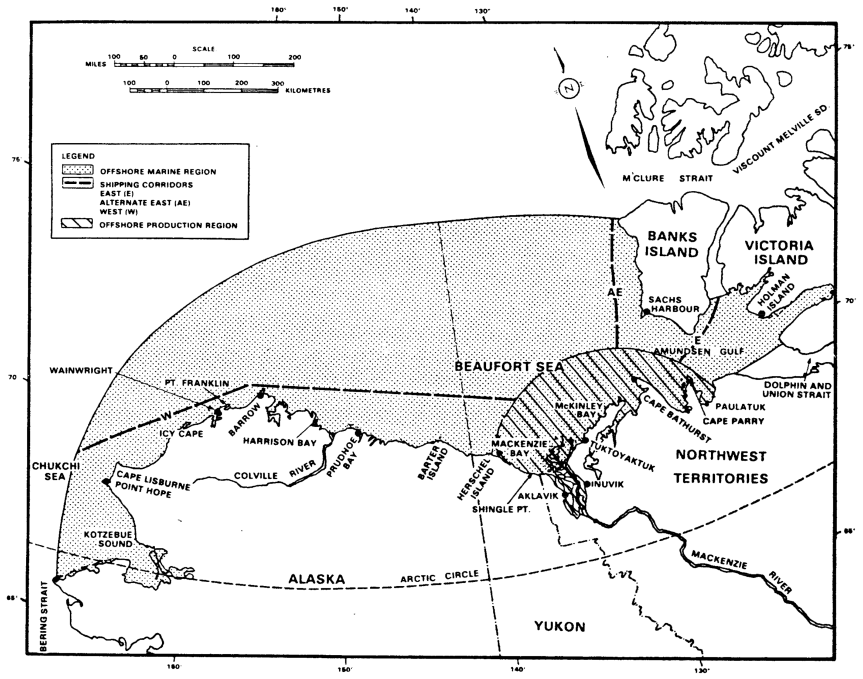

Figure 1.1: Map of Beaufort Sea, [3].

difficult to quantitate ice loads precisely.

The purpose of this thesis is to develop a concept for a floating oil production platform for year-round operation in the Beaufort Sea. Ice loads on the platform will be calculated for a range of different ice conditions. Together with the capabilities of the stationkeeping system, ice loads will be used to assess the operability of a year-round production platform in the Beaufort Sea. The need for such a platfrom is largely governed by the hydrocarbon resources available in the Beaufort Sea, and this will therefore be assessed next.

According to a U.S. Geological Survey [4] the Arctic could hold up to 22 % of the remaining undiscovered hydrocarbon resources. Roughly 240 GOEB (billion oil-equivalent barrels) have been discovered in areas above the Arctic circle, and it is expected that the undiscovered amount is 403 GOEB [17]. A large amount of the undiscovered resources are assumed to be gas and natural gas liquids, while undiscovered oil resources accounts for 12 %.

Hamilton [17] has estimated that about 40 billion barrels of oil could lie in areas with more than 100 m water depth. Further, three-fourths of

this amount is found in four regions: The Canadian Beaufort Sea, East Greenland, West Greenland/East Canada and East Barents Sea. The gas-related (gas and natural liquid gas) resources are expected to be much larger, but due to higher expenses for transport compared to oil and abundance of gas closer to the markets, deep water Arctic gas will not be economic to produce in the near future. Hamilton [17] therefore concludes that deep water Arctic oil fields will be developed first.

One of the most important factors to establish before considering oil production in the Beaufort Sea is the required size to ensure an economic project. Factors such as remoteness, lack of infrastructure and short season for construction, installation and maintenance leads to increased expenses for development, installation and maintenance. Hamilton [17] suggests that minimum oil field size will be roughly 500 million to 1 billion oil-equivalent barrels (OEB) for a deep water Arctic oil field to be economic. An oil field of this size is conceivable. Of oil and gas fields discovered above the Arctic circle, 61 of them are larger than 500 million OEB. 11 of these are oil fields.

This shows that the need for a floating production platform in the Beaufort Sea is realistic, and that increased activity in this area can be expected in the future.

1.1 Experience with Floating Vessels in the Beaufort Sea

The use of floating offshore structures for hydrocarbon exploration and production in ice infested waters has been limited. However, from the mid 1970s to early 1990s ice reinforced drillships and a conical drilling vessel, the Kulluk, were used in the Beaufort Sea for exploration drilling. They were used in water depths up to 80 m. The Canmar drillships were normally used in the summer months and early fall, but with the support of ice breakers the drilling season was extended and stationkeeping in a variety of different ice conditions was possible, according to Wright [47].

Even though the drillships worked quite well with proper ice management, several lessons and limitations were noted as described by Wright [47]:

- Ice management support had a very significant effect in providing drillships with the ability to stationkeep in ice. Also, ice monitoring

and ice alert procedures were developed to increase the safety and reduce downtime which turned out to be very successful.

- The drillships capability to break ice had essentially no impact on their stationkeeping performance in ice, since the ice management vessels performed all ice breaking
- The fixed orientation of the drillships had a huge effect on ice loads experienced depending on the ice drift direction. Ice forces were relatively low when ice drift was against bow or stern, but much higher when ice drift was from either sides.
- The weak moorings of the drillships were not capable of resisting the forces caused by high concentrations of thick moving ice or large floes, within acceptable tolerances for offset and line tension.
- Since mooring lines came off the deck and through the water line they were exposed to moving ice. Ice would often get entangled in the lines causing an increase in line tension
- Ice clearing around the ships was very important regarding ice forces. Good ice clearance resulted in low ice forces while poor ice clearance, and resulting ice build-up, resulted in high forces.

All these factors were taken into consideration when designing the second generation Arctic drill unit, the Kulluk, shown in Figure 1.2. To minimize the icebreaking and clearance ice forces that the vessel would experience from any direction, it provided an omnidirectional capability to resist ice actions. The mooring system was much stronger compared to the drillships so that it could operate in heavier ice conditions and thus extend the season. Further, the mooring system was submerged to decrease the risk of ice becoming entangled in the mooring lines. It was also necessary to develop a new ice management system to deal with the more difficult ice conditions experienced in an extended operation season.

One of the features used was a downward sloping hull. By utilizing a sloping hull the incoming ice is broken in bending which corresponds to a low force. Near its bottom an outward flare ensures that ice is cleared efficiently, to avoid ice interfering with mooring lines and risers and to avoid ice getting trapped in the moon-pool.

The Kulluk was designed to operate in 1.2 m of unbroken level ice. This required an ideal mooring layout which was in most cases not met, and as

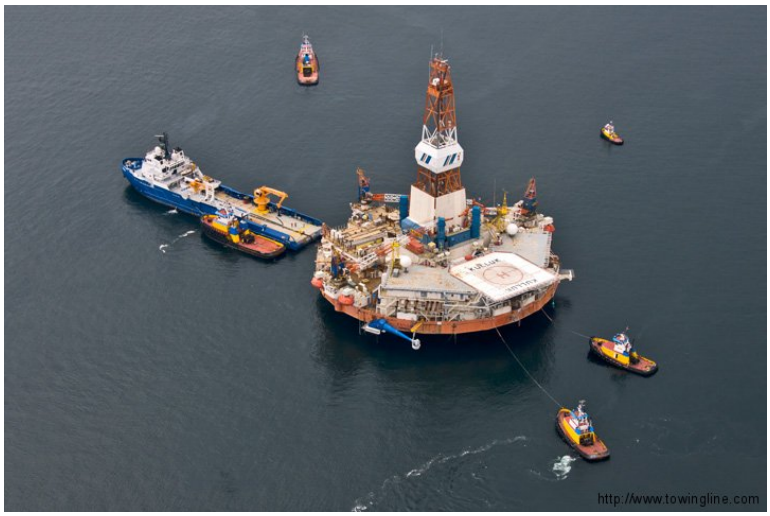

Figure 1.2: Picture of the Kulluk, [41].

a result maximum allowable ice thickness was lower. It is also important to appreciate the fact that level ice is seldom found in the Beaufort Sea. This required icebreakers to handle large ridges, hummock fields and large multi-year floes.

All of the vessels mentioned so far have been used for drilling, and during the months with the most extreme ice conditions they were moved of site. Extending to year-round production, the platform must be able to operate in all ice conditions. In some cases ice loads will exceed the capabilities of the stationkeeping system and ice management system. This will require disconnection of the platform from the mooring system, risers and umbilicals before it is towed away.

1.2 Outline of Thesis

The main focus in this thesis is on selection of an appropriate platform type for year-round production in the Beaufort Sea. Ice conditions are determined and these are used to evaluate ice loads on the platform. A stationkeeping system is selected, and ice loads and restoring forces are compared to evaluate the viability for the proposed design. It is therefore natural to divide the thesis into chapters covering the different topics.

Chapter 2 gives an analysis of the Beaufort Sea and the environmental

conditions. Special focus is given to the ice conditions that can be encountered, and a design basis is selected.

In chapter 3 the functional requirements of the platform are specified, with a focus on the location of the platform and its functions such as the required production amount, the export system for offloading hydrocarbons, and its performance in ice.

Chapter 4 covers the selection of platform type. Important factors that will govern the selection are presented and important ones such as ice loading, hull geometry and ice management is covered in detail. Further, different platform types are considered individually considering their performance in ice. A platform type is selected for further analysis.

In chapter 5, ice loads on the selected platform are calculated for a range of different ice conditions based on the design conditions determined in chapter 2.

A stationkeeping system in form of mooring is selected in chapter 6. Parameters for the system is selected, and the restoring coefficients are found. Using a maximum allowable horizontal displacement of 5% water depth, the maximum allowable horizontal load is determined. Also, maximum mass of colliding ice feature is found.

In chapter 7 the ice loads and restoring loads are compared, and the viability of the selected platform is analysed. The operability of the platform is discussed, and the requirements of the ice management system are decided.

Conclusion and recommendation for further work is given in chapter 8.

In appendix A the plastic limit analysis by Ralston is presented with the objective of determining coefficients in the equations for horizontal and vertical level ice loads on cones. Appendix B gives the theoretical solution of ridge breaking load by Wang. For all calculations performed a MATLAB program was written, which is presented in appendix C. The program is also checked against numerical examples in literature to verify that it performs calculations correctly.

Chapter 2

The Beaufort Sea

The area of interest is the Beaufort Sea. It is located north of Alaska and north-west of Canada, as seen in figure 2.1. This area was extensively explored in the 1970s and 1980s [21], and there is a fair amount of information available considering climate and ice conditions.

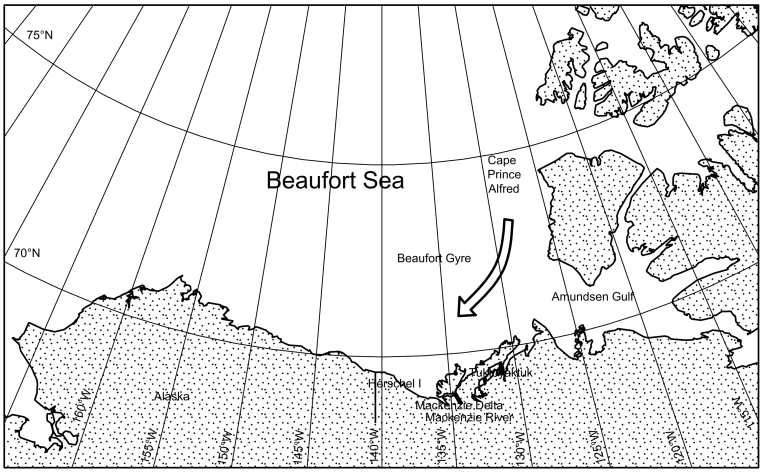

Figure 2.1: Map of Beaufort Sea [21].

Before looking into type of platform in detail it is important to gather information on the environmental conditions in the area. Bathymetry, winds, currents, waves and ice conditions will be looked into.

2.1 Bathymetry

According to ISO-19906 [21] there are three main bathymetric features in the southeastern Beaufort Sea:

- The continental shelf, sloping gently from the coastline to approximately 100 m water depth;
- The continental slope, angling steeply from the edge of the shelf to water depths of several 1000 m; and
- The trench-like Mackenzie/Herschel Canyon which transects a portion of the shelf.

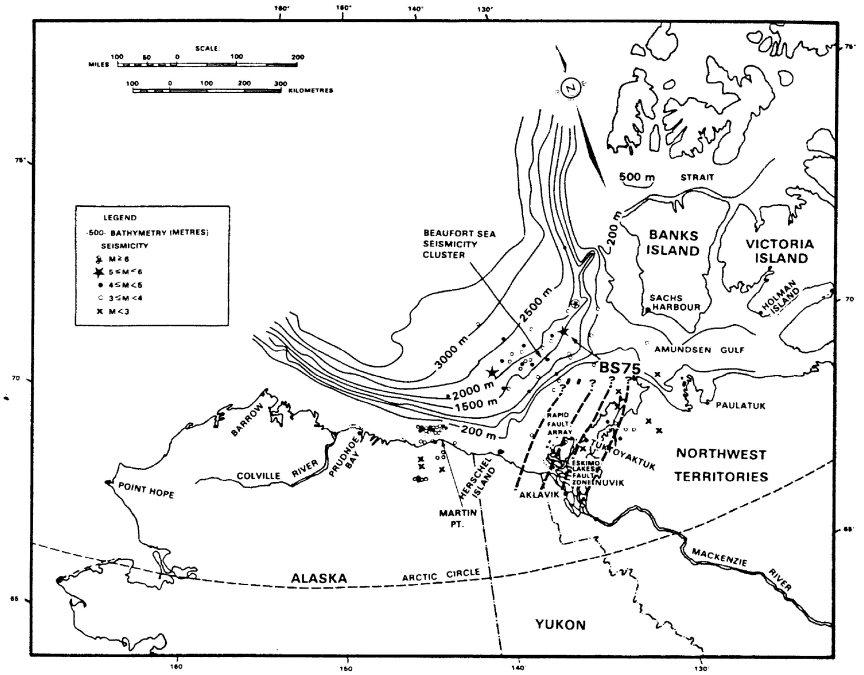

Figure 2.2: Bathymetry of the Beaufort Sea, clearly showing the steep continental slope and difference in width of continental shelf from Canadian to US Beaufort Sea. [3].

As can be seen in Figure 2.2 the continental slope is very steep. This is a challenge concerning any subsea installations needed on a potential oilfield. An example is the Ajurak oilfield which is explored by Imperial Oil where

the water depth varies between 60 m and 1200 m [6]. The location of the platform is assumed to be over the continental slope, at a water depth of 500 m.

2.2 Winds

Wind is important regarding ice drift, and creation of waves. During the late summer and early fall, when ice usually is offshore, strong winds create high waves. This because the fetch, which is the extent of open water over which the wind blows, is at its largest.

The coastal winds in the Beaufort Sea is strongly governed by the high coastal lands and the large thermal contrast between the sea and land. These circulations, driven by the temperature difference between the land and the sea, results in onshore breezes in summer and offshore breezes from the pack ice edge or open water in the winter.

Several wind analysis have been performed, as stated by *Beaufort Sea Production Environmental Impact Statement* [3]. Once every 50 years, winds with an hourly average of 29 m/s can be expected. Depending on location this varies somewhat, with higher values in the western part of the Beaufort Sea. 1-minute averages have also been determined in other studies, with a higher value of 39 m/s.

2.3 Waves

Knowledge of wave climate is important as it governs the design of the platform; and any offshore operations such as installing platform at site, performing maintenance or offloading hydrocarbons to tankers.

Wave height is one of the important parameters, which is governed by the wind strength, how long the wind blows, the water depth and the fetch. In the Beaufort Sea the fetch is limited due to presence of ice and local land mass. Therefore, normal sea states are less severe compared to the North Sea and other offshore areas with hydrocarbon exploration and production.

Beaufort Sea Production Environmental Impact Statement [3] presents several studies of the wave climate in the Beaufort Sea. The wind-generated waves dominate the energy spectrum, and the large

wind-waves have average periods from 6 s to 8 s while rarely exceeding 10 s.

In high ice concentrations (larger than 7/10) waves of significant height will not occur. Therefore, waves loads will not be considered further since it is the performance of the platform in ice that is of interest.

2.4 Currents

The mean circulation pattern in the Beaufort Sea is governed by the clockwise circulation of the Beaufort Gyre. In western parts the current speed has been estimated between 0.05 m/s and 0.1 m/s [3], [21].

2.5 Ice Conditions

Information on ice conditions is based on Cammaert and Muggeridge [5], ISO-19906 [21] and *Beaufort Sea Production Environmental Impact Statement* [3]. All give an extensive analysis of ice conditions and features, but since the ISO-standard is newer it is preferred for data.

Occurrence of ice in the Beaufort Sea is on average between October and July, but it can also vary to late September to mid-August. The ice conditions in the Beaufort Sea can be categorized in three main regions:

1. Arctic polar pack zone;
2. seasonal or transitional (shear) zone; and
3. landfast ice zone.

The Arctic polar pack extends into the Beaufort Sea, but this varies a lot depending mainly on the wind regime. According to Cammaert and Muggeridge [5] the southern limit is approximately 72°N, while ISO-19906 [21] defines the limit from Cape Prince Alfred off Banks Island southwestward to some 200 km north of Herchel Island and then westward some 200 km off the Alaska north coast. This means that the Arctic polar pack is located over the deeper parts of the Beaufort Sea. The ice type is mainly multi-year ice with a level ice thickness of up to 5 m. First-year ice reach a maximum of 2 m. Ridges are also found with thicknesses up to 25 m. When estimating the ice loading of ridges it is also important to

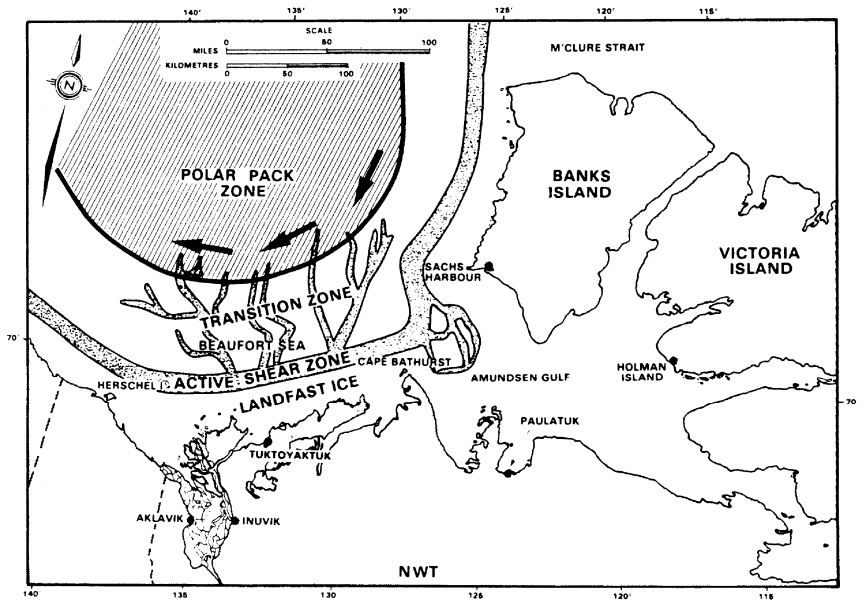

Figure 2.3: Winter ice zones of the Beaufort Sea [3].

include the probability of occurrence of such ice features. Cammaert and Muggeridge [5] states that only one out of 100 have a keel depth greater than 15 m. A common assumption of occurrence is 5 ridges per kilometre, leading to a ridge with keel depth greater than 15 m occurring every 20 km.

The landfast zone extends from the shore out to approximately 20 m water depth. Floating platforms will not be used in such water depths, and this zone will therefore not be explained further. Figure 2.4 gives an example of the extent of the landfast ice and where the season transitional zone starts.

2.5.1 Seasonal Transitional Zone

The seasonal transitional zone lies between the landfast zone and the Arctic polar pack, and is the most interesting regarding a floating production platform. The width of the zone varies between a couple of kilometres to 300 km, both from year to year and during a season. It is generally wider in the Canadian Beaufort than off Alaska. Ice type in this zone is mainly first-year ice, but there is also presence of multi-year ice. This zone has mean ice drift speeds between 0.035 m/s and 0.15 m/s, with a maximum of 0.35 m/s. Ice drift speeds also vary seasonally as seen in Figure 2.5. As a

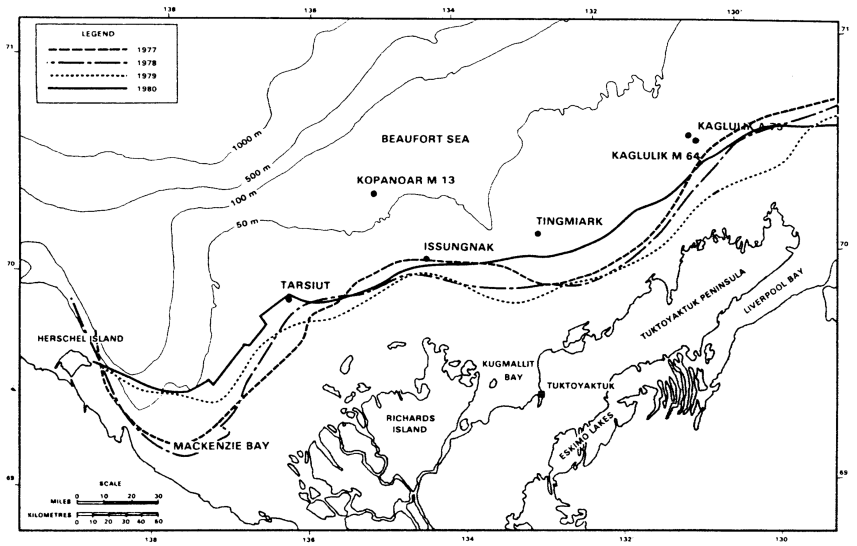

Figure 2.4: Extent of landfast ice in the Beaufort Sea between 1977-1980, [40].

result of the ice drift, deformation and ridging occurs in the seasonal zone.

Pressure ridges are important as they are common in the Beaufort Sea. They pose a great threat to any floating platform due their size. It is common to distinguish between first-year and multi-year ridges. A typical cross-section of a first-year ridge is given in Figure 2.6.

First-year ridges are larger, but weaker compared to multi-year ridges. Under the sail there is a relatively thin consolidated layer of ice, while the keel is made up of unconsolidated blocks. If a first-year ridge survives several summers and becomes a multi-year ridge, melted ice fills the voids between the blocks and when it refreezes the keel is consolidated. Multi-year ridges are therefore much stronger compared to first-year ridges and they have a more rectangular, smoothed shape. Timco and Burden [42] have analysed measurements of both first-year and multi-year ridges to obtain a relationship between sail height and keel depth. They give a sail to keel ratio of 1:3.3 for multi-year ridges, and 1:4.4 for first-year ridges. Sand and Horrigmoe [36] also presents an idealized multi-year ridge model which has the same sail to keel ratio, and that also gives ratios for the top and bottom width of the ridge. This is given in Figure 2.7.

When designing a platform for operation in areas where ridges are

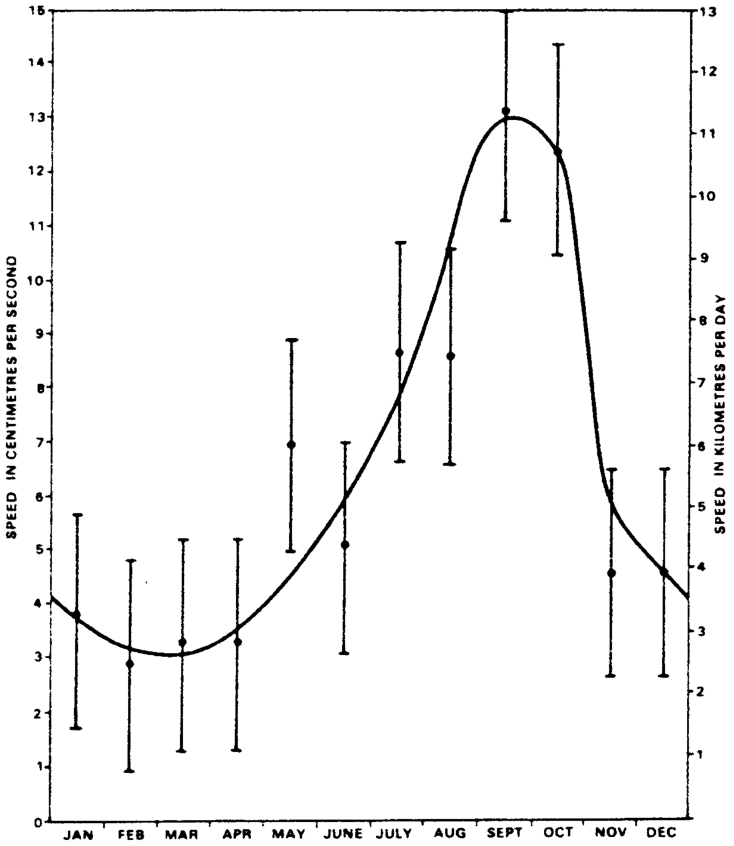

Figure 2.5: Seasonal variation of ice drift speeds in the seasonal transitional zone. Measured between 1975 to 1978. [3].

encountered the probability of encounter is an important aspect. Some studies on the probability of encounter versus the sail height is given by Wright and Schwab [49] in Figure 2.8.

This suggests that one ridge out of 10 has a heigh of 2 m, while only one out of 1000 is likely to be higher than 5 m. The probability for multi-year ridges has not been found. Due to the melting and re-freezing which smooths multi-year ridges the dimensions may be somewhat smaller. As mentioned earlier this will lead to an increase in strength compared to first-year ridges.

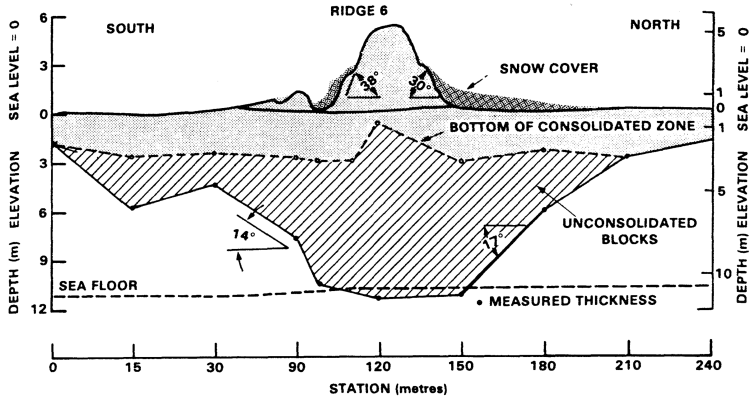

Figure 2.6: Cross-section of first-year ridge based on measurements, [3].

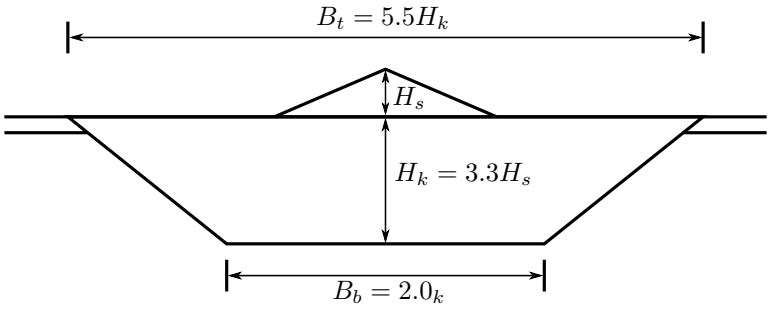

Figure 2.7: Idealized ridge model, used by Sand and Horrigmoe [36].

2.5.2 Extreme Ice Features

Regarding extreme ice features there are two types that must be taken into consideration; ice islands and multi-year hummock fields. Ice islands are of glacial ice and can be very large with an area of up to 700 km^2, while thickness range from 30 m to 60 m [3]. Although dangerous for any offshore structure, they are very rare.

Multi-year hummock fields are formed at the intersection between the landfast zone and the seasonal transitional zone along the western edge of the Canadian Archipelago. Crushing and overriding of multi-year ice sheets results in large fields of ice blocks and ridges parallel to shore. Ridges can be up to 20 m high and be grounded in up to 60 m water depth. If these hummock fields survive one summer or more they can become completely consolidated and break away from landfast ice sheet [3].

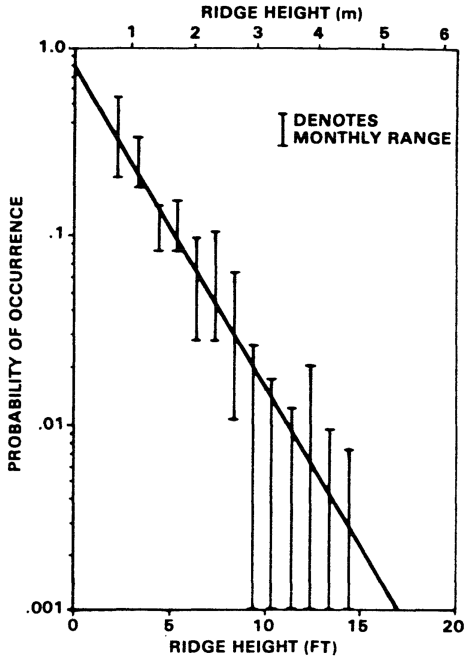

Figure 2.8: Probability of finding first-year ridges of a given sail height in the seasonal zone of the Beaufort Sea, [49].

2.5.3 Ice Season

Besides the ice conditions the ice season is also a very important factor as it governs the operability of the platform. Ice season length will govern the need for ice management throughout the year. During summer months with little ice the platform may be able to operate without any icebreakers, while during winter months icebreakers are required.

Information about the ice season is based on the *Beaufort Sea Production Environmental Impact Statement* [3]. While the ice break-up pattern for the landfast and transitional zones are similar each year, the rate of break-up and at which point the ice clears completely vary from year to year. This is due to the difference in wind and temperature. Break-up starts in the transitional zone, with flaw leads being created. Ice clears first in the Canadian part and ice tends to move into the Alaskan part, which means that the Alaskan part clears more slowly. Maximum open water extent is usually reached in September. The ice edge moves northward as melting occurs. Number of ice floes increase as ice melts, and reach a maximum

in early summer. Size of seasonal floes versus number of floes is given in Figure 2.9.

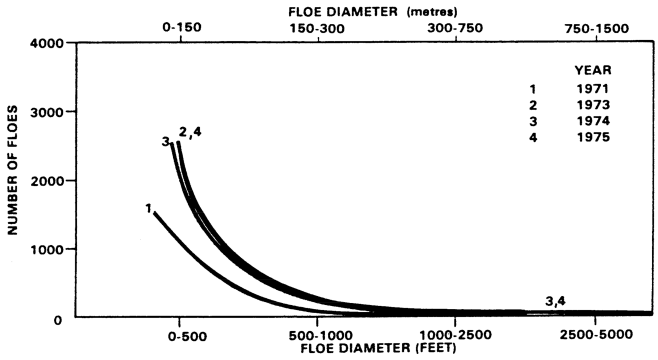

Figure 2.9: Size distribution of seasonal floes in the transitional zone in summer, [3].

The seasonal floes tends to be smaller in dimensions compared to the multi-year floes. Figure 2.10 gives the size distribution of multi-year floes. The multi-year floes are thus of largest threat since they are larger.

Freeze-up starts in the coastal areas between late September and late October. The exact start date depends on the conditions during the summer. A cold summer will result in an early start. When freeze-up has started it usually takes two weeks before the Beaufort Sea is completely covered. The polar pack tends to move southerly in the fall, but is stopped when the seasonal zone is sufficiently developed to halt this movement.

The summer ice conditions will vary depending on the predominating wind direction. In years with predominant onshore winds multi-year ice will be pushed south, into coastal waters. If winds are mainly offshore, the ice edge tends to move north.

For level ice the largest thicknesses occur just before ice starts to melt, as seen in Figure 2.11. This also shows the difference in thickness between landfast ice and ice in the transitional zone. The landfast ice tends to become thicker compared to the ice in the transitional zone.

2.5.4 Conclusion

It remains to establish the design basis for the platform in terms of ice conditions. Table 2.1 gives a summary of the general ice condition in the

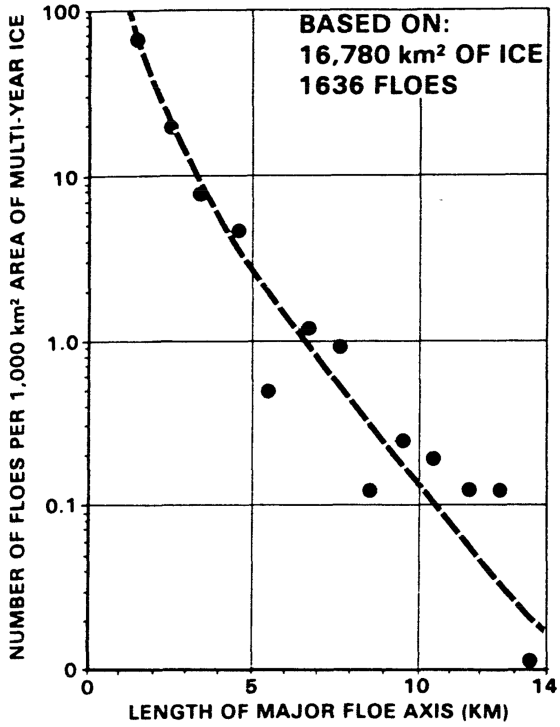

Figure 2.10: Mean number of multi-year ice floes in pack ice between 70°-72° N, 127°-138° W in September and October 1980, [3].

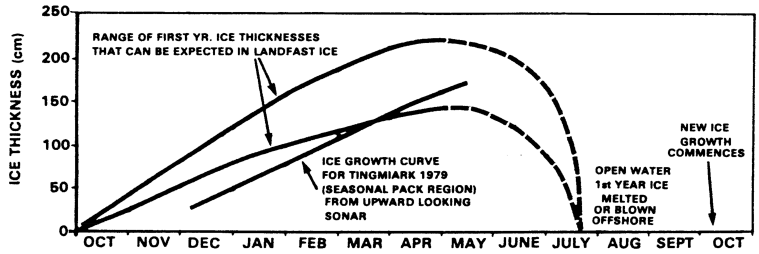

Figure 2.11: Annual ice growth for landfast and seasonal zones, [3].

Beaufort Sea.

For ridges it is the multi-year type that is of largest threat due to keel being consolidated. Interaction between ridges and structure will result in large loads and maximum size has to be determined. An increase in loads with increasing size of ridge is expected, but a larger ridge also makes it easier to detect by an ice management system. First-year ridges consists of a sail,

Table 2.1: Ice data for Beaufort Sea. Values from ISO-19906 [21]. $*$ means no data available.

Parameter	Average annual value	Ranges of annual value
First-year		
• floe thickness, [m]	1.8	1.5 to 2.3
• ridges		
◦ sail height, [m]	5	3 to 6
◦ keel depth, [m]	25	15 to 28
• rubble fields		
◦ sail height, [m]	5	3 to 6
◦ length, [m]	100 to 1000	100 to 1000
Multi-year		
• ice thickness, [m]	3 to 6	2 to 11
• floe thickness, [m]	5	2 to 20
• ridges		
◦ sail height, [m]	$*$	$*$
◦ keel depth, [m]	20	10 to 35
• rubble fields		
◦ sail height, [m]	2 to 5	3 to 6
◦ length, [m]	750	50 to 2300
Ice movement		
• drift speed offshore, [m/s]	0.08	0.06 to 1.0
Ice islands		
• mass, [10^6 tonnes]	10	$*$

keel and a consolidated layer between them. Since the keel is made up of unconsolidated slushy blocks it is the consolidated layer that governs the loads on the platform.

Regarding ice islands, an impact with the platform is not very likely since the ice islands are rare features in the Beaufort Sea. Still, maximum ice island mass can be determined in terms of the capacity of the stationkeeping system.

Large multi-year floes are present in the Beaufort Sea. Interaction with a floating structure might occur. How to analyse the interaction will depend somewhat on the season. During summer multi-year ice floes will drift according to wind and currents, and the drift speed tends to be higher compared to in winter. In winter floes will be embedded in the ice cover, and as such being driven by the overall ice movement. ISO-19906 [21] suggests that maximum ice drift speed can be up to 1 m/s, while Cammaert and

Muggeridge [5] suggests a maximum value of 0.35 m/s. For further analysis the largest value will be used.

Selection of design conditions is needed to perform ice load calculations. There are generally five interaction scenarios between platform and ice, and the following ice conditions for each scenario is assumed:

- Level ice of 2 m thickness
- First-year ridge with keel depth of 25 m and sail height of 5 m
- Multi-year ridge, 20 m thick, with the dimensions following the idealized ridge model in figure 2.7.
- Large ice feature colliding with platform. An average mass of ice islands is given by ISO-19906 [21] as 10×10^6 t. This is used to compare the capabilities of the mooring system.
- Managed level ice where the floe thickness is 2 m. Also managed ice features such as ridges should be checked to test the effect ice management.

It must be noted that ice information based on literature gives uncertain values as it is based on different measurements throughout the area. To design a safe structure for a specific location it is necessary to perform measurement of ice conditions at the specific location. This is the only way to ensure accurate information on the ice conditions and any location-specific ice features.

Chapter 3

Functional Specifications

Before selecting the type of platform it is important to specify the functional requirements of the platform. This is an extensive task largely governed by the following factors

- location
- functions
- production amount
- export system
- performance in ice
- open water performance

These factors will be considered in general terms, while chapter 4 will cover some of the topics more in detail.

Location

The proposed location of the platform is in the deeper parts of the Beaufort Sea, meaning any parts where the water depth exceeds 100 m. As a result the platform will be placed in the transitional shear zone. Several new areas of interest currently being surveyed are located above the continental slope, and relevant water depths are therefore down to 1000 m. For this thesis a water depth of 500 m will be chosen.

Functions

As stated in chapter 1 oil fields are of main interest since deep water Arctic gas fields are expected to be less economic in comparison. Further, a potential oil field must be large to ensure that the project is economic. The platform should be able to sustain year-round production. Due to the apparent need to disconnect from the risers and mooring system, it is envisioned that the platform can use a turret and buoy connection to ease the operation.

Performance in Ice

As already stated, the platform should be able to sustain year-round production. Ice loads are expected to vary a lot depending on the ice conditions, and as an initial assumption, the platform should only be able to operate by itself in moderate ice conditions. The requirement for the platform is therefore that it should be able sustain production in unmanaged level ice being 2 m thick. In thicker ice or for larger ice features, ice management shall be present to reduce the loads within the limitations given by the stationkeeping system. For extreme ice features that are unmanageable by icebreakers the platform must be able to disconnect from the mooring system, risers and umbilicals. The icebreakers must therefore be able to safely tow the platform, alternatively with the assistance of dedicated tugs, away from the extreme ice feature.

Open Water Performance

The ability to sustain production is governed by many factors. For a floating production platform the horizontal displacement from the equilibrium position is important, as this governs the stress in risers and umbilicals. A limit for the horizontal displacement is therefore set to 5 % of the water depth. If there is a risk of exceeding this limit, the production must be stopped and the platform disconnected from the risers. For open water performance this means that the platform must be able to operate in the sea states that are expected in the Beaufort Sea. As seen in section 2.3, the wave conditions are expected to be less severe than in the North Sea. This means that a conventional platform design most likely will be able to operate in the sea states found in the Beaufort Sea. However, this is not in the scope of the thesis, and it will not be considered any further.

Production Amount

A large daily production rate is required due to the required oil field size. Large production platforms such as the Terra Nova FPSO had an expected production amount of 150 000 bopd [19]. This will therefore be chosen as the required production rate for the platform. Besides production equipment there is also a need for storage of oil. The platform should be able to store at least the amount accumulated during 10 days, that is 1 500 000 bbl.

Export System

The most appropriate export system for this production platform is offloading to shuttle tankers. This gives a certain flexibility of where to deliver oil. Offloading can be either directly from the platform to the tanker, or using a loading buoy placed a certain distance away from the platform. Using an external loading buoy will require that the buoy itself is designed to handle loads due to ice. Therefore, it seems more appropriate to perform offloading directly between platform and tanker. This is a critical operation which is further complicated with the presence of ice. The tanker must be able to stay at the selected position for offloading while maintaining a safe distance to the platform. To reduce ice loads on the tanker, it can be placed in the wake of the platform during offload.

Chapter 4

Selection of Platform Type

Selection of the most appropriate platform type is a challenging task. Several judgements must be made based on the functional requirements which are established in in chapter 3. These are primarily driven by the characteristics and fluid properties of the reservoir that is going to be developed [13], but also on location of field and export system. Factors for deepwater platforms will first be considered in general, before usage in ice and in the Beaufort Sea is considered.

The two most important functional requirements for the topside is whether or not to have surface or subsea trees (dry and wet trees respectively) and whether to incorporate drilling or workover capability on the platform. Factors that affect these decisions are number of wells, top-hole locations, well production profiles, recovery mechanism and fluid characteristics [13].

As stated by D'Souza and Basu [13] the main difference between these two solutions is the lower capital cost of a wet tree platform and higher cost of drilling and workover of subsea wells with a MODU (Mobile Offshore Drilling Unit) versus the higher capital costs and complexity and lower drilling and well intervention costs of a dry tree platform.

Ronalds [34] has classified different platform types for deepwater applications, and the floating platforms can be grouped as in table 4.1.

Table 4.1: Classification of platforms according to important functional requirements. *Mobile Offshore Drilling Unit.

	Trees	**Workover**	**Drilling**
FPSO	Subsea	Intervention vessel	MODU*
Semi	Subsea	Intervention vessel	MODU
		Platform	Platform/MODU
Mini-TLP	Subsea	Intervention vessel	MODU
TLP	Surface	Platform	Platform/MODU
Spar	Surface	Platform	Platform/MODU

As seen in Table 4.1 the semi-submersible has been used in configurations with and without workover and drilling capabilities.

Platforms with surface trees give the best recovery factors since they provide direct downhole access for well intervention and management of the reservoir. Subsea trees gives a larger flexibility with placement of wells and may be beneficial when the reservoir requires spread wells to ensure optimum production [13].

The weight of a platform with dry trees is substantially larger than a platform with wet trees, especially if a drilling rig is also installed. D'Souza and Basu [13] presents a comparison where it is found that dry tree with drilling doubles the topside weight compared to wet tree without drilling. Thus, the capital cost increases, the complexity of the project increases and it takes longer time before first oil is delivered.

Installing the topside on the hull is also important to consider and there are two main procedures, either offshore lift or quayside lift. Offshore lifting is limited by the capability of the available crane vessel. This method is used for Spars and mini-TLPs, and maximum crane vessel capacity is at the moment about 12 000 t [13]. For larger Spars it may be necessary with several offshore lifts, which will increase the costs quite a lot. In the Beaufort Sea any offshore lifting must take place in the months with least presence of ice. Depending on location, there may be some individual ice floes present that must be managed so that they do not interfere with the operation. The cost and complexity of installing a topside on a Spar hull is thus larger compared to the other structures. In the Beaufort Sea, quayside lifting seems preferable since the presence of ice may interfere with offshore lifting operations.

The water depth where the platform will be operating is also an important

factor for selection of platform type. Figure 4.1 shows the approximate maximum water depth for several platform types. As seen, all floating platforms can operate in moderate to deep waters. Limiting factors for water depths are technical and commercial constraints on stationkeeping system and riser system.

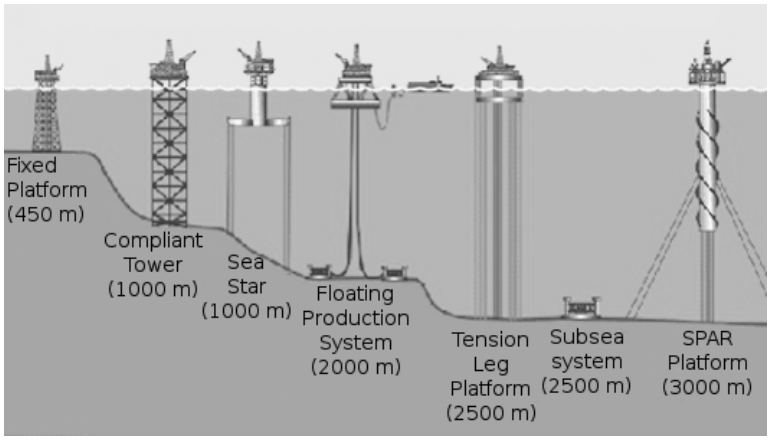

Figure 4.1: Typical maximum water depths of different offshore structures [27].

The process of selecting platform type is further complicated when the platform is to be used in the Beaufort Sea. For any Arctic area there are several extra factors to consider as stated by Aggarwal and D'Souza [1]:

- Remoteness of field;
- limited access to field due to presence of ice;
- lack of infrastructure, both offshore and onshore;
- short drilling and installation season; and
- transportation of products to markets.

It is evident that the capital expenditure (CAPEX) and operational expenditure (OPEX) will be high compared to a similar platform in the North Sea. As discussed in chapter 1 an oil field in the deeper parts of the Beaufort Sea has to be large to be economic to develop. A large oil field requires a high production rate, which in turn requires a large platform.

According to Aggarwal and D'Souza [1] there are two development alternatives for deep water Arctic fields: either subsea to shore or floating platform to shore. The subsea to shore solution will not be covered any further, but it is important to also consider this solution for any field development.

For a floating platform in the Arctic it is required that it is able to disconnect from the stationkeeping system to protect it against large ice features. To be able to disconnect the wells have to be placed subsea, which removes the possibility for conventional dry tree platforms.

Including the previous considerations for deep water production platforms there are several other considerations when moving to Arctic areas. They can be summed up accordingly, based on Aggarwal and D'Souza [1]:

1. Very large topside to meet requirements for high production rate.
2. Large number of risers and mooring lines.
3. Platform and subsea equipment must withstand environmental forces, including ice forces.
4. Hull designed to reduce the ice loads.
5. System for detaching platform from risers and mooring in case of collision with large ice features. It must be quick and reliable.
6. The platform must have means of self-propulsion or tugs in the vicinity to tow it away after detaching.
7. Complexities in construction and installation of platform. Keywords are remoteness of field and limited period with benign weather and ice conditions.
8. Top side must be winterized.
9. Quayside installation of topside or in sheltered waters. Transportation will be longer due to remoteness.

Point number four is regarded as one of the most important factors for ice loading and thus requirements for stationkeeping system, and it must be considered early in the design process. Ice management is also important to consider, as it also influences the ice loads.

4.1 Ice Loading and Structure Geometry

The use of floating platforms in ice is limited compared to fixed structures. Aggarwal and D'Souza [1] states that existing fixed platforms in ice may experience maximum ice loads from 500 MN to 1000 MN for multi-year ice and large ice features. Further, they state that the maximum capacity of the stationkeeping system for the Terra Nova FPSO is roughly 20 MN. The ice loads from multi-year ice and large ice features are thus much larger than the capabilities of a feasible stationkeeping system. Methods to decrease the ice loads are therefore important to consider when designing a floating production platform for the Beaufort Sea.

Ice loading and failure modes of ice will be covered more in detail later, but in general ice failure in crushing yields much higher loads compared to failure in bending. Therefore, the platform should have sloping sides near the waterline, as shown in Figure 4.2. Aggarwal and D'Souza [1] suggests that downward sloping sides are best for floating structures. Ice will not accumulate on the platform but is cleared around and beneath it. This is also beneficial for any mooring system, as a downward sloping platform will be subjected to an upward vertical force limiting the slackening of mooring lines. This is important since the slackening of mooring lines will result in larger horizontal displacements under the influence of ice.

Figure 4.2: Breaking ice using downward and upward slopes.

Semi-submersibles and TLPs are usually multileg structures. In some cases ice may accumulate between the legs and lead to large ice forces. There are three main features seen with multileg structures, as pointed out by Løset et al. [26]: mutual influence of legs; sheltering and jamming effects; and non-simultaneous maximal actions on legs. One of the main results is that multileg structures may experience substantial larger ice loads due to ice rubble accumulating between legs. Due to non-simultaneous maximal forces on different legs, the platform may also be subjected to yawing. If a multileg structure is considered, these effects have to be studied extensively to make sure that the stationkeeping system is able to withstand these effects.

Protection of stationkeeping system and risers from ice is also important. Ice may pile up on risers and mooring lines and cause damage. Therefore, methods of protecting these systems must be incorporated in the design.

4.2 Ice Management

Ice management may also be required to further decrease ice loading and assure effective ice clearance. According to ISO-19906 [21] there are three levels of design approaches: passive, semi-active and active, which assumes different levels of ice management.

For the passive level there is no ice management, and the platform is designed to withstand all of the expected ice and other environmental loads. Stationkeeping is also passive, meaning that the platform is free to weathervane without the use of thrusters. The platform is not able to disconnect from the mooring system. For the semi-active design approach there is no ice management, but the platform is able to disconnect from the stationkeeping system and move off location. The active design approach assumes an active ice management system to avoid certain ice conditions. If ice conditions become to severe the platform is designed to disconnect from the stationkeeping system and move off location.

In this thesis an active design approach is selected, as deducted by the functional specifications. The platform will thus operate in managed ice, but it is assumed that it can operate in level ice without ice management. Further, it should be able to withstand large ice features broken into pieces with size comparable to the platform itself. In the event of ice loads exceeding the capabilities of the stationkeeping, caused by ice that is unmanageable by the ice management system, the platform is disconnected and moved off location.

Selection of ice management system is very often based on experience of ice management personnel, and ISO-19906 [21] recommends the use of such input. At an early stage it is suitable to study the previous use of ice management systems. The previously mentioned drilling vessel, the Kulluk, had up to 4 PC4[1] icebreakers which gave an approximate downtime of 10 %, but the Kulluk did not operate year-round. This suggests that the number of icebreakers required for year-round operation is higher, but this may also be balanced by a stronger stationkeeping system. A compromise will

[1] Polar Class 4

most likely be appropriate, by introducing a stronger stationkeeping system while at the same time keep at least two icebreakers during winter for ice management. Due to offloading to tankers it may also be necessary to have smaller icebreakers and tugs to assist during these operations. Experience with offloading in ice is limited, but the Varandey FOIROT (Fixed Offshore Ice Resistance Oil Terminal) in the Barents Sea provides valuable insight and is presented by Riska [33]. Offloading from the terminal to shuttle tankers is performed year round, and tankers are designed to break ice which means that they need little support from icebreakers. At the location of the terminal there is however icebreakers and support icebreaking tugs present that can assist in operations if needed.

4.3 Platform Types

Considering all possible floating structures in this context, they can be grouped accordingly:

- ship-shaped hulls (e.g. FPSO (floating production, storage and offloading)) and FSO (floating storage and offloading)) or barge units
- column-stabilized (e.g. semi-submersible), and spar and buoy type units

The platform types considered most interesting will now be discussed individually with the aim of determining the most suitable for hydrocarbon production in the Beaufort Sea. A rough estimate of the possible ice loads due to level ice of 2 m thickness will also be done using Korzhavin's formula given by Løset et al. [26] as:

$$F = IKm\sigma_c Dh \tag{4.1}$$

I is the indentation factor taking into account the ice properties and the correlation between the ice thickness and the structure's diameter. It also takes into consideration the confinement; that is, how the stress/strain field influences the ice strength. K is a contact factor. Løset et al. [26] states that the product IK should be between 0.45 and 0.55, based on recommendations from the American Petroleum Institute. m is a shape factor for the structure, found as 0.9 for a cylinder and 1 for flat structure.

D and h are the diameter of the structure and ice thickness. σ_c is the unconfined compressive strength of the ice. This value can vary quite a lot due to ice crystallography, how the ice is loaded and the strain rate. A value of 2 MPa is assumed [5], which is for first-year ice. Korzhavin's formula was developed for narrow bridge pillars and should be used cautiously on wide structures such as platforms. Still, it is useful to get an indication of loads on the various platforms.

An initial estimate of the available restoring forces due to horizontal displacement is also needed to compare against the ice load estimates. This will give an idea of the capabilities of the platforms in ice. The comparison of ice loads and restoring forces can also give indications on whether the platform must be specifically designed for operations in ice, or if standard shapes are good enough. Aggarwal and D'Souza [1] states that a typical FPSO mooring system, using turret mooring, has restoring forces of roughly 20 MN. This value will be used for all platform types considered, as all are expected to use mainly mooring lines for stationkeeping. Restoring forces from the mooring system can of course be highly varying depending on the selection of mooring system parameters, but as an initial estimate this value is deemed appropriate.

It is assumed that the platforms will operate with a certain amount of ice management, but the extent will depend on the platform type. Different platform types will thus have somewhat different operation concepts.

4.3.1 Spar platform

Sablok and Barras [35] presents the Spar platform for use in Arctic areas, with focus on Barents Sea and East Coast Canada. The Spar platform exhibits low motion characteristics in response to environmental loads compared to other structures. The separation between centre of gravity and centre of buoyancy gives the Spar excellent stability. This is achieved by installing heavy ballast at the platform keel, which lowers the centre of gravity. As a result the draught of Spar platforms is large ($>\sim 90$ m), and they are only suitable for larger water depths.

There are three types of Spar platforms; classic Spar, truss Spar and cell Spar. All are explained in detail by Sablok and Barras [35]. The classic spar is a large cylinder comprising of three main parts. The upper part is a cylindrical hard tank that provides buoyancy to support the topside, hull, mooring and risers. Further down is the mid section which is a cylindrical

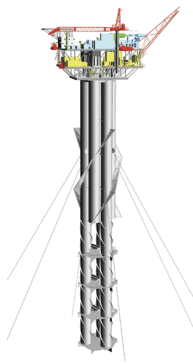

Figure 4.3: Cell Spar platform, [30].

shell that is flooded. This provides structural separation between the upper part and the ballast. At the bottom, fixed ballast is installed. The truss Spar is a modification of the classic Spar where the cylindrical shell is replaced by a truss section with heave plates. This reduces the weight of the platform, and decreases environmental loads and heave motion. The third option is a cell Spar, in which the large single cylinder of the classical Spar is replaced with several small diameter cylinders joined in a symmetric pattern. This reduces the cost and complexity of building the platform, making it feasible for smaller deepwater field developments.

The classic Spar is recognized as a good alternative for Arctic areas where ice breaking is required [35]. It also gives the best shielding of risers along the full length of the Spar, and it provides storage of oil.

Assuming a waterline diameter of 40 m, the ice load is estimated to 72 MN using Equation 4.1. This is beyond the given stationkeeping capabilities of 20 MN. To improve ice breaking capabilities the Spar can be conically shaped at the waterline. Further, Sablok and Barras [35] proposes to have two operational draughts. In ice the Spar is kept at the "ice-draught" with the waterline at the cone-shaped part. In other conditions the Spar is kept at "storm-draught" with the waterline at the neck of the Spar. This is seen in Figure 4.5.

Regarding collision with extreme ice features such as icebergs and ice islands, the loads on the Spar will be larger than the capacity of practical mooring systems. It is therefore required that the Spar is able to disconnect from the mooring system and risers, and that it can be towed away in event of a collision. This alternative would require a two piece hull where the upper

main hull can be disconnected and towed away, while the lower hull stays on location. The lower hull supports the disconnected risers and mooring lines, while the upper hull supports the topside and all systems for production including crude storage. When disconnected the upper hull is stable by itself, and it can be towed away.

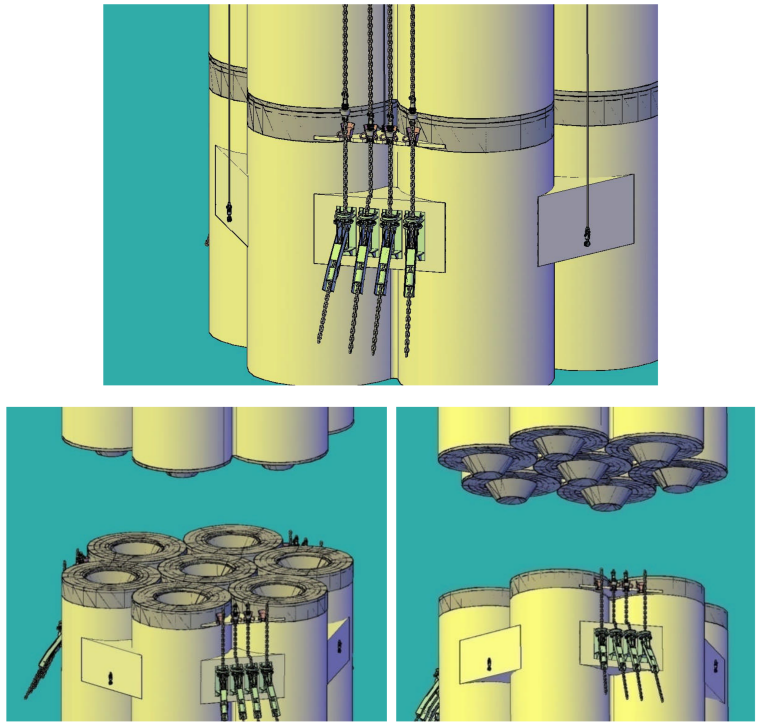

Figure 4.4: Lower part of a detachable Spar platform, [35].

A combination of a detachable Spar with conical transition operating at two different waterlines will require a significant ballast system. As stated by Aggarwal and D'Souza [1] the difference in WL 1 and WL 2 (ref. Figure 4.5) would be around 15 m. Towing should be performed with the waterline at a large diameter due to stability. This requires deballasting beyond WL 2 and distance between WL 1 and tow water line would be even more than 15 m. The operation of towing away the Spar is thus more complex compared to other hull forms.

Regarding ice management the operational concept of a Spar is comparable to the Kulluk, in that it can be designed to withstand a certain amount of level ice by itself and requiring assistance with heavier ice features. Since

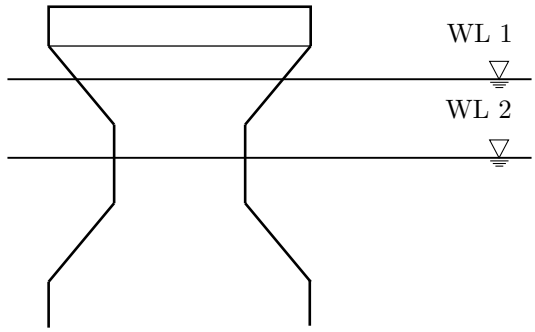

Figure 4.5: Figure of upper part of Arctic Spar. WL 1 is waterline when in ice, and WL 2 is in other conditions.

the risers and mooring lines are protected the task of the ice management is to reduce the global ice loading on the platform.

4.3.2 FPSO

There are two types of FPSOs, either ship-shaped or buoy shaped. They will be treated individually.

Tanker Based FPSO

Widely applied on several oilfield, the ship-shaped FPSO is a popular choice. Two FPSOs are also installed at the East Coast of Canada where there may be presence of ice during winter. The FPSO houses all equipment necessary for production and offloading. Ample storage space is provided, which eliminates the need for an external storage facility. Stationkeeping is usually achieved by using conventional mooring. To reduce the environmental loads, weather-vaning is achieved by using single point mooring often in the form of an internal turret connected to a buoy. A singe point mooring also allows for ice-vaning, reducing the ice loads on the FPSO [47].

For a FPSO using turret mooring the anchor lines attach to the buoy which is submerged, and they are thus protected from ice. The turret also holds risers from the subsea templates. This system is very practical in Arctic areas, because it is relatively easy and quick to disconnect from the buoy and move away in case of any unmanageable ice features drifting towards the FPSO. A typical turret is shown in Figure 4.7.

Figure 4.6: Terra Nova FPSO. It utilizes a turret mooring assisted by a DP-system. [11].

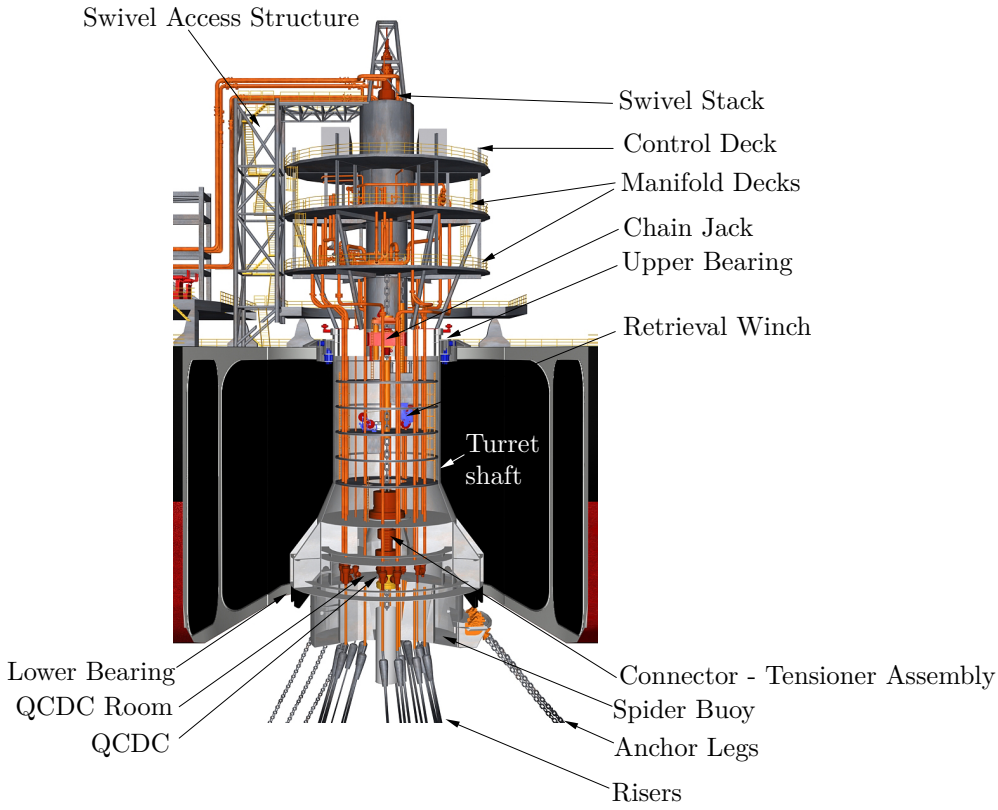

Figure 4.7: Turret system of Terra Nova FPSO. At disconnection the spider buoy is released, and it moves to a depth of 35 m to protect it from ice. [19].

To increase ice-vaning capabilities, active stationkeeping based on a Thruster Assisted Position Mooring System (TAPMS) can be used. This is implemented on the Terra Nova FPSO [25]. Nonetheless, a ship-shaped FPSO seems less favourable for hydrocarbon production in the Beaufort Sea. The shape will make it vulnerable to ice drifting towards its sides, which may be the case if ice drift direction changes and the FPSO is unable to change its heading due high ice concentration. A lot of the ice management resources must thus be spent on ensuring proper heading of the FPSO, and ice clearance if proper heading is unattainable.

Circular FPSO

Similar to a Spar platform, the circular FPSO consists of a circular hull. This shape is not vulnerable to changing ice drift direction, as long as the mooring system is designed to be symmetrical around the vessel. Sevan Marine is currently designing such FPSOs, and is delivering one unit to the Goliat field in the Barents sea [38].

Assuming a waterline diameter of 100 m the estimated level ice loading is 180 MN. This suggests that a circular FPSO should be designed as a downward sloping cone to reduce the ice loading. This solution has many similarities to the Kulluk drilling vessel, which has showed good ice capabilities in the Beaufort Sea [47].

Figure 4.8: Example of circular FPSO, the Sevan Voyageur by Sevan Marine [37].

Connection to mooring system and risers can be through a turret, giving

it the same benefits as a conventional ship-shaped FPSO. To improve its capabilities when detached from the mooring system, it is also possible to equip the circular FPSO with thrusters. As the design is not dependable on ice drift direction, there is not need for the circular FPSO having the capability to rotate around the turret.

The circular FPSO does not have the same problems with ice drift direction as the conventional FPSO. Ice management requirements are comparable to the Kulluk, due to the similarities in shape.

Regarding installation and commissioning of such a platform, Aggarwal and D'Souza [1] proposes that the topside is integrated at quayside and that hull with integrated topside is towed to the platform cite and connected to a pre-installed mooring system. This was seen in the introduction of this chapter as being the preferred method for the Beaufort Sea.

4.3.3 Semi-submersible

The semi-submersible is a very popular platform type for drilling, and it is also becoming increasingly popular for production. It uses conventional anchoring, DP, or a combination for stationkeeping. One of the limitations is the lack of (or very limited) oil storage capacity on board. This requires a floating storage and offloading unit or continuous offloading to shuttle tankers or through pipelines.

Figure 4.9: A semi-submersible platform, the drillrig "Eirik Raude" owned by Ocean Rig, [28].

To decrease ice loading on the semi-submersible downward sloping cones

can be installed on all columns. It is also important to ensure that ice accumulation between legs is avoided due to the large increase in ice loads that this may lead to. Detachment of the semi-submersible requires multipoint detachment of mooring lines as they are connected to the semi-submersible at different locations. This may also be the case for risers, depending on their layout. Detachment of a semi-submersible is therefore much more complex than a single point detachment commonly used for FPSOs. Due to the shape of the semi-submersible the mooring lines and risers will also be exposed to ice, which may lead to damage if ice accumulates.

The geometry of a semi-submersible and a TLP can be assumed to be equal, having four columns with diameters of 25 m. Using Equation 4.1 and assuming that the ice loading is shared between two columns, the predicted ice load is 90 MN.

Due to the shape of the semi-submersible and TLP, with possible problems of ice entanglement and jamming, the requirements of the ice management system is further increased. The broken ice must be small enough to pass as freely as possible through the platform. It must also be small enough to ensure that local loads on risers are low to limit damage on them.

4.3.4 TLP

A tension leg platform uses vertical steel tendons for stationkeeping and a typical hull consists of four vertical air-filled columns supported by pontoons, much similar to a semi-submersible. The tendons will limit the vertical motion, but at the same time allow for horizontal motion. At the seabed the tendons are connected to templates which are piled into the ground. One serious drawback is that the TLP cannot disconnect from the tendons, and in the event of a collision with a large ice feature it does not have the ability to be moved away. Regarding oil storage and ice interaction the TLP is comparable to the semi-submersible. That is, it has limited storage capacity and the same problems with risers exposed to ice. If a potential TLP design would use downward breaking cones, there is a risk of ice interacting with the tendons.

Since the shape and dimensions of a conventional TLP are assumed to be equal to a semi-submersible, as deducted from Figure 4.10, the ice loads are expected to also be similar in magnitude.

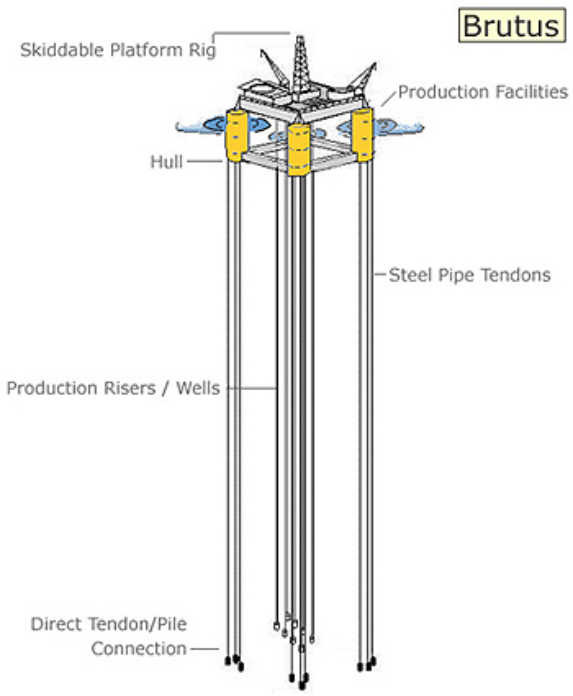

Figure 4.10: Typical TLP, [31].

There are also proposals for a single column hull with a conical transition in the waterline. This will reduce the ice loads compared to a conventional TLP or semi-submersible shape. Including the vertical tendons there is also a conventional mooring system to reduce the horizontal displacements due to ice. This is called a hybrid TLP [1]. Still, this design will have difficulties regarding disconnection from tendons.

4.4 Conclusion

Different platform alternatives have now been presented, with a focus on hydrocarbon production and operations in ice. To operate effectively in ice, methods to reduce ice loads are needed so that the capabilities of the mooring system are not exceeded.

If there is a risk of the platform encountering ice features that would lead to loads exceeding the capabilities of the stationkeeping system, and that are not manageable by ice breakers, the platform must be able to disconnect

from the mooring system and risers. This procedure should be quick and as easy as possible, which can be achieved with a single point detachment in form of turret and buoy.

In areas with moderate ice loading and where detachment is not required the Spar platform is a good candidate. There are several concepts with Spars that are detachable, but compared to the circular FPSO the operation seems more complex and time consuming. The use of either semi-submersibles or TLPs is limited by the inherent multi-column design, difficult and time consuming disconnection or lack of this feature, exposure to ice and limited oil storage.

Estimates of ice loads on the different platform types are 72 MN, 90 MN and 180 MN for the Spar, Semi-submersible/TLP, and circular FPSO. It is clear that measures must be taken to reduce ice loads, as the restoring load was found to be roughly 20 MN.

Ice load reduction can be achieved by designing the platform with sloping sides accompanied with ice management. It is assumed that the platform normally operates in managed ice, but that it can operate in unbroken ice with a thickness of up to 2 m. If an event arises that limits the ice management the platform should however be able to operate in unbroken ice for a limited period. Any further conclusion on ice management and what the platform should be able to handle without it must be judged after the ice loads and restoring forces have been studied more in detail.

Based on the discussion a circular FPSO seems preferable compared to the other platform types presented. It can be built to decrease ice loading, it has a single point detach/reattach buoy that supports mooring lines, risers and umbilicals and it can be fitted with thrusters for self propulsion. It also has large storing capacity and can facilitate a large topside to ensure high production rate.

The following shape is proposed for the platform:

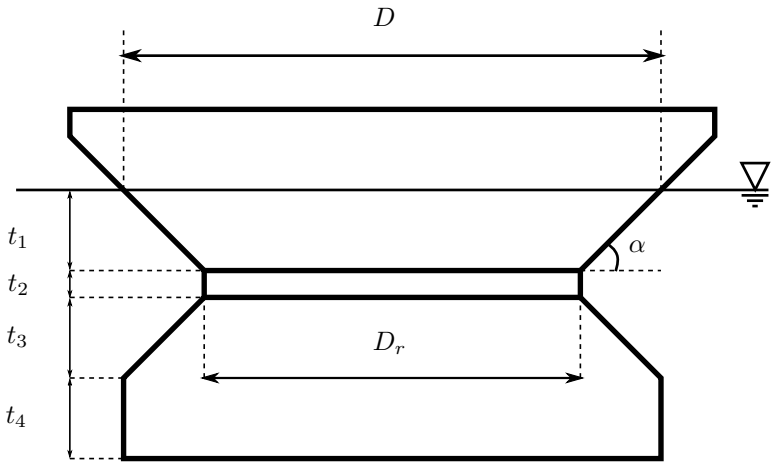

Figure 4.11: Sketch of platform with dimensions.

with the following dimensions

$$D = 100\,\text{m}, \qquad D_r = 70\,\text{m}, \qquad t_1 = 15\,\text{m},$$

$$t_2 = 5\,\text{m}, \qquad t_3 = 15\,\text{m}, \qquad t_4 = 15\,\text{m},$$

$$\alpha = 45°$$

The dimensions are only initial assumptions needed to perform the ice load calculations. Other considerations such as storage capacity and open water performance may however dictate changes in dimensions.

Chapter 5

Ice Loads

In this chapter several methods for calculating global ice loads on the platform are presented. All input parameters for the calculations are selected and the results are presented.

There are several structure-ice interaction scenarios to consider for a floating production platform in the Beaufort Sea:

- Level ice
- Broken ice
- Ridges
- Hummock fields
- Ice islands

Regarding the stationkeeping capabilities of the platform, it is the global ice loads that are of main interest. According to ISO-19906 [21] the following conditions shall be considered, and the governing ones shall be used in the design:

1. quasi-static actions due to level ice (first-year, rafted or multi-year), where inertial action effects within the structure can be neglected;
2. dynamic actions due to level ice (first-year, rafted or multi-year), where inertial action effects within the structure are influential and a dynamic analysis is required;

3. quasi-static actions due to ice rubble and ridges, where inertial action effects within the structure can be neglected;
4. impacts from discrete features such as icebergs, ice islands and large multi-year or first-year ice features;
5. quasi-static actions from features lodged against the structure, driven by surrounding ice or directly by metocean actions;
6. adfreeze action effects, including the frozen-in condition; and
7. thermal action effects;

There are thus many analyses required, but at an early stage in the design process it is suitable to look into the static loading in the most common ice conditions for the area of interest.

There are generally four different ice-structure interaction modes as stated by Løset et al. [26]: *limit stress*, *limit momentum*, *limit force* and *splitting*.

Limit stress is when the stress in the ice reaches a maximum limit, such as compressive, shear, tensile, flexural or buckling strength. This is used when ice fails close to the structures, such as level ice breaking in bending when interacting with a cone structure. An unlimited driving force of the ice is assumed.

Limit momentum considers the kinetic energy of an ice feature, and when this energy is insufficient for the structure to penetrate significantly into the ice. Thus, the ice feature comes to a halt. This procedure is good when studying freely floating icebergs or ice islands colliding with the structure. For this interaction mode, loads exerted on the structure will also depend on how the ice floe will behave after the impact. After a while it may move around the structure, but this requires that ice concentration is relatively low and that the structure is not very wide. The other option is that the ice floe due to high ice concentrations will become stuck in front of the structure. This leads to the next interaction mode.

Limit force arises when an ice floe stops in front of the structure. Forces from surrounding ice features, wind and current will be transmitted through the ice floe on to the structure. If forces are sufficiently large, the structure will start to penetrate into the ice and as such *limit stress* is initiated. If forces are too small and the surrounding ice is weaker than the floe at the structure, rafting and ridging will start at the back of the ice floe. Ice will

accumulate. For the first alternative it is crucial to recognize the difference from the normal *limit stress* scenario. Since the ice floe has come to a halt and starts to move again, the velocity is generally lower. This usually corresponds to a higher force.

Splitting usually corresponds to the lowest ice forces. A crack is formed in the ice, starting where the ice hits the structure. The direction is away from the structure. This is usually the case for structures with sharp corners, but it can also occur for circular structures.

One must also look into the failure mode of ice against the structure, since the maximum pressure the ice can withstand is dependent on failure mode. Thus, maximum loads on a structure will also depend on the failure mode. What type of failure mode that will arise depends on many different factors such as the stress distribution, ice velocity and the geometry of the structure. Type of failure mode can also change for the same structure, due to changes in velocity, ice pile up and changing ice characteristics.

Generally, crushing will yield high loads, while for instance bending corresponds to lower loads. Therefore, it is usually beneficial with sloping structures as this ensures failure in bending.

Løset et al. [26] gives the most common failure modes for ice, presented in figure 5.1.

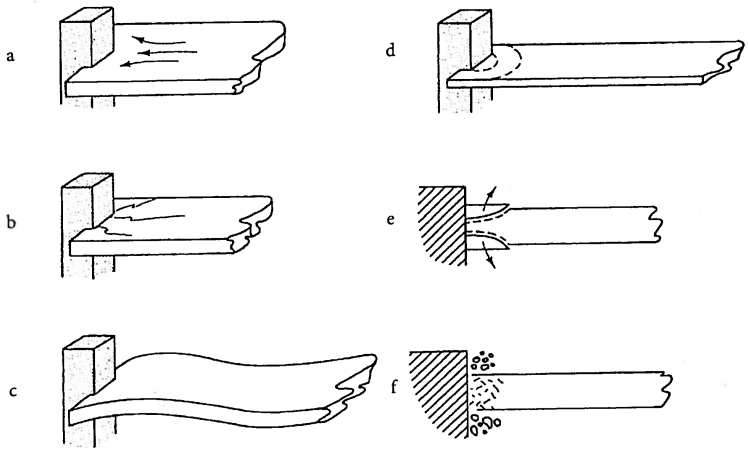

Figure 5.1: Failure modes of ice. a) creep, b) radial cracking, c) buckling, d) circumferential cracking, e) spalling and f) cruching, [26].

5.1 Ice interaction with Sloping Structures

The process of ice interacting with a sloping structure can be divided into several stages. First the ice sheet drifts towards the structure, slides along the surface of the structure and fails in flexure. Due to the motion of the ice sheet, the piece broken off will continue to move along the slope and it may be broken into smaller pieces. This process is repeated several times, causing smaller and smaller pieces to slide along the surface. For an upward sloping structure, the typical interaction is shown in Figure 5.2. The resulting ice load has a vertical and horizontal component, and generally these components are lower for a downward breaking structure compared to an upward breaking structure of same size and slope angle.

For a downward sloping structure, stage a) and b) can be expected to be somewhat similar as for an upward sloping structure. As the process continues ice pieces are pushed further down and around the structure before surfacing at the sides or behind the structure due to their buoyancy. Ice rubble may also accumulate, especially for wide structure.

Two different types of sloping structures are most common. A conical shape

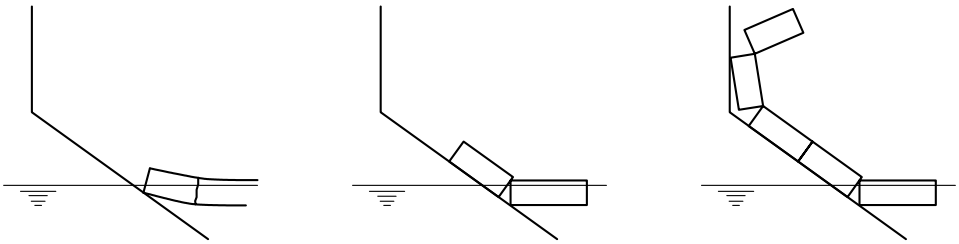

Figure 5.2: Ice interacting with an upward sloping structure, [21]. a) ice sheet approaches the structure, b) ice begins to fail and ride up face of structure, and c) ice blocks ride up face of structure and are turned back at vertical face.

is often preferred due to its symmetrical plan shape. The other alternative is the multi-faceted cones with flat, sloping faces.

5.2 Level Ice Loads

Two different methods to calculate level ice loads on sloping structures are now presented, namely the methods developed by Ralston and Croasdale.

5.2.1 Ralston

Based on a 3D elastic plastic analysis of the ice sheet interacting with a cone-shaped structure, Ralston [32] developed equations for horizontal and vertical forces:

$$F_H = \left[A_1\sigma_f h^2 + A_2\rho_w g h D^2 + A_3\rho_w g h(D^2 - D_r^2)\right] A_4 \tag{5.1}$$

$$F_V = B_1 F_H + B_2\rho_w g h(D^2 - D_r^2) \tag{5.2}$$

where ρ_w is the density of water, σ_f the flexural strength of ice, D the waterline diameter of the structure, D_r the diameter at the height of the ice rubble, and h the level ice thickness. A_1, A_2, A_3, A_4, B_1 and B_2 are coefficients given in Figure 5.3.

The two first terms in Equation 5.1 are due to breaking of the advancing ice sheet, while the third term results from the broken ice sliding over the

surface of the cone. Thus, coefficients A_1 and A_2 are dependent on the parameter $\rho_w g D^2/\sigma_f h$ and coefficients A_3 and A_4 are functions of cone angle and coefficient of friction between ice and structure.

Vertical force, found using Equation 5.2, is a function of the horizontal force and coefficients B_1 and B_2 which also depend on the cone angle and coefficient of friction between ice and structure.

Instead of using Figure 5.3 to determine coefficients, Ralston also gives an outline of the plastic limit analysis to determine these coefficients. This method is presented in appendix A.

In the original equations by Ralston, Equations 5.1 and 5.2, it is assumed that the leading side of the structure is covered by a single thickness layer of broken ice. This is not a realistic representation as ice tends to pile up. A modified version of Ralstons Equation is therefore presented by Løset et al. [26] to correct for this effect.

$$F_H = \left[A_1 \sigma_f h_1^2 + A_2 \rho_w g h_1 D^2 + A_3 \rho_w g h_2 (D^2 - D_r^2)\right] A_4 \tag{5.3}$$

$$F_V = B_1 F_H + B_2 \rho_w g h_2 (D^2 - D_r^2) \tag{5.4}$$

where h_1 is the level ice thickness and h_2 is the thickness of ice covering the leading side of the cone assumed to be $h_2 \approx 2h_1 \approx 2h$.

Since the platform chosen is to be shaped as a downward sloping cone, it is necessary to further modify the formulation by Ralston. API [2] suggests the following equations for ice forces on downward sloping cones, where ρ_w is replaced with the buoyancy $\rho_w - \rho_i$.

$$F_H = \left[A_1 \sigma_f h^2 + A_2 (\rho_w - \rho_i) g h D^2 + A_3 (\rho_w - \rho_i) g h (D^2 - D_r^2)\right] A_4 \tag{5.5}$$

$$F_V = B_1 F_H + B_2 (\rho_w - \rho_i) g h (D^2 - D_r^2) \tag{5.6}$$

ρ_i is the density of ice. Only a single ice thickness layer is assumed for this formulation. Now D_r is the diameter at the depth of the ice rubble ride-down, assumed to be at the end of the cone shape (at t_1 in Figure 4.11).

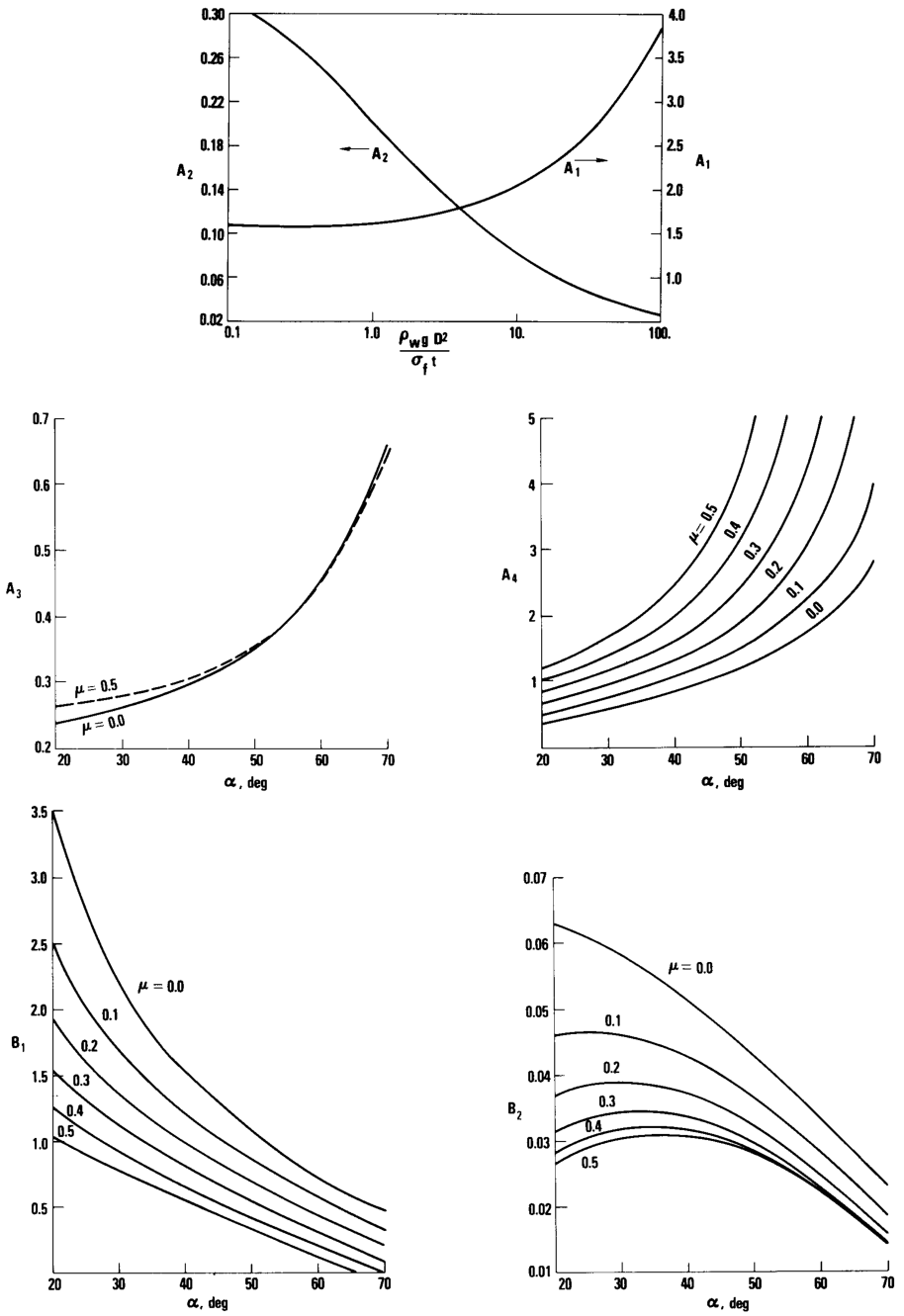

Figure 5.3: Coefficients for Ralston's solution, [32].

5.2.2 Croasdale

Croasdale developed a 2D model to estimate ice loads on a plane slope. This was later developed into a 3D model and both methods are presented by Croasdale and Cammaert [10]. This method is not based on the same theory of elastic plastic analysis as the method by Ralston. Instead this method is based on analysis of a semi-infinite elastic beam on an elastic foundation [26].

The full 3D method from Croasdale and Cammaert [10] is rather lengthy, and only presented for upward cones. Therefore, a formulation consisting of 3D breaking theory and 2D ride-up/down theory is used. The use of 2D ride-up compared to 3D will overestimate the force component, which is appropriate in an early design phase. The horizontal force on an upward cone is found as

$$F_H = C_1 D \sigma_f \left(\frac{\rho_w g h^5}{E}\right)^{1/4} \left(1 + \frac{\pi^2 L}{4D}\right) + C_2 t_h h D \rho_i g \tag{5.7}$$

where C_1 and C_2 are coefficients depending on the slope angle and coefficient of friction between material of structure (in this case steel) and ice. E is the elastic modulus of ice, L is the characteristic length of an ice beam on an elastic foundation, and t_h is the maximum rubble height. Coefficients C_1, C_2, and characteristic length L are found using the following formulae

$$C_1 = 0.68 \frac{\xi_1}{\xi_2} \tag{5.8}$$

$$C_2 = \xi_1 \left(\frac{\xi_1}{\xi_2} + \cot(\alpha)\right) \tag{5.9}$$

$$\xi_1 = \sin(\alpha) + \mu \cos(\alpha) \tag{5.10}$$

$$\xi_2 = \cos(\alpha) - \mu \sin(\alpha) \tag{5.11}$$

$$L = \left(\frac{E h^3}{12 \rho_w g (1 - \nu^2)}\right)^{1/4} \tag{5.12}$$

where ν is the Poisson's ratio of ice. The slope angle α is defined from the horizontal plane, taken as positive for upward sloping cones.

Timco and Cornett [43] later developed a formulation for downward sloping structures, where the horizontal force is given as

$$F_H = C_3 D\sigma_f \left(\frac{\rho_w g h^5}{E}\right)^{1/4} \left(1 + \frac{\pi^2 L}{4D}\right) + C_4 t_s h D(\rho_w - \rho_i)g \tag{5.13}$$

C_3 and C_4 are coefficients depending on the slope angle and coefficient of friction (μ), and t_s is the ice rubble depth which is assumed to be equal to the draught of the cone section. Coefficients C_3 and C_4 are found using the following formulae

$$C_3 = 0.68\frac{\xi_3}{\xi_4} \tag{5.14}$$

$$C_4 = \xi_3 \left(\frac{\xi_3}{\xi_4} - \cot(\alpha)\right) \tag{5.15}$$

$$\xi_3 = \mu\cos(\alpha) - \sin(\alpha) \tag{5.16}$$

$$\xi_4 = \mu\sin(\alpha) + \cos(\alpha) \tag{5.17}$$

The slope angle is defined from the same horizontal plane, but taken as negative for downward sloping cones. The equations by Croasdale are derived finding the vertical load that will break the ice beam, and the relationship between vertical and horizontal force is used to give Equations 5.7 and 5.13. This relationship is found as (for downward slope with negative angle)

$$F_H = F_V \frac{\mu\cos(\alpha) - \sin(\alpha)}{\mu\sin(\alpha) + \cos(\alpha)} = F_V\xi \tag{5.18}$$

5.3 First-year Ridge Loads

First-year ridges are found where ice starts rafting and eventually form ridges. They consist of a sail, a consolidated layer and a keel. The sail and keel consist mainly of loose ice rubble, while the consolidated layer is formed by several layers of rafted ice sheets that have frozen together.

An upper bound estimate of the loads by first-year ridges is given by

$$F_H = F_c + F_k \tag{5.19}$$

where F_c is the load contribution of the consolidated layer, and F_k is the contribution of the keel. The contribution of the sail is usually neglected since its volume is small compared to the keel. The contribution from the consolidated layer can be found using level ice methods, where h is replaced with the thickness of the consolidated layer h_c. The thickness of the consolidated layer is difficult to estimate as this will vary geographically. ISO-19906 [21] suggests to use $h_c = 2h$ if no field data is available, which is a valid assumption if the ice sheet has grown under the same conditions as the ice ridge.

There are several approaches and theories for calculating first-year ridge loads on offshore structures. Timco et al. [44] have evaluated several methods and compared results to measurements on the Molikpaq structure. They identify several inadequacies of the methods and advise caution when using them. Still, to get an overview of the magnitude of the loads the method by Dolgopolov and Mellor will be used. It should be noted that these two methods are for vertical structures, and loads may therefore be somewhat overestimated.

5.3.1 Dolgopolov

The theory by Dolgopolov is based on observation from experiments and parallels with granular material, [44]. The horizontal force is given as

$$F_k = h_k D_e q \left(\frac{h_k \gamma_e \eta^2}{2} + 2\eta c \right) \tag{5.20}$$

h_k is the keel depth of the ridge, D_e is the effective structure diameter taken as the diameter D, γ_e is the effective buoyant density, c is the apparent cohesion, and η is the passive pressure coefficient given as

$$\eta = \sqrt{\frac{1 + \sin(\omega)}{1 - \sin(\omega)}} \tag{5.21}$$

where ω is the angle of internal friction. The factor q is a shape factor that

depends on the keel depth and the structure width. Timco et al. [44] give this shape factor as

$$q = 1 + \frac{2h_k}{3D_e} \tag{5.22}$$

According to Kärnä and Nykänen [24] this is not correct, instead it should be

$$q = 1 + \frac{2B_s}{3D_e} \tag{5.23}$$

where B_s is the width of the sail of the ridge. This was also checked against the original paper by Dolgopolov et al. [12], and it was found that Equation 5.23 was indeed correct. Further, Kärnä and Nykänen [24] suggests that B_s is equal to $h_k/4$.

γ_e, the effective buoyant density, is given as

$$\gamma_e = (1 - n)(\rho_w - \rho_i) g \tag{5.24}$$

where n is the void ratio, taken as 0.3. Several properties have to be defined. The cohesion c is set to 1.5 kPa and the angle of internal friction ω to 45°.

5.3.2 Mellor

The method by Mellor is also presented by Timco et al. [44]. This method proposes that the rubble in the keel and sail slip along planes that make a constant angle with the horizontal. As such this method also includes the contribution from the ridge sail. API RP 2N [2] suggests this method, amongst others, to determine loads from first-year ridges.

The horizontal force from the sail is given as

$$F_s = \frac{1}{2} D_e \eta^2 (1 - n) \rho_i g h_s^2 + 2 D_e c \eta h_s \tag{5.25}$$

The horizontal force from the keel is given as

$$F_k = \frac{1}{2} D_e \eta^2 (1 - n)(\rho_w - \rho_i) g h_k^2 + 2 D_e c \eta h_k \tag{5.26}$$

Total force is then found by summing up the contribution of the keel and sail. Properties are the same as for the method by Dolgopolov. If q is set to unity the method by Dolgopolov yields the same result as the keel load from Mellor.

5.4 Multi-year Ridge Loads

As stated in the description of the ice conditions in section 2.5, one important design criterion in the Beaufort Sea is multi-year ridges. Two methods to calculate loads on the platform from multi-year ridges will now be presented. As previously mentioned the multi-year ridges tend to be more smoothed, but due to consolidation of ice rubble much stronger.

5.4.1 Elastic Ridge Bending - Ralston

Ralston [32] presents a method developed by Croasdale where the failure of a multi-year ridge against a conical structure is treated using the theory of elastic beams on elastic foundation. There are two main events during the interaction: initial crack formation and hinge crack formation, both shown in figure 5.4.

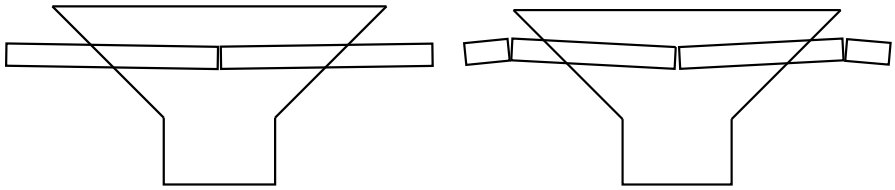

(a) Initial crack **(b)** Hinge crack

Figure 5.4: Initial and hinge cracks for the ridge model by Ralston.

To estimate the forces corresponding to these events it is necessary to assume the following: the initial failure is analogous to an infinite floating ice beam subjected to a vertical load; the hinge crack formation is analogous to the simultaneous failure of two semi-infinite floating beams subjected to vertical loading. The forces are given as [32]

$$F_v^{\infty} = \frac{4I\sigma_f}{y_t l}, \quad \text{(Initial crack)} \tag{5.27}$$

$$F_v^{\infty} = \frac{6.20 I \sigma_f}{y_b l}, \quad \text{(Hinge crack)} \tag{5.28}$$

I is in this case the second moment of area for the ridge cross section. A rectangular cross section is assumed in the calculations. y_t and y_b are the distances from the neutral axis to the top and bottom of the ridge. l is the characteristic length of the ridge given as

$$l = \sqrt[4]{\frac{4EI}{k}} \tag{5.29}$$

where k is the foundation modulus given as $\rho_w B g$.

The horizontal force will depend on the angle of inclination and the friction coefficient, and is found using Equation 5.18.

It has so far been assumed that the ridge is long. If the same theory is applied to shorter ridges the predicted force will increase with decreasing length, as stated by Ralston [32], and he therefore suggests that the method outlined is rather uncertain. Other methods should be included when estimating multi-year ridge loads.

5.4.2 Plastic Limit Method - Wang

Wang [46] presents a method of estimating the breaking loads from a multi-year pressure ridge on a conical structure. It is based on an upper bound plastic limit method, where the rate of external work (force $\times$ velocity) is equated to the rate of internal work (potential energy of the ice and work of deforming the plastic hinges). The internal work depends on the assumed position of the plastic hinges, and the position of the hinges are determined when the rate of internal work is a minimum. The deformation and location of the hinges are shown in Figure 5.5.

The position of the hinge cracks are determined by three unknown distances a, b and d. Wang [46] determines these distances by minimizing the rate of internal work with respect to the distances by a numerical trial and error procedure. When the distances are known, the forces can be determined. He further describes 5 possible hinge crack combinations with the first type, the Long Ridge Type I, being the most likely breaking pattern for long ridges. It is therefore considered further.

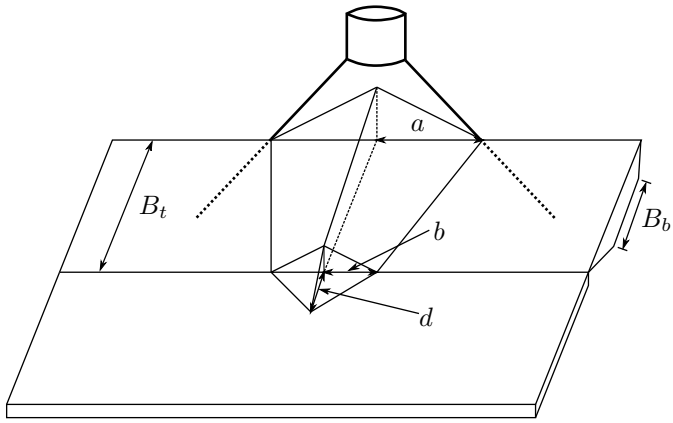

Figure 5.5: Figure of the deformation of Long Ridge Type I. This sketch shows the ridge breaking upwards. For a downward sloping cone the deformation is similar but directed downwards instead.

Nevel [29] simplified the equations for the Long Ridge Type I, by giving an analytical solution. This method is also used in the API standard [2]. The method assumes a ridge cross-section as shown in Figure 5.6.

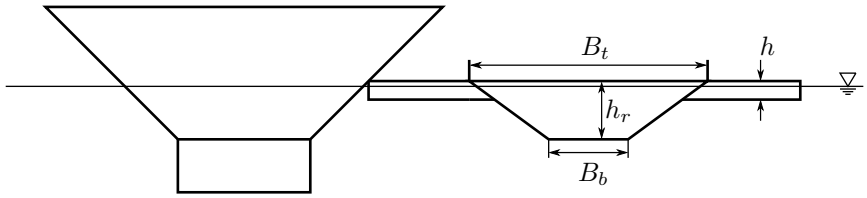

Figure 5.6: Figure of ridge with assumed cross-section, interacting with a platform shaped as a downward sloping cone.

The result of the analysis gives the following expression for the vertical force

$$F_V = \frac{\sigma_r h_r^2 \left(AF_a - BF_b\right)}{3} \tag{5.30}$$

where σ_r is the strength of the ridge ice, h_r is the thickness of the ridge and variables A, F_a, B and F_b are given in appendix B. The horizontal force is found by using Equation 5.18, defined in Section 5.2.2. The horizontal force is thus a function of the inclination angle of the platform and the friction coefficient between platform and ice.

This method does not take into consideration the ride-down loads, but

purely the breaking loads exerted on the platform during impact. Also, the effect of the ridge sail is neglected. This seems as a valid assumption for multi-year ridges since their shape tends to be more rectangular and smoothed.

5.5 Limit Momentum

For large ice features colliding with the platform the *limit momentum* interaction mode can be used to determine the maximum mass of an ice feature given a horizontal displacement of the platform, velocity of ice feature and stiffness of the stationkeeping system.

A large drifting ice floe is assumed to collide with the platform and its kinetic energy will be transferred to the platform. At the contact point between ice and platform the collision will result in crushing of ice. Some of the kinetic energy is thus used to crush the ice, while the largest amount is assumed to be taken up as potential energy by the stationkeeping system. Assuming that the ice floe collides head-on with the platform in surge direction and that crushing is neglected, the following relationship between the kinetic and potential energy can be established

$$\frac{1}{2}Mv^2 = \frac{1}{2}k_g x^2 \tag{5.31}$$

M and v are the mass and velocity of the ice floe; and k_g and x are the global stiffness of the stationkeeping system and the displacement of the platform. Since the maximum displacement of the platform is given as 5 % of the water depth, maximum ice floe mass can be determined as

$$M_{max} = \frac{k_g x^2}{v^2} \tag{5.32}$$

The only unknown variable is the global surge stiffness k_g, which is determined later, in chapter 6. It is expected that the ice drift velocity varies seasonally, with higher values during the summer. During winter the surrounding ice will govern the drift velocity of the floe, while in summer the wind and current acting on the floe itself will be governing. The drift speeds during the summer may therefore be larger, which means that the maximum mass that the platform can withstand is lower.

5.6 Ice Loads in Managed Ice

It is foreseen that ice management in one form or another will be utilized for the floating platform. The methods of estimating ice loads in managed ice have been treated by Croasdale, Bruce, and Liferov [9], and these methods will now be utilized to test the effect of ice management.

Three interaction scenarios are proposed:

- Scenario 1: Thick ice features broken into large pieces.
- Scenario 2: All ice broken into small pieces - minimal pressured ice.
- Scenario 3: All ice broken into small pieces - pressured ice present.

5.6.1 Scenario 1

The thick ice feature can for instance be a large pressure ridge or any other ice feature expected to result in large ice loads on the platform. This feature is broken into pieces by large icebreakers, and the size of the broken pieces are similar in size as the platform. Figure 5.7 shows this scenario.

As the ice pieces move against the platform the ice loads on the platform will be limited by the failure of the pack ice at the back of the ice pieces. The interaction process between ice pieces and platform can influence the loads, for example the interaction with a sloping structure will result in ice pieces being submerged. Regardless of interaction process the upper bound load is given by Croasdale, Bruce, and Liferov [9] as

$$F_{S1} = phD \tag{5.33}$$

where h is the ice thickness at the back of the ice piece, D is the width of the ice piece taken as the width of the structure (diameter at waterline for a circular structure). p is the pressure imposed by the surrounding pack ice at the back of the ice feature, seen in Figure 5.7. Croasdale, Bruce, and Liferov [9] propose the following value for p

$$p = 2h^{0.25}D^{-0.54} \tag{5.34}$$

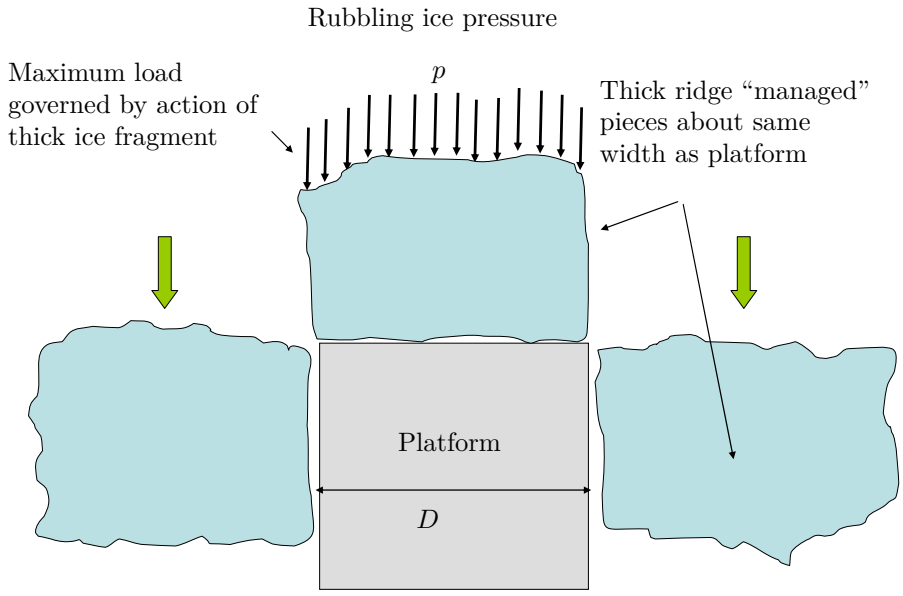

Figure 5.7: Scenario 1, ice feature broken into large ice pieces by icebreakers, [9].

5.6.2 Scenario 2

In this scenario all ice is broken into small pieces, and there is minimal pressured ice around the structure. This means that the ice pieces can move around the structure. The scenario is shown in Figure 5.8.

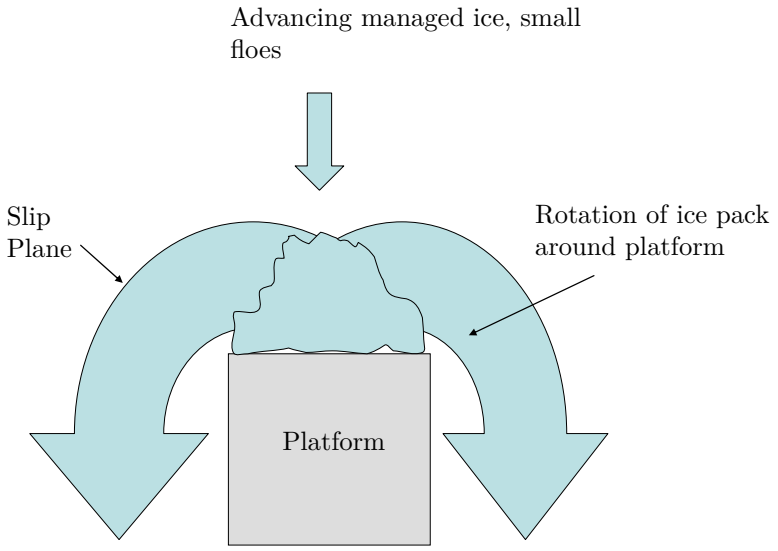

Figure 5.8: Scenario 2, small ice floes hit the structure and are rotated around the platform, [9].

The load on the structure under this scenario is found as

$$F_{S2} = KqDh_f \tag{5.35}$$

where K is a bearing capacity factor which relates the length of the slip planes to the width of the structure. h_f is the managed ice rubble thickness and q is the average shear strength of the ice rubble along the slip planes. Croasdale, Bruce, and Liferov [9] use a value of 6 for K, and q may be approximated as

$$q = \frac{K_0 \gamma_e \tan(\phi)}{2} + c \tag{5.36}$$

γ_e is the buoyant weight of the ice rubble given as $(1-n)(\rho_w - \rho_i)$ where n is the porosity/void ratio of the ice rubble taken as 0.3. K_0 is the ratio between the vertical and lateral rubble pressure which is set to 1 if assuming loose rubble. ϕ and c are the friction and cohesion of the ice rubble. Croasdale, Bruce, and Liferov [9] suggest that the values of ϕ and c are set to zero and 1500 Pa, based on calibration with results obtained in full-scale measurements on the Kulluk.

5.6.3 Scenario 3

The last scenario to consider in managed ice is very similar to scenario 2, but now there is pressured ice around the structure. As seen for the Kulluk, this leads to a wedge of ice rubble forming upstream of the platform exemplified in Figure 5.9.

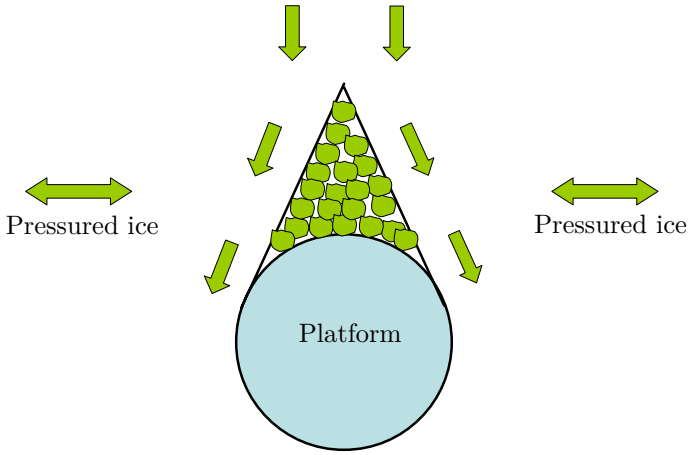

Figure 5.9: Scenario 3, ice floes are confined in front of the platform due to pressured ice, [9].

Using the approximation shown in Figure 5.10 the loads on the rubble wedge is given as

$$F_{3Sw} = pDh_f \left(1 + \frac{\mu}{\tan(\theta)}\right) \tag{5.37}$$

Including the friction of the ice on the platform the total ice load in scenario 3 is

$$F_{S3} = pDh_f \left(1 + \frac{\mu}{\tan(\theta)}\right) + 2pD\mu h_f \tag{5.38}$$

Croasdale, Bruce, and Liferov [9] state that an average value for p is 25 kPa, based on measurements performed in 1986. Further, different values of p was used to compare the results with measured values on the Kulluk. They found that $p = 25$ kPa gave too high results, while $p = 15$ kPa provided a better fit. A value of 15 kPa will therefore be used in calculations.

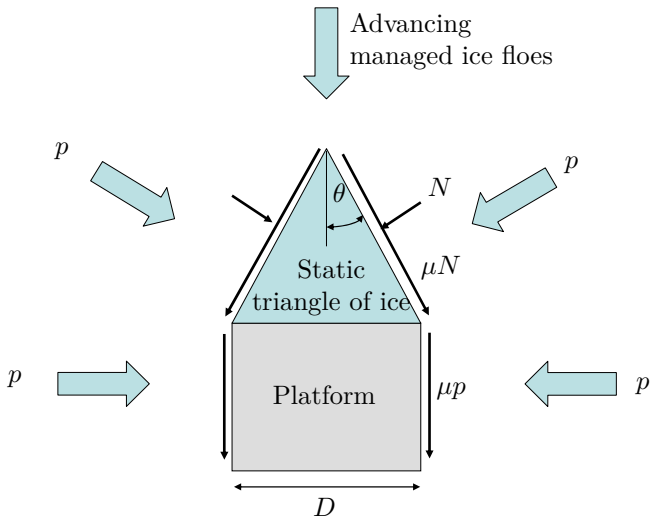

Figure 5.10: Simplification of scenario 3, [9].

The vertical forces in the three scenarios are determined using Equation 5.18, defined in Section 5.2.2.

5.7 Limit Force

After the *limit momentum* interaction scenario there are generally two outcomes. If ice concentration around the structure is low the ice feature may rotate around the structure. However, if the structure is wide and the ice concentration is higher the ice feature may become stuck in front of the platform. Forces from the surrounding ice features, wind, and current will be transmitted through the feature on to the structure.

For an ice feature colliding with the platform the *limit momentum* interaction mode has been used to estimate maximum mass of ice feature given a maximum allowable displacement of 25 m. When it stops the question arises of whether the driving forces are high enough to initiate further penetration or not. Croasdale [8] gives Equation 5.39 for the *limit force* load valid when ridge building occurs behind the ice feature, and wind and current acts on the ice feature

$$F_{lf} = \underbrace{C_w \rho_a V_w^2 L^2}_{\text{wind}} + \underbrace{C_c \rho_w V_c^2 L^2}_{\text{current}} + wL \tag{5.39}$$

C_w and C_c are the wind and drag coefficients for the ice feature. Croasdale [8] uses a value of 2×10^{-3} for C_w. ρ_w and ρ_a are the water and air densities, and V_w and V_c are the wind and current velocities. L is the width and length of the ice feature, assuming that the feature is square. w is the average pack-ice force over the width of the floe. It is thus a ridge building force, given as force per unit length.

The purpose of this method is to compare the results with the loads estimated by the *limit stress* approach for the same floe. The *limit stress* method may yield very high loads for large and thick floes. This raises the question of whether or not the environmental loads from wind, current and ridge building can generate such high loads. This method represents interaction between floe and platform during winter, due to the ridge building force being included.

Wind and current velocities have been estimated in sections 2.2 and 2.4. Croasdale [8] includes only the contribution from wind and ridge building, and since no current drag coefficient has been found the same is done in the calculations. It remains to estimate the size of the floe, L, and the ridge building force, w. The ridge building force depends on the ice thickness, and Croasdale [8] presents Figure 5.11 showing the variation. The mid-value of 1×10^5 N/m is selected for calculations, but it is important to appreciate that the value increases with increasing ice thickness.

The size and number of floes are connected in that most of the floes are rather small. For multi-year floes Figure 2.10 shows measurements performed in September and October 1980. Smaller floes occur more often than larger floes. Since a conservative approach is wanted, the size L is set to 10 km. Average annual thickness of multi-year floes is 5 m referring to Table 2.1. Due to the selected floe being rather large, the thickness will most likely also be larger. Therefore, a thickness of 15 m is selected.

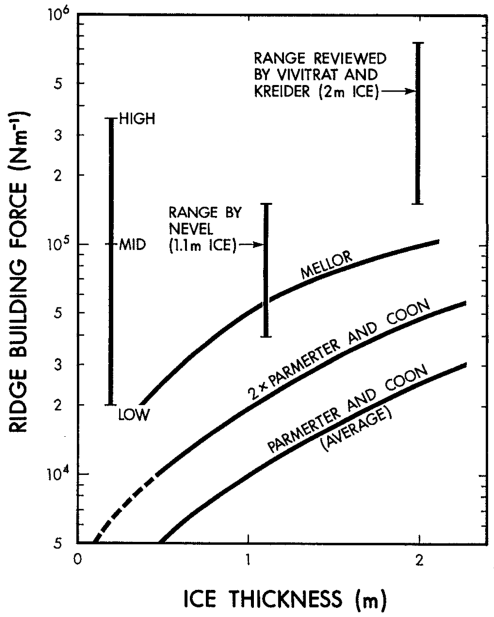

Figure 5.11: Values of ridge building forces, [8]. Croasdale [8] suggests the values 2×10^4 N/m, 1×10^5 N/m, and 3.5×10^5 N/m for all thicknesses.

5.8 Input for Ice Load Calculations

Different methods for determining ice loads in various ice conditions have now been presented. Some input parameters have been defined based on literature and design basis for the platform. Table 5.1 gives a summary of all the user-defined parameters that are needed to run the MATLAB program. Symbols follow the same convention as in the MATLAB program.

Table 5.1: Input to ice load calculations. Symbols follow the same convention as in MATLAB.

Parameter	Symbol	Value	Unit
Environmental parameters			
Acceleration of gravity	g	9.81	[m/s^2]
Density of sea water	ρ_w	1025	[kg/m^3]
Density of air	ρ_a	1.225	[kg/m^3]
Maximum wind speed	V_w	39	[m/s]
Water depth at location of platform	d	500	[m]
Platform dimensions			
Waterline diameter	D	100	[m]
Rubble ridedown diameter	D_r	70	[m]
Slope angle	α	-45	[deg]
Depth of sloping part	t	15	[m]
Level ice parameters			
Friction coefficient	μ	0.1	[-]
Density of ice	ρ_i	917	[kg/m^3]
Flexural strength of ice	σ_f	500	[kPa]
Elastic modulus of ice	E	5	[GPa]
Poisson ratio	ν	0.3	[-]
Level ice thickness	h	2	[m]
Ice ridge parameters			
Keel depth, first-year ridge	h_k	25	[m]
Sail height, first-year ridge	h_s	5	[m]
Sail width, first-year ridge	B_s	6.25	[m]
Thickness of consolidated layer, FY-ridge	h_c	4	[m]
Angle of internal friction, FY-ridge	ω	45	[deg]
Void ratio	n	0.3	[m]
Thickness of multi-year ridge	h_r	20	[m]
Top width of ridge	B_t	110	[m]
Bottom width of ridge	B_b	40	[m]
Strength of ridge ice	σ_r	500	[kPa]
Managed ice parameters			
Thickness of managed floes	h_f	2	[m]
Porosity of ice	e	0.3	[-]
Ice rubble friction coefficient	ϕ	0	[-]
Ice rubble cohesion	c	1.5	[kPa]
Bearing capacity	K	6	[-]
Vertical/lateral rubble pressure ratio	K_0	1	[-]
Ice pressure	p	15	[kPa]
Angle of stationary ice rubble block	θ	45	[deg]
Floe parameters			
Length and width of ice floe	L	10000	[m]
Thickness of ice floe	L	15	[m]
Ridge building force	w	100	[kN/m]
Wind drag coefficient	C_w	2×10^{-3}	[-]
General			
Ice drift speed	V	0.08	[m/s]

5.9 Results

Results from calculations are presented in Table 5.2.

Table 5.2: Results from ice load calculations. *initial/hinge crack as explained in section 5.4.1.

	Horizontal force [MN]	**Vertical force** [MN]
Level ice		
• Ralston	14.70	15.44
• Croasdale	11.47	9.386
First-year ridge		
Rubble:		
• Dolgopolov, keel	159.6	130.6
• Mellor, keel and sail	202.7	165.8
Consolidated layer:		
• Ralston	41.37	43.1
• Croasdale	28.87	23.62
Total (using Ralston):		
• Dolgopolov + consolidated layer	200.9	173.7
• Mellor + consolidated layer	244.1	208.9
Multi-year ridge		
• Ralston	93.94/145.6*	76.86/119.1*
• Wang	227.4	186.0
Managed ice		
• Scenario 1	39.57	32.37
• Scenario 2	1.800	1.473
• Scenario 3	3.900	3.191
Limit force		
• Croasdale	1373	-

5.10 Conclusion

For ice loads due to level ice, the methods by Croasdale and Ralston both give loads of the same order of magnitude. Higher results are seen for Ralston's method. The reason for this difference may be connected to the underlying theory applied. While Croasdale uses a semi-infinite beam on an elastic foundation, which is a 2D assumption, Ralston applies a plastic limit analysis which takes into consideration 3D effects. As mentioned in section 5.2.2, the method by Croasdale is also corrected for 3D effects. Further,

since the platform under consideration is assumed to be wide, meaning that its width is much larger than the ice thickness, a 2D method should be appropriate. Reasons for the difference in the results are therefore difficult to pin-point. Compared to loads estimated by Korzhavin's formula in section 4.3 the loads calculated by Croasdale and Ralston are much lower. This clearly shows how sloping sides will reduce the ice loads on the platform.

Ice management was also considered to reduce the ice loads on the platform. For level ice, loads in managed ice is calculated in scenario 2 and 3. Scenario 2 where all ice is broken into small pieces and there is minimal ice pressure gives a horizontal force that is roughly 12 % of the fore estimated by Ralston's method and 16 % of the force estimated by Croasdale's method. This indicates that ice management has a substantial effect on the ice loads exerted on the platform. Scenario 3 gives higher loads due to the presence of pressurized ice compared to scenario 2. Horizontal force in scenario 3 is approximately 27 % and 34 % of ice forces estimated by Ralston's method and Croasdale's method. This shows that loads are reduced significantly even in pressured ice.

Methods by Dolgopolov and Mellor have been used to estimate loads for first-year ridges. Both methods are in reasonable agreement, and this is also expected since setting the shape factor $q = 1$ in Dolgopolov's equation will yield a result identical to the keel force by Mellor. Dolgopolov yields a horizontal load of 159.6 MN, while Mellor yields a somewhat higher load of 202.7 MN. Mellor includes the sail rubble, which may explain the higher load. The contribution of the consolidated layer was calculated using the methods by Ralston and Croasdale, with a thickness of the consolidated layer equal to $2h$. Horizontal forces from the consolidated layer are 41.37 MN and 28.87 MN. Total horizontal force is now found by adding the contribution from the rubble (keel and if included, sail) and the consolidated layer. Using the force from Ralston, total forces from the ridge on the platform are 200.9 MN and 244.1 MN.

Compared to level ice loads, the increase in loads is significant. As pointed out by Timco et al. [44] the methods used have several inadequacies, and results should only be taken as an initial estimate. For instance, both methods do not take into account the other dimensions of the ridge such as length and widths. Further, the structure is assumed to have vertical sides. Another interesting observation is that the consolidated layer yields lower loads than the rubble, although it was expected to be the other way around. The reason for this may be that methods by Dolgopolov and Mellor assumes a vertical structure, while the contribution of the consolidated

layer was calculated using methods by Ralston and Croasdale that take into consideration the sloping sides.

Results for loads due to multi-year ridges are more scattered, but both methods show an increase in loads compared to level ice. The horizontal loads estimated using the method by Ralston are 93.94 MN for the initial crack, and 145.6 MN for the hinge crack. Using the method by Wang, horizontal load is 227.4 MN. Wang and Ralston uses different cross-sectional shapes for the ridges. Although ridges are comparable in size the calculated ice loads are different for the two different methods. The different theories applied may be the reason to the difference. Ralston [32] suggests that the method he developed has some uncertainties regarding the effect of the length of the ridge. The method by Wang is therefore preferred, especially since it is used in the API RP 2N [2]. Wang's method only estimates the breaking load of the ridge, so no forces due to ride-down is included. The magnitude of the breaking load is therefore assumed to be governing.

Comparing loads from first-year and multi-year ridges, loads are very similar in magnitude if multi-year ridge results from Ralston are neglected. It was expected that multi-year ridges would lead to higher results. The reason for this may be that the rubble loads estimated by Dolgopolov and Mellor assumes a vertical structure, while the method by Wang assumes a downward breaking structure. Loads by Dolgopolov and Mellor may therefore be overestimating the real loads. Also, the first-year ridge is 5 m thicker than the multi-year ridge, which also leads to somewhat higher loads from the first-year ridge.

To reduce loads from ridges it is possible to break the ridge up into smaller pieces. Loads in this condition is estimated using equations in scenario 1 of managed ice, giving a value of 39.57 MN. This clearly shows the effect of ice management on the loads exerted on the platform. It is assumed that loads are governed by the rubbling ice pressure behind the ice piece, and the accuracy will therefore depend on the accuracy of the ice pressure. Ideally, it should be based on measurements at the location of the platform, but since this is not available, values from literature have been used.

As very large and thick multi-year floes may be encountered in the Beaufort Sea, the *limit momentum* and *limit force* interaction modes were presented to analyse the event of the platform colliding with such ice features. Results from the *limit momentum* interaction mode requires the global stiffness of the stationkeeping system, and will therefore be covered after the stationkeeping system has been introduced and analysed. The

impact between platform and ice feature is assumed to be head on. If the impact is eccentric, energy will also be used to rotate the ice feature and platform. Hydrodynamic effects on the ice feature such as added mass will also influence the collision. Since the platform will start to move as a result of the impact, the added mass of the platform itself should also be considered. At this point these effects have not been included. Equations to evaluate loads on structures using *limit momentum* interaction scenario are presented by ISO-19906 [21]. However, these can not be used for compliant structures such as a moored platform. The energy consideration presented based on the surge/sway stiffness of the mooring system is therefore judged as an appropriate method to estimate maximum mass of ice features. Since no other terms that corresponds to energy dissipation is included (for example crushing of ice and local dissipation) the maximum mass estimated will be conservative.

For the *limit force* interaction mode, the underlying question is whether or not if the environmental driving forces on the floe are large enough to initiate *limit stress* interaction mode. If this is the case the loads on the platform are governed by the *limit stress* interaction mode. If not, loads on the platform are governed by the *limit force* interaction mode. For the particular ice floe chosen, the *limit force* is 1373 MN. Using a thickness of 15 m and assuming that the floe breaks in bending, *limit stress* loads by Ralston and Croasdale are found as 327.6 MN and 354 MN. The driving force is thus far large enough to initiate the *limit stress* interaction mode, and loads on the platform is limited by the *limit stress* loads.

As ice is broken during interaction with the platform, there will accumulate ice rubble in front of and around the platform. ISO-19906 [21] indicates that ice rubble accumulation will depend on factors such as slope angle, platform width, effects from snow, and roughness of ice sheets. If a substantial amount of ice rubble accumulates the load required to push more ice through the rubble will increase. Eventually it will become so large that the failure mode switches to failure of the oncoming ice against the ice rubble. Loads on the platform can in this case be estimated by the ridge building load. Since the platform is relatively wide there is a risk of ice accumulation. To judge if ice rubble accumulation is going to happen, model tests may be performed.

Ice drift speed will also influence the failure mode of ice sheet on sloping structures. At high speeds ISO-19906 [21] suggests that the failure mode may change from bending to shear, especially at higher ice thicknesses. This change is due to inertial effects, and may result in increase of loads.

The velocity effects will also depend on factors such as slope angle, sloping surface roughness and ratio between ice thickness and waterline width of platform. ISO-19906 [21] suggests that full-scale data should be used to determine the degree and sense of velocity effects. If no data is available it is suggested to increase loads if ice speeds are above 0.5 m/s. Even though maximum ice drift speed is set to 1 m/s in table 2.1, this is maximum value in summer for individual floes drifting under the influence of wind and current. During winter when level ice is present, ice drift speeds are expected to be well below 0.5 m/s. The effect of high ice drift speed is therefore not considered important for the Beaufort Sea.

The methods and results presented in this chapter only give static loads, meaning that only maximum or mean (depending on method) ice forces are found. Taking level ice loads as an example, the process can be divided into three phases: breaking of ice, rotating broken ice piece to align with sloping side and sliding along sloping side. The loads on the platform will therefore vary with time, typically with larger loads during breaking.

Shkhinek et al. [39] suggest several reasons why the use of static methods on floating anchored structures may give poor results:

- Due to anchored structure being compliant the ice load is a function of mutual ice-structure displacement and velocity.
- The position of the contact area between ice and structure is constantly changing over time.
- Besides maximum ice loads, the whole load time history should be determined. This because resonance motions can arise at certain ice load frequencies.
- Ice sheet may be subjected to 3D deformation, and the use of 2D assumption must be done with great care.

Shkhinek et al. [39] present a method where equations of motion of the structure is solved together with the equation of motion of the ice sheet. Their approach also takes into account that the slope angle for a conical structure is not constant over the width of the platform. According to Shkhinek et al. [39] this approach gives good results compared to results obtained in experiments performed by other authors.

At an early stage the static methods presented in this thesis is deem appropriate for initial design, and a dynamic model is not developed due

to the complexity. However, it is natural that the next step would be to develop a dynamic model to check the results obtained from the static analysis.

To make sure that the MATLAB program performs calculations that are correct, it was used to calculate loads for different numerical examples found in literature. This analysis is presented in appendix C, and it is found that the program calculates correctly.

As loads now have been calculated, the next step is to choose an appropriate stationkeeping system and estimate the restoring loads that it can generate.

Chapter 6

Stationkeeping

For any floating structure the positioning and motion control system is crucial to its performance. There are generally three different systems to apply: conventional mooring, dynamic positioning (DP) or a combination of the two. All have the same task of counteracting the environmental loads and assure that the structure holds the wanted position within an allowable variation. Due to the moderate water depth of 500 m it is probable that conventional mooring with anchors will be used. This chapter contains an analysis of a mooring system in terms of restoring forces and coefficients.

6.1 Mooring

A conventional mooring system is made up of several mooring lines attached between the structure and anchors at the seabed. Usually the mooring lines are placed in a spread system to ensure sufficient restoring forces. There are two groups of mooring-systems: catenary mooring and taut mooring. The difference is in materials used for mooring lines and how the mooring lines are shaped. A comparison is shown in Figure 6.1. Taut mooring is usually deployed in large water depths, using wires or fibre ropes for mooring lines. Catenary mooring is used in shallow to moderate water depths, and usually consists of chains. One fundamental difference is the angle at which the mooring lines arrive at the seabed. Catenary lines arrive horizontally, which means that anchors are subjected only to horizontal loads. Taut lines arrive at an angle which means that the anchors will be subjected to vertical as well as horizontal loads. There is also a difference in how the restoring

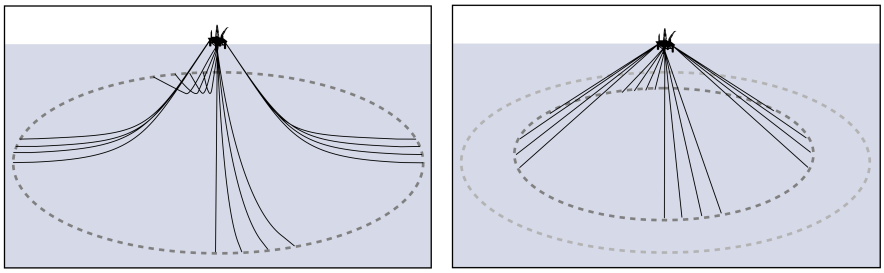

(a) Catenary system **(b)** Taut system

Figure 6.1: Comparison of catenary and taut mooring. Taut mooring systems will have a smaller footprint compared to a similar catenary mooring system. [45].

forces are generated by the different systems. For the taut system restoring forces are generated by the elasticity of the mooring lines, while for the catenary system it is mainly the weight of the mooring lines that generates the restoring forces. In this thesis a catenary system is analysed, since the water depth is moderate and well within the range of such a system.

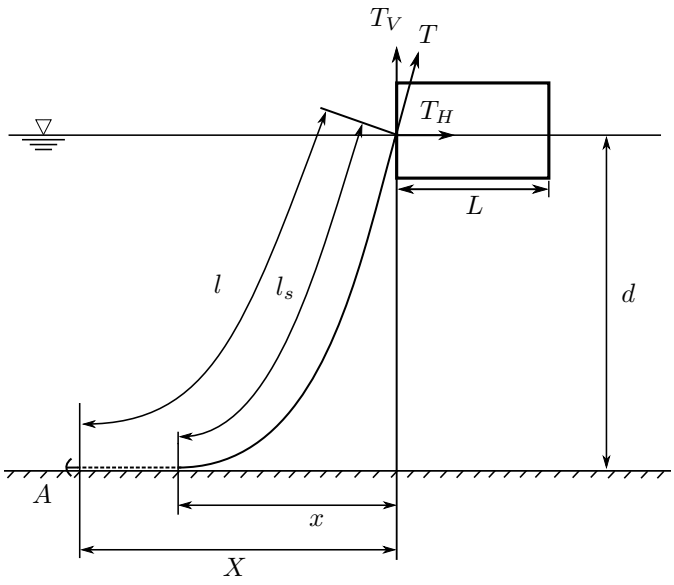

Figure 6.2: Catenary mooring line.

A catenary spread generates a non-linear restoring force that increases with the horizontal displacement of the structure. All lines have a pretension

to restrict the movements of the structure, and this influences the stiffness of the system. The following simplified analysis is based on Faltinsen [15], and gives a linear restoring force depending on the horizontal offset of the platform.

In Figure 6.2 a catenary mooring line is shown, connected between an anchor at A and a floating structure. By neglecting bending stiffness, elasticity, dynamic effects and the water drag on the mooring lines the catenary equations can be written as [15]

$$T_V = wd \tag{6.1}$$

$$T = (T_H^2 + T_V^2)^{1/2} = T_H \cos\left(\frac{wx}{T_H}\right) + wd \tag{6.2}$$

$$X = l - l_s + x = l - d\left(1 + 2\frac{T_H}{wd}\right)^{1/2} + \frac{T_H}{w}\cosh^{-1}\left(1 + \frac{wd}{T_H}\right) \tag{6.3}$$

T is the total line tension and T_H and T_V are the horizontal and vertical components. The total length of the inelastic caternary line is $l = l_b + l_s$ where l_b is the length of the part resting on the seabed and l_s is the part suspended between seabed and platform. w is the weight per unit length of the chain in water and d is the water depth. x is the horizontal distance from where the catenary line leaves the seabed to the platform, and X is the horizontal distance from the anchor to the vessel. Typically the ratio X/h is in the range 5-20, as proposed by Hansen [18].

It is foreseen that the platform will connect to a buoy that holds mooring lines, risers and umbilicals. The mooring system in Figure 6.3 is proposed, with 24 identical mooring lines connected to the turret. There are four connection points on the buoy, which means that the mooring lines are connected in groups of six. Mooring lines are equally spaced with an angle of 15° between them.

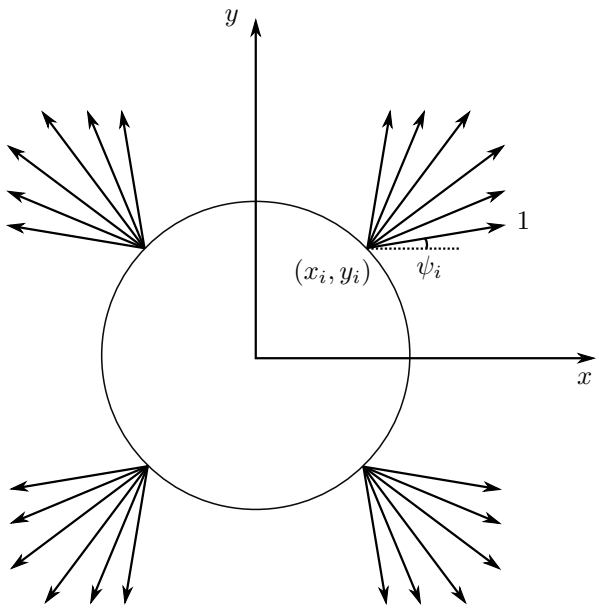

Figure 6.3: Turret with 24 mooring lines attached. There are four attachment points on the turret, each with six mooring lines connected. The angle ψ_i for each line is relative to the positive x-axis. For line number 1 the angle is thus 7.5°, and for subsequent lines increases with 15° going counter-clockwise.

Total restoring forces and moments are found by summing up the contributions from each of the individual mooring lines.

$$F_1^M = \sum_{i=1}^{n} T_{Hi} \cos(\psi_i) \tag{6.4}$$

$$F_2^M = \sum_{i=1}^{n} T_{Hi} \sin(\psi_i) \tag{6.5}$$

$$F_6^M = \sum_{i=1}^{n} T_{Hi} \left[x_i \sin(\psi_i) - y_i \cos(\psi_i) \right] \tag{6.6}$$

T_{Hi} is the horizontal tension of each mooring line, and ψ_i is the angle between the positive x-axis and mooring line i. x_i and y_i are the x and y coordinates of the connection point of mooring line i. The stiffness of the mooring system can also be determined, and this can be used to determine the restoring force as a function of the horizontal offset of the platform. It

is also needed in the *limit momentum* approach in section 5.5 to determine the maximum mass of ice feature. The stiffness of each individual mooring line can be determined as the derivative of T_H with respect to X at $(T_H)_M$. $(T_H)_M$ is the tension at the equilibrium position, i.e. the pretension of the line. An analytical expression can be obtained by differentiating Equation 6.3, given by Faltinsen [15] as

$$k_i = \frac{dT_H}{dX} = w \left[\frac{-2}{\left(1 + 2\frac{(T_H)_M}{wd}\right)^{1/2}} + \cosh^{-1}\left(1 + \frac{wd}{(T_H)_M}\right) \right]^{-1} \tag{6.7}$$

To find the global restoring coefficients the contribution of each mooring line is summed up in the respective direction giving the following

$$C_{11}^M = \sum_{i=1}^{n} k_i \cos^2(\psi_i) \tag{6.8}$$

$$C_{22}^M = \sum_{i=1}^{n} k_i \sin^2(\psi_i) \tag{6.9}$$

$$C_{66}^M = \sum_{i=1}^{n} k_i \left[x_i \sin(\psi_i) - y_i \cos(\psi_i)\right]^2 \tag{6.10}$$

The other restoring coefficients C_{12}^M, C_{21}^M, C_{16}^M, C_{61}^M, C_{62}^M, and C_{26}^M are zero since the mooring system is symmetric about the $x-z$ plane and the $y-z$ plane. It is assumed that the pretension is equal in all lines. This combined with the symmetric geometry of the mooring system leads to $C_{11}^M = C_{22}^M$. At the first stage it is mainly horizontal displacement that is of interest. If ice hits so that the force resultant works through the centre of the platform it will move purely translatory. If loads act off-centre the platform will start to move translatory while also starting to rotate. The movement of the platform will thus depend on contact point and angle relative to the centre of the platform. Translatory movements will be considered further.

6.1.1 Mooring System

The selection of parameters for the mooring system is not straight forward. Equations presented will only give a simplified analysis of catenary mooring lines. Thus it cannot be used where elasticity must be taken into consideration or where buoys are used along the mooring lines.

Minimum length of mooring line can be determined as a function of water depth, d; maximum allowable tension, T_{max}, in line; and the weight per unit length of the line in water, w.

$$l_{min} = d\left(2\frac{T_{max}}{wd} - 1\right)^{1/2} \tag{6.11}$$

T_{max} is assumed to be equal to the minimum breaking strength (MBS) of the chain. Selected mooring line characteristics are given in Table 6.1.

Table 6.1: Mooring line characteristics.

Parameter	**Value**	**Unit**
Water depth	500	m
Unit weight of chain	4500	N/m
Minimum breaking strength (MBS)	31	MN

This gives a minimum length of roughly 2600 m. However, this is not a fixed value as other considerations may require a different length, and it is therefore increased to 3000 m. The pretension of the mooring lines is also an important parameter for the characteristics of the system, and it is assumed to be 30 % of MBS. The value of MBS is cited in Aggarwal and D'Souza [1], based on a value used by Jannes Snel in his Master's thesis (2008). This is based on the value for one of the strongest chains available. Using the presented mooring line characteristics in Table 6.1, the horizontal distance X is found as 2888 m.

The mooring system characteristics can now be determined. Using Equation 6.7 the stiffness of individual mooring lines is determined. This is used in Equation 6.9 to determine the global stiffness of the mooring system as 12 times the individual mooring line stiffness, seen in equation 6.12. Results are presented in Table 6.2.

$$C_{11}^M = C_{22}^M = \sum_{i=1}^{12} k_i \cos^2(\psi_i) = 12k_i \tag{6.12}$$

Table 6.2: Mooring system characteristics.

Parameter	Value	Unit
Individual mooring line stiffness	1.7792×10^5	N/m
Global surge/sway stiffness	2.135×10^6	N/m

Since the maximum allowable horizontal displacement is given as 5 % of water depth, it is possible to determine the maximum horizontal environmental force. With a water depth of 500 m the maximum allowable horizontal displacement is 25 m, giving a maximum horizontal force of 53.38 MN. This means that the platform under a horizontal loading of 53.38 MN will be displaced 25 m. Due to the platform and mooring system being symmetric, this is the same regardless of which direction ice acts on the platform.

As the platform is displaced, tension in the different mooring lines will change. In lines with an increase in distance X, the increase in tension must be checked to ensure that it does not exceed the MBS. If the platform is displaced in negative x-direction, referring to Figure 6.3, lines 1 and 24 will experience the largest increase in distance X. These lines will therefore have the largest tension.

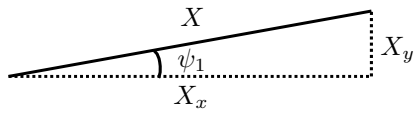

Figure 6.4: Relationship between horizontal distance X and horizontal distance along the x-axis for anchor line 1.

In the equilibrium position the horizontal distance X is equal for all lines. Figure 6.4 shows distance X, and the components along the x-axis and y-axis for anchor line 1. These distances are given as

$$X_x = X\cos(\psi_1) = X\cos(7.5) \tag{6.13}$$

$$X_y = X\sin(\psi_1) = X\sin(7.5) \tag{6.14}$$

As the platform is displaced 25 m along the negative x-axis the distance X_x is increased with 25 m, while X_y is constant. This will change the angle between the x-axis and the mooring line, and it can be shown that the new angle is given as

$$\psi_{1,ext} = \arctan\left(\frac{X_y}{X_x + 25}\right) \tag{6.15}$$

The distance X of lines 1 and 24 is increased to X_{ext}, which is found as

$$X_{ext} = \frac{X_x + 25}{\cos(\psi_{1,ext})} \tag{6.16}$$

For the particular mooring system selected, X_{ext} becomes 2912.79 m. Equation 6.3 can now be used iteratively to determine the horizontal tension in the line. When this is known the total tension in the line is found as

$$T = T_H + wd \tag{6.17}$$

The tension in lines 1 and 24 increase to roughly 18.1 MN, which is 58.4 % of MBS. This is well below the MBS, and is found acceptable.

Due to the assumption of catenary mooring lines, the anchors can only be subjected to horizontal loading. If an anchor is subjected to vertical loading it will start to move. This happens if l_s is equal to l. l_s is given as [15]

$$l_s = d\left(1 + 2\frac{T_H}{dw}\right)^{1/2} \tag{6.18}$$

Assuming displacement in negative x-direction again, horizontal tension in lines 1 and 24 is 15.85 MN when the platform is displaced 25 m. This gives a suspended length of 1942.22 m, which is well below the total length of 3000 m. Anchors at lines 1 and 24 will therefore not start to move. This

indicates that the allowable horizontal displacements are well within the capabilities of the mooring system.

6.2 Dynamic Positioning

Dynamic positioning using thrusters for stationkeeping is also a possibility, either individually or in combination with a mooring system. With the selected platform it seems preferable, based on existing platforms, to use mooring for stationkeeping since the platform does not need the ability to ice vane. Thrusters could be fitted to aid in moving the platform after disconnection. DP will therefore not be covered any further, but in deeper waters the use may be more preferable.

6.3 Conclusion

A stationkeeping system has now been introduced in form of a 24 line mooring system. Appropriate lay-out and characteristics have been selected to estimate maximum restoring force. The calculations are based on a maximum allowable horizontal displacement of 5 % water depth. Table 6.3 shows the mooring system characteristics.

Table 6.3: Mooring system characteristics when platform is displaced 25 m in negative x-direction.

Parameter	**Value**	**Unit**
Global Surge/sway stiffness	2.135×10^6	N/m
Maximum allowable displacement	25	m
Maximum allowable horizontal load on platform	53.38	MN
Maximum tension in lines when platform is displaced in negative x-direction	18.1	MN

Inelastic catenary equations have been used for the analysis, and factors such as bending stiffness, dynamic effects and water drag on the mooring lines have been neglected. Nonetheless, as an initial analysis the results seems valid when compared to for instance the mooring system used for the Terra Nova FPSO. Maximum capacity of its mooring system is 20 MN according to Howell and Duggal [19].

Chapter 7

Operability

In this chapter the ice loads and restoring forces from the stationkeeping system are compared. This will aid in the conclusion on operability of the platform. Further, ice management will also be analysed more in detail based on the conclusions on ice loads and restoring forces.

7.1 Ice Loads and Restoring Forces

Ice loads have been calculated for the design basis selected. Results are presented in Table 5.2, and they are discussed in section 5.10. The ice load results are also presented in Figure 7.1, together with the maximum allowable horizontal load represented by the red horizontal line.

Table 7.1: Explanation of method numbers in Figure 7.1.

Number	Ice load method
1	Level ice, Ralston
2	Level ice, Croasdale
3	First-year ridge, Dolgopolov + consolidated layer (Croasdale)
4	First-year ridge, Mellor + consolidated layer (Croasdale)
5	Multi-year ridge initial crack, Ralston
6	Multi-year ridge hinge crack, Ralston
7	Multi-year ridge, Wang
8	Managed ice, scenario 1
9	Managed ice, scenario 2
10	Managed ice, scenario 3

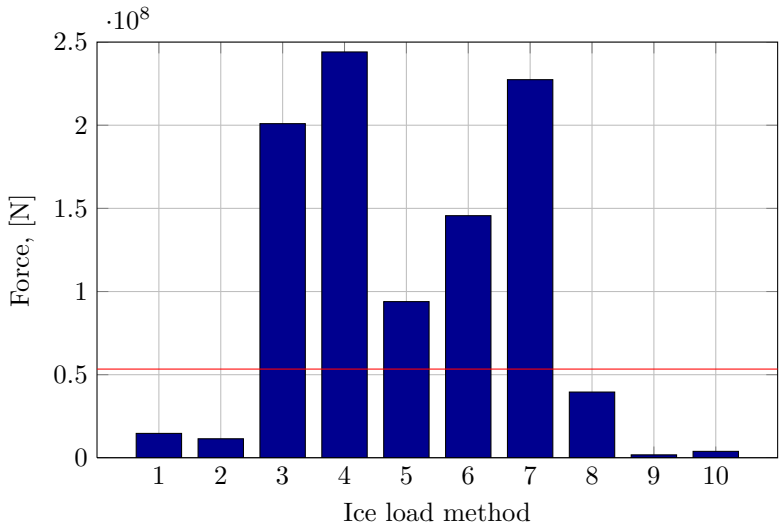

Figure 7.1: Horizontal ice loads in different conditions compared to maximum allowable load, given by the horizontal red line. Explanation of method number is given in Table 7.1.

Ice loads in 2 m level ice have been evaluated using methods by Ralston and Croasdale. Both results are lower than maximum allowable load, which suggests that the platform is able to operate in level ice on its own. In reality the ice cover is never homogeneous, meaning that level ice of constant thickness seldom is found. Other ice features such as rafted ice and hummock fields may increase the ice loads further. This implies that a certain ice management should be upheld at all times, to ensure that the loads are kept below the capacity of the mooring system. According to results obtained from calculations in scenario 2 and 3 (methods 9 and 10 in Figure 7.1), the ice loads in level ice can be reduced significantly with ice management.

Columns 3 and 4 show loads due to first-year ridges, and loads exceed maximum allowable load. Results are very consistent, which was expected. Both methods use more or less the same equations with the difference being that the sail contribution is included by Mellor. Based on loads the platform is not able to withstand an impact with a first-year ridge having a keel depth of 25 m. Both methods are presented in API RP 2N [2], and can be used with a certain confidence for initial estimates of loads. However, as explained by Timco et al. [44] both methods have several shortcomings and results should be used with care.

Loads due to multi-year ridges have also been estimated and are represented by columns 5, 6 and 7 in Figure 7.1. Results are well above the maximum allowable load. This suggests that the platform is not able to withstand the impact of a multi-year ridge with a thickness of 20 m. The method by Wang is preferred since it is presented in API RP 2N [2].

All methods use simplified ridge cross-sections for the calculations. For certain ridges, these simplifications may lead to uncertain estimates of loads. At an early design stage the methods are deemed appropriate to get an order of magnitude of the loads than can be expected.

For ridges and large ice features, scenario 1 in managed ice estimates loads on the platform assuming that ice features are broken into pieces with size comparable to the dimensions of the platform. The result is represented by column 8 in Figure 7.1. Loads at roughly 40 MN can be expected, which is below the maximum allowable load. The platform is thus able to operate in managed ice ridges, which further strengthens the viability of the concept. By managing large ice features into smaller pieces, loads can be brought below the capabilities of the stationkeeping system.

Limiting driving force was also estimated for a floe measuring $10\,000\,\text{m} \times 10\,000\,\text{m} \times 15\,\text{m}$ subjected to a wind with speed 39 m/s and a ridge building force of 100 kN/m. The driving force on such a floe is 1373 MN, indicating that *limit stress* can initiate. Using level ice methods by Ralston and Croasdale, the *limit stress* loads for ice with thickness of 15 m are 327.6 MN and 354 MN. *Limit stress* will therefore initiate, leading to loads far exceeding the capabilities of the stationkeeping system. These loads are not included in Figure 7.1 due to axis scaling.

To conclude, the platform with the selected geometry and mooring system should be able to operate in moderate level ice without the need for ice management. In more severe ice conditions ice loads increase significantly, and the need for ice management is clear. The ice load calculations in managed ice clearly shows how loads are reduce, which is essential to ensure year-round production.

7.1.1 Ice Loads in Varying Ice Conditions

So far calculations have been performed only for specific ice conditions. It is also interesting to calculate ice loads for a range of ice conditions such as level ice thickness, ridge thickness and managed floe thickness. Therefore,

plots have been made for the following ice conditions:

- Level ice with thickness from 0 m to 6 m, Figure 7.2.
- First-year ridges with keel depth from 5 m to 30 m, Figure 7.3.
- Multi-year ridges with thickness from 10 m to 35 m, Figure 7.4.
- Managed ice with pack ice thickness from 0 m to 4 m, and ice floe thickness from 0 m to 4 m, Figures 7.5 and 7.6.

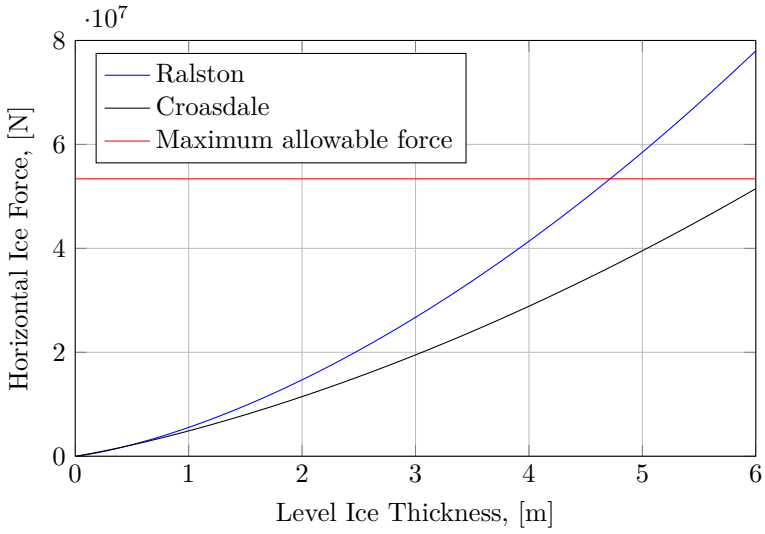

Figure 7.2: Level ice loads plotted against level ice thickness calculated using methods by Ralston and Croasdale. Red line represents the load that leads to maximum displacement of 25 m of the platform.

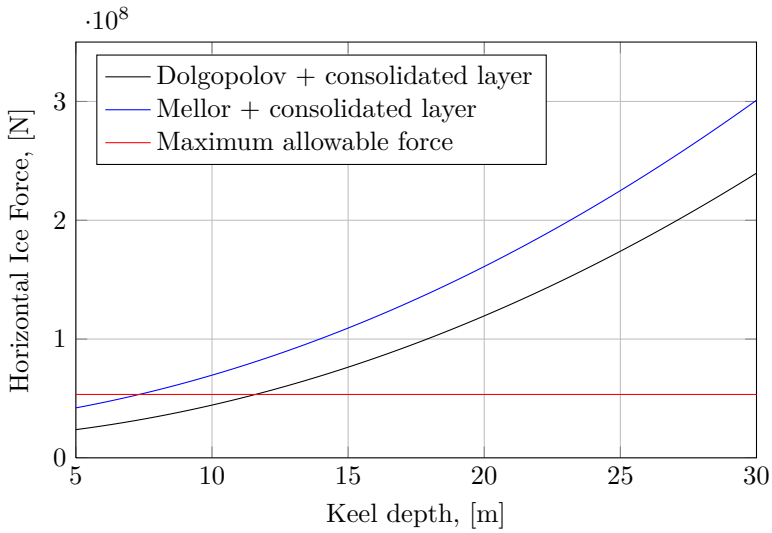

Figure 7.3: First-year ridge load plotted against keel depth, calculated using methods by Dolgopolov and Mellor. Red line represents the load that leads to maximum displacement of 25 m of the platform.

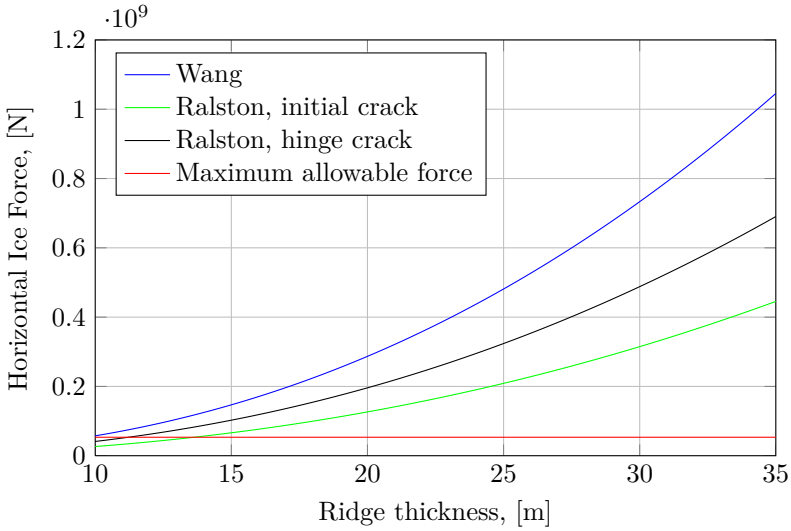

Figure 7.4: Multi-year ridge load plotted against the ridge thickness, calculated using methods by Ralston and Wang. Red line represents the load that leads to maximum displacement of 25 m of the platform.

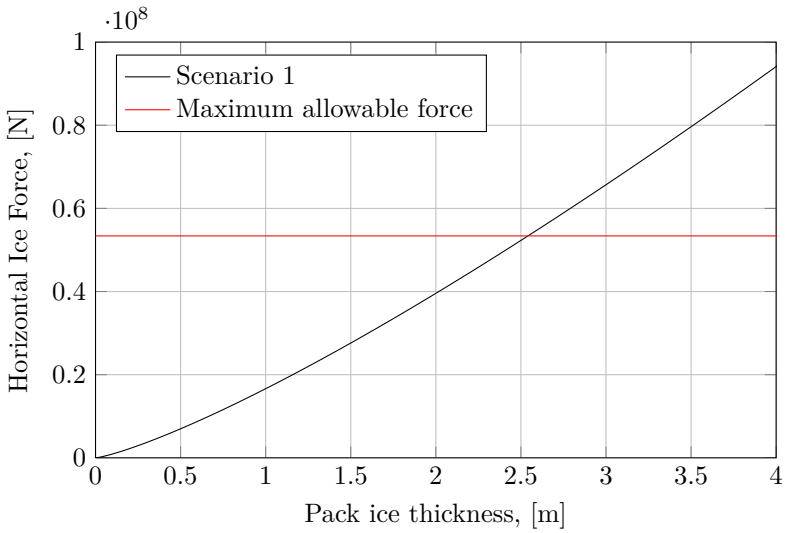

Figure 7.5: Ice loads in scenario 1 of managed ice plotted against the pack ice thickness. Large ice features are broken into pieces comparable in size to the platform. Red line represents the load that leads to maximum displacement of 25 m of the platform.

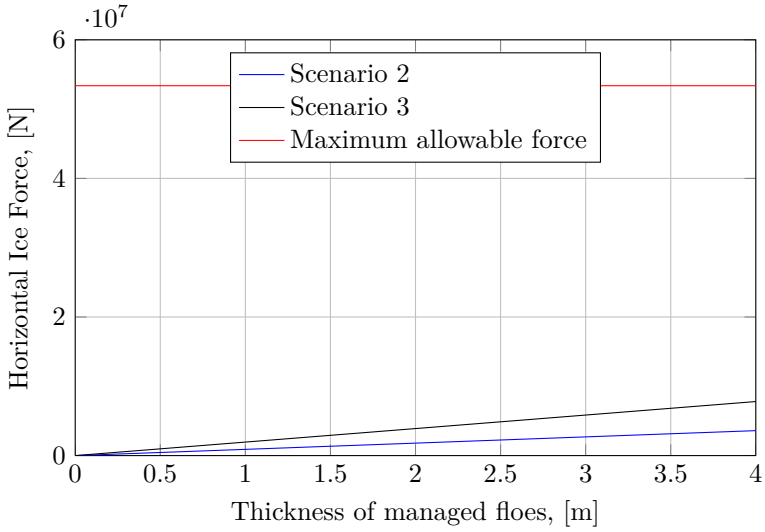

Figure 7.6: Ice loads in scenario 2 and 3 of managed ice plotted against the floe thickness. Level ice is broken into small pieces in both scenarios, with the difference being that ice pressure is present in scenario 3 resulting in somewhat larger loads.

Figure 7.2 indicates that the platform is able to operate within the requirements even at large level ice thicknesses. Estimated maximum level ice thickness is 6 m and 4.6 m based on the methods by Croasdale and Ralston. This indicates that the selected platform and mooring system will have good performance in level ice. Requirements for ice management is therefore limited in level ice.

Loads due to first-year ridges are plotted in Figure 7.3, and loads increase with increasing keel depth. For both methods the maximum allowable load is reached at the lower end of the keel depth scale, roughly around 5 m to 10 m. The platform is thus only able to withstand loads by smaller ridges. Average annual keel depth for first-year ridges is 25 m according to ISO-19906 [21] (see also Table 2.1), and it is clear that the load from such a ridge far exceeds the capabilities of the mooring-system.

For interaction with multi-year ridges the loads increase significantly compared to level ice. Figure 7.4 gives ridge loads for a range of ridge thicknesses between 10 m and 35 m. Only smaller ridges with a thickness less than 10 m can be tackled by the platform itself. Based on previous discussion the method by Wang is deemed the most reliable, and this is also the method that results in the highest loads. For the average annual multi-year ridge thickness of 20 m, loads will exceed the maximum allowable load. This suggests that in the event of such a ridge colliding with the platform, ice management must be initiated to break up the ridge. If this is not successful the platform must be disconnected and towed away.

If comparing a first-year ridge to a multi-year ridge, where both have the same keel depth, loads for multi-year ridges are highest. Selecting a keel depth of 25 m, load by first-year ridge is 261.8 MN using method by Mellor. For a multi-year ridge with a thickness of 25 m (sail is neglected) method by Wang yields a load of 330.7 MN.

Regardless of either first-year or multi-year ridges the probability of encounter is also an important factor to consider. Loads increase with ridge dimension, but the probability of encounter decreases with increasing dimensions. As seen in Figure 2.8 it is 100 times more likely to encounter a first-year ridge with a sail height of roughly 1.8 m, compared to a first-year ridge with a sail height of 5 m.

Figures 7.5 and 7.6 show ice loads on the platform in different kinds of managed ice. Scenario 1 estimates loads of large ice features broken into pieces of size comparable to the platform itself. The upper bound of this

force is limited by the driving force at the back of the ice feature, which again is dependant on the pack ice thickness. Figure 7.5 suggests that maximum load will be reached at a pack-ice thickness of roughly 2.5 m. This result is also largely dependant on the pressure of the pack-ice, and since this is determined using an empirical relationship it is difficult to validate the results. Still, reduction in loads compared to unmanaged ridges is clear.

In managed level ice the loads on the platform are reduced significantly compared to unmanaged ice. There is a small increase in loads with increasing thickness of managed floes, but this is moderate as seen in Figure 7.6. Scenarios 2 and 3 estimates loads well below maximum allowable, and the platform should therefore be able to operate safely in managed ice.

As the mooring system characteristics are known and a range of ice drift speeds have been defined, it is possible to estimate maximum mass of ice feature colliding with the platform, referring to the *limit momentum* interaction mode in section 5.5. Ice drift speed can vary between 0.06 m/s and 1 m/s according to ISO-19906 [21], giving a maximum mass from 1.334×10^9 kg for 1 m/s to 3.707×10^{11} kg for 0.06 m/s. The variation of maximum mass with ice drift speed is presented in Figure 7.7. For the average annual drift speed of 0.08 m/s maximum mass is found as 2.081×10^11 kg. An ice island in the Beaufort Sea has an average annual mass of 10×10^6 t, according to Table 2.1. In the event of an impact, and assuming that the drift speed is 0.08 m/s, the mooring system should be strong enough. The resulting horizontal displacement should only be around 5.5 m. Local deformation of the ice floe and platform at point of contact has been neglected. In reality this will also absorb some of the energy, and in certain cases the local deformation may be unacceptable. Structural concerns may therefore be more important when considering a collision with a large ice feature. In any case the platform should be disconnected before it collides with an ice feature.

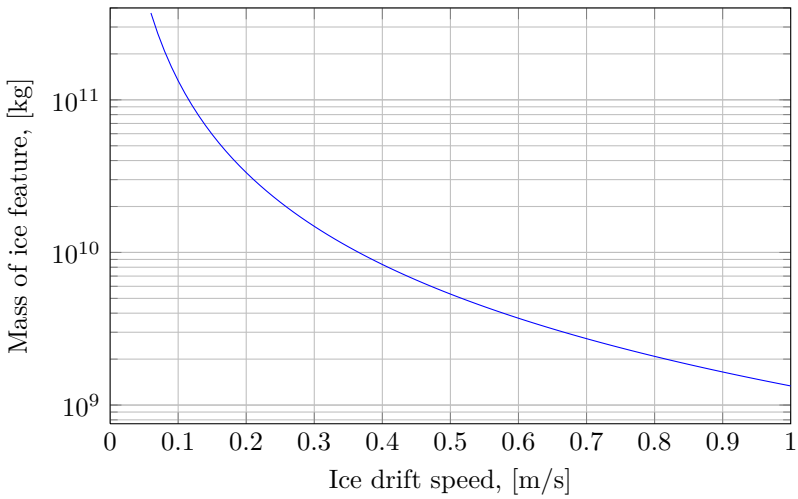

Figure 7.7: Maximum mass of ice feature as a function of the ice drift speed. Increasing ice drift speed reduces the maximum mass of the ice feature that the stationkeeping system is able to withstand.

7.2 Ice Management

The results obtained show that ice loads will vary a lot, depending on ice conditions. In level ice calculations suggests that the platform can operate without the assistance of icebreakers. As the platform encounters any other ice features such as ridges and floes, loads will exceed the maximum allowable load defined by the mooring system and as such ice management is required. A typical example of ice management is shown in Figure 7.8.

For a production platform the main objective of the ice management system is to ensure safe operation and minimize downtime related to ice. There must be a reliable ice surveillance system to detect, forecast and track ice features. Since the platform is able to withstand a certain amount of ice by itself the task of the ice management system is to manage larger ice features that lead to loads far too high for the stationkeeping system. The primary objectives are thus, as proposed by Coche, Liferov, and Metge [7]:

- Ensure detecting, tracking and forecasting of the ice features
- Manage ice features to ensure that the platform can maintain production

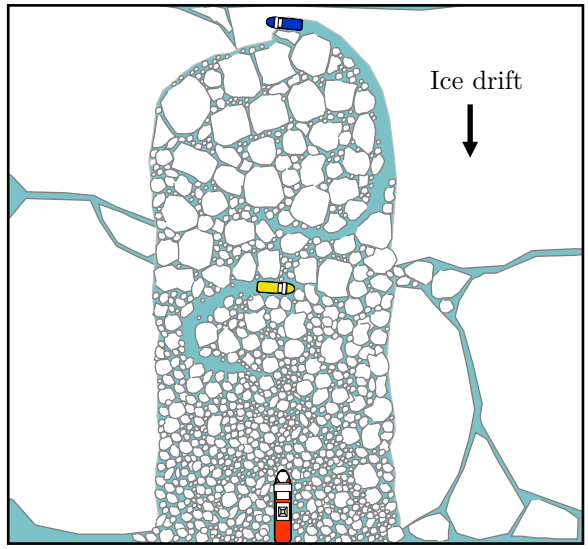

Figure 7.8: Typical ice management. Platform is represented by the red ship. The largest icebreaker is working furthest away from the platform, doing the first ice breaking. Closer to the platform the smaller icebreaker continues ice breaking, reducing the floe size further. [16].

It is foreseen that the icebreakers are designed to also perform the task of field support vessels. As proposed by Coche, Liferov, and Metge [7], the secondary objectives of the ice management system are:

- Assist in marine operations such as route planning for tankers and assistance during offloading
- Assist during disconnection and reconnection, and towing of platform
- Assist during emergencies

Keinonen [22] identifies the difference in ice management for a platform compared to traditional escort of vessels in transit. For traditional icebreaking, the objective is to create a channel for a transiting vessel. The icebreakers can find routes circumventing larger ice features. Ice management for a stationary platform is different in that it must deal with whatever ice that drifts towards the platform, up to the limit defined for disconnection. Ice drift direction is also prone to change rapidly which further increases the challenges for the icebreakers.

The most effective way to manage ice is to operate icebreakers in systematic patterns updrift of the platform. Typical fleet patterns are given in Figure 7.9.

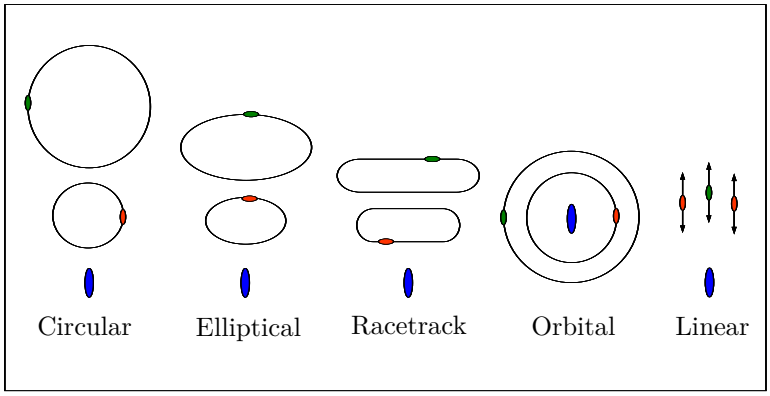

Figure 7.9: Typical ice management patterns. Usually the green icebreaker is larger than the red one. [16].

These patterns assumes one icebreaker per pattern, but it is also possible to use two or more icebreakers in the same pattern to increase the efficiency. This will however require a certain distance between icebreakers to ensure a safe operation.

Most patterns assume a size difference between icebreakers, with the largest icebreaker working furthest away from the platform. This breaks ice into floes, and if necessary uses ramming to break up larger ice features. Closer to the platform a smaller icebreaker is used to further decrease ice floe size. Since it operates in pre-broken ice it can operate at higher speeds.

The distance from where icebreakers operate to the platform is also an important factor to consider. The channel created by the icebreakers may miss the platform due to the ice drift curvature. It therefore seems preferable to manage ice close to the platform. This conflicts with the need for sufficient shutdown and disconnect time. The selection of distance between ice breaking and platform is therefore a compromise between the two considerations. For most platforms there will also be an exclusion zone defined, which typically is set to 500 m. Coche, Liferov, and Metge [7] suggests the zones in Figure 7.10 to be defined, with the following explanation.

- GSZ, General Surveillance Zone. Different surveillance techniques are

used to identify the potential ice threats. At this point the ice is usually three to seven days from the platform.

- TAZ, Threat Assessment Zone. An icebreaker confirms the potential threats and starts to manage threats that can be managed. It further assesses how ice management shall continue. At this point the ice is one to three days from the platform.
- PMZ, Physical Management Zone. Standard ice management is started, and the ice is usually 24 to 6 hours from the platform. The objective of this zone is to prevent ice threats to cross the planned disconnection limit (PDL) usually situated six hours from the platform.
- EDZ, Emergency Disconnection Zone. This zone shall protect the emergency disconnect limit situated 15 minutes from the platform.

The disconnection limits are defined based on the time it takes to disconnect the platform. Controlled disconnection will take a considerable amount of time since the following stages must be performed as presented by Howell and Duggal [19]:

1. Shutdown production;
2. de-pressurize gas injection, gas lift, and water injection lines;
3. pig and flush hydrocarbons from production/test lines;
4. close upper and then lower quick connect and disconnect (QCDC) valves;
5. disconnect QCDC valves;
6. de-pressurize and vent umbilicals and disconnect J-plates;
7. flood turret to waterline; and
8. disconnect main connector that releases spider buoy.

A typical disconnection takes from four to six hours as indicated by Howell and Duggal [19] and Coche, Liferov, and Metge [7]. Most of the time is spent on pigging and flushing of production lines. In an emergency disconnection

Table 7.2: Explanation of ice management zones in Figure 7.10.

GSZ	General Surveillance Zone
TAZ	Threat Assessment Zone
PMZ	Physical Management Zone
PDL	Planned Disconnection Limit
EDL	Emergency Disconnection Limit
EXZ	Exclusion Zone
EDZ	Emergency Disconnection Zone

the procedure is more or less the same, but no pigging and flushing is performed. An emergency disconnection will typically take 15 minutes.

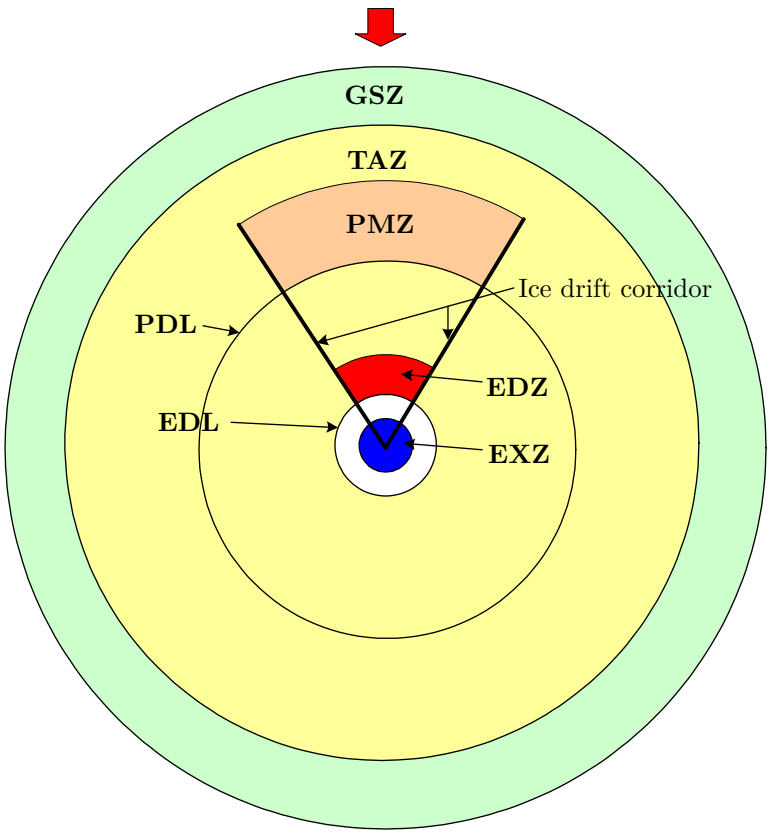

Figure 7.10: Ice management zones. Zones are explained in Table 7.2. [7].

Large ice features such as ice islands will most likely be impossible to break

up into smaller pieces by the icebreakers. The alternative solution is to try and change the trajectory of the ice island by pushing or towing it.

As seen by ice load calculations both first-year and multi-year ridges lead to very large loads. Multi-year ridges are consolidated due to melting and re-freezing and must be managed by ramming or towing. First-year ridges consist of loose rubble in keel and sail. Keinonen [22] suggests that by using icebreakers with azimuth thrusters first-year ridges can be managed more easily compared to ordinary icebreakers. The icebreaker moves along a severe ridge and directs its propeller wake towards the keel of the ridge, effectively washing the keel away. The remaining sail and consolidated layer collapses due to loss of buoyancy. The advantage of this technique is that larger ridges are more easily dismantled, due to the increased weight of the sail.

In the unlikely event of disconnection, the towing of the platform may be challenging due to high ice concentrations. An increased number of icebreakers working as tugs may therefore be required during the winter.

7.3 Operability of Platform

Ice loading has now been discussed and compared to the restoring forces from the mooring-system. Further, ice management has also been analysed based on the results for ice loads and restoring loads and general remarks. The main objective is to make sure that the platform is able to sustain year-round production. The following operability scheme is suggested.

During open water season the platform is accompanied by a single vessel. The objective of this vessel is to assist offloading to the tankers, and managing any multi-year floes on collision course with the platform. In the unlikely event of the platform being disconnected, this vessel will also be used for towing of the platform and assisting with disconnection and reconnection to the buoy.

As ice formation starts the ice management is kept unchanged, until the ice conditions become more severe during November and December. At this point it will be necessary to introduce a second icebreaker, and the two icebreakers can maintain typical ice management patterns as given in Figure 7.9. Towards the end of the ice season the ice conditions may have worsened further, introducing the need for a third icebreaker. This may be used to ensure ice clearing around the platform in case of pressured ice

and assist tankers with offloading. Due to the severity of ice conditions in the Beaufort Sea it is foreseen that each oil tanker will have a dedicated icebreaker for transit, which also assists in offloading. The need for a third icebreaker will also most likely vary from year to year, as severity of ice conditions also will vary from year to year.

Selecting an appropriate ice management system must also be based on economical considerations. The day rate of icebreakers is high, and the introduction of additional icebreakers will increase the operational costs. This must be weighted against the risk of disconnection and downtime, resulting in loss of income.

A conservative operability chart of the platform is given in Figure 7.11 showing the extent of the ice season and ice management.

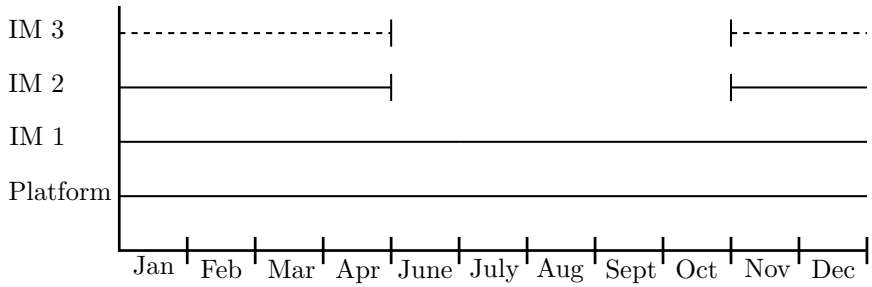

Figure 7.11: Operability of platform in terms of ice management. One vessel is present year round. This is seen as necessary due to multi-year ice, and also if the platform needs to disconnect. In the ice season a second icebreaker is added, and a third if necessary. Need for the third icebreaker will depend on the annual ice severity. In some years it may be needed, while in others not.

Operability of the Kulluk was discussed in Section 4.2. It was accompanied by up to four icebreakers, and it did not operate year-round. Number of icebreakers selected in this thesis may therefore seem somewhat underdimensioned. As pointed out by Wright [48] the Kulluk was designed to withstand global loads of 750 t, corresponding to roughly 7.4 MN. The mooring system selected in this thesis has a limit of 53.38 MN, which is almost four times higher. As such, the increased need for ice management is to some degree balanced by a stronger mooring system.

7.4 Summary

To summarise the operability, the circular platform with mooring for stationkeeping shows to be a promising concept assuming that an effective ice management system is present. The platform with mooring system operating in level ice is shown conceptually in Figure 7.12.

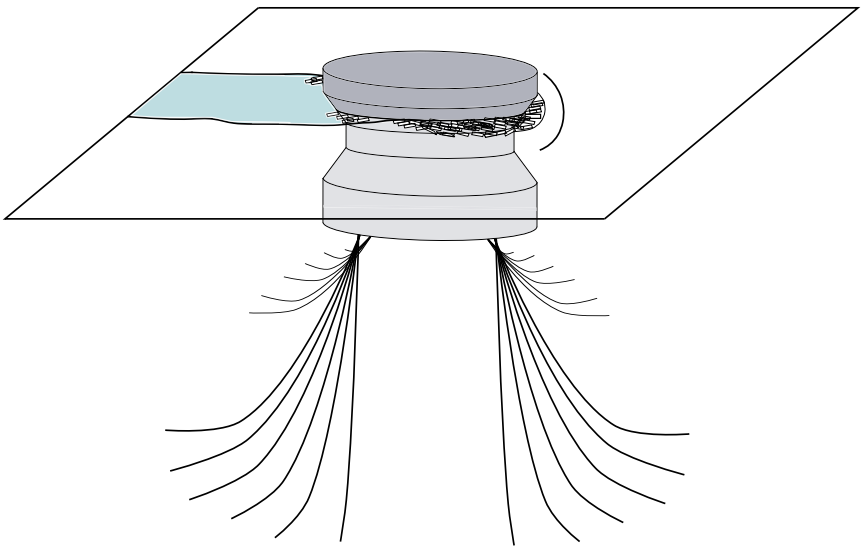

Figure 7.12: Platform operating in unbroken level ice. The radial cracking pattern is a typical breaking pattern for conical structures. Ice floes are further broken into smaller pieces that clear around and beneath the platform.

In short, the proposed platform uses a circular design with downward sloping sides to reduce the ice loading. Based on the water depth and previous experience with similar platform types, conventional mooring is chosen for stationkeeping. A 24-line system with catenary anchor lines and conventional anchors is proposed. The capability of the mooring system is exceeded in any ice other than level ice and managed ice. Ice management is therefore required to prevent loads on the platform to exceed the capabilities of the mooring system. It is foreseen that there is one icebreaker present year-round, due to the risk of multi-year ice. When ice season starts, another icebreaker is introduced to ensure proper ice management. If required, a third icebreaker can be included. The icebreakers must also work as field support vessels, being able to tow the platform in case of disconnection and assist during disconnection and

reconnection.

For offloading of oil, the use of shuttle tankers is proposed. They must be designed to operate in ice, and it is foreseen that they are accompanied by dedicated icebreakers during winter. During offloading the tanker is located in the wake of the platform to shelter it from ice.

Chapter 8

Conclusions and Further Work

The main goal of this thesis was to develop an oil production platform for year-round operation in the Beaufort Sea. A platform type was selected based on an analysis of the available platform types. It was found that a circular FPSO, albeit being subjected to large ice loads assuming vertical sides, was most appropriate due to insensitivity to ice drift direction. Also, using a turret system the platform is able to quickly disconnect and reconnect if required. To reduce ice loads on the platform it was decided to use sloping sides.

The environmental conditions in the Beaufort Sea have been analysed, with a focus on the ice conditions. Ice conditions were divided into level ice, first-year ridges, multi-year ridges, large floes and ice islands. Design conditions were chosen based on data from ISO-19906 [21]. Platform dimensions and ice conditions were used in several methods to calculate ice loads on the platform. It was found that ice loads are lowest in managed ice and level ice. In other ice conditions ice loads increase significantly.

To test the effects of global ice loads on the platform a conventional mooring system with 24 mooring lines was chosen for stationkeeping. This was analysed using inelastic catenary equations, giving a maximum allowable horizontal load of 53.38 MN. Compared to ice loads, only level ice and managed ice results in loads below this limit. This clearly shows the need for ice management.

An ice management system has been proposed, with one ice breaker being

present year-round. The need for a year-round icebreaker is based on the presence of multi-year ice in the Beaufort Sea. During the ice season an additional icebreaker is introduced, and optionally a third if ice conditions are very severe. Seasonal and year-to-year variations in ice conditions will dictate the need for the third icebreaker.

Based on this, the concept of a floating production platform using mooring for stationkeeping is judged to be achievable, given that an efficient ice management system is used. Operating such a platform in ice infested waters clearly increases the complexity compared to a similar platform in ice free waters. It should however be within achievable limits with the use of ice management.

For further work the dimensions of the platform must be checked, and of course the open water performance must be analysed in terms of stability and operating in waves. Regarding ice loads, it is natural that a full dynamic analysis as discussed in section 5.10 is used to verify ice loads. Also, numerical methods for ridges and floes can be used to further verify the ice loads. For analysis of mooring system the next step would be to use mooring software such as MIMOSA. This will give a more accurate and realistic analysis of the mooring system compared to the simplified methods used in this thesis. Analysis of the structural integrity of the platform is also required, as local ice loads may lead to deformation and failure of the structure.

The MATLAB program developed for the analysis is rather simple, but it has proven as a good tool to test the effect of changing parameters on the ice load results. It is also a possibility to further develop this program to handle more ice load calculation methods, or to implement numerical methods. In general, the program would also benefit from some restructuring.

Factors connected to the offloading procedure is also important to consider. This is a critical operation, and important to ensure year-round operation of the platform. Number of tankers and routes from terminals to platform must be taken into consideration. This is a large task which requires information on ice conditions along possible routes in the Beaufort Sea.

Since the concept of a floating production platform in the Beaufort Sea is rather new, with no real life examples in equally harsh conditions it is natural that the platform concept is tested in model scale. Ice loads can be estimated experimentally, and factors such as ice clearing and interaction with mooring lines and risers can be verified visually.

References

[1] R. Aggarwal and R. D'Souza. "Deepwater Arctic - Technical Challenges and Solutions". OTC paper no. 22155. Arctic Technology Conference. 2011.

[2] API. *Reccomendend Practice for Planning, Designing and Constructing Structures and Pipelines for Arctic Conditions*. API Recommended Practise 2N. API RP 2N. American Petroleum Institute, 1995.

[3] *Beaufort Sea Production Environmental Impact Statement*. Tech. rep. Six Volumes. Calgary: Dome Petroleum Ltd., Esso Resources Canada Ltd., and Gulf Canada Resources Inc., 1982.

[4] K. J. Bird, R. R. Charpentier, D. L. Gautier, D. W. Houseknecht, T. R. Klett, J. K. Pitman, T. E. Moore, C. J. Schenk, M. E. Tennyson, and C. J. Wandrey. *Circum-Arctic Resource Appraisal: Estimates of Undiscovered Oil and Gas North of the Arctic Circle*. U.S. Geological Survey Fact Sheet 2008-3049, 4 p. 2008. URL: http://pubs.usgs.gov/fs/2008/3049/.

[5] A. B. Cammaert and D. B. Muggeridge. *Ice Interaction With Offshore Structures*. 115 Fifth Avenue, New York: Van Nostrand Reinhold, 1988. ISBN: 0442216521.

[6] Chevron. *Canada Fact Sheet*. 2011. URL: http://www.chevron.com/documents/pdf/canadafactsheet.pdf (visited on 05/23/2012).

[7] E. Coche, P. Liferov, and M. Metge. "Ice and Iceberg Management Plans for Shtokman Field". OTC paper no. 22103. Arctic Tehcnology Conference. 2011.

[8] K. Croasdale. "The Limit Driving Force Approach to Ice Loads". OTC paper no. 4716. Offshore Technology Conference. 1984.

[9] K. Croasdale, J. Bruce, and P. Liferov. “Sea Ice Loads Due To Managed Ice”. POAC09-31. Port and Ocean Engineering under Arctic Conditions. 2009.

[10] K. Croasdale and A. Cammaert. “An Improved Method for the Calculation of Ice Loads on Sloping Structures in First-year Ice”. *Hydrotechnical Construction* Vol. 28.No. 3 (1994).

[11] Daily Business Buzz. *Terra Nova FPSO SUNCOR*. URL: http://www.nl.dailybusinessbuzz.ca/photo/Terra-Nova-FPSO-SUNCOR-1683319 (visited on 05/20/2012).

[12] Y. Dolgopolov, V. Afanasiev, V. Koren’kov, and D. Panfilov. “Effect of Hummocked Ice on the Piers of Marine Hydraulic Structures”. IAHR. 1975, pp. 469–477.

[13] R. D’Souza and S. Basu. “Importance of Topsides in Design and Selection of Deepwater Floating Platforms”. OTC paper no. 22403. Offshore Technology Conference. 2011.

[14] ExxonMobil. *Arctic Leadership*. 2008. URL: http://www.imperialoil.ca/Canada-English/Files/EM_Arctic_leadership_brochure.pdf (visited on 05/23/2012).

[15] O. M. Faltinsen. *Sea Loads on Ships and Offshore Structures*. The Edinburgh Building, Cambridge CB2 2RU, UK: Cambridge University Press, 1990. ISBN: 0521458706.

[16] J. Hamilton, J. Blunt, D. Mitchell, and T. Kokkinis. “Ice Management for Support of Arctic Floating Operations”. OTC paper no. 22105. Arctic Tehcnology Conference. 2011.

[17] J. M. Hamilton. “The Challenges of Deep Water Arctic Development”. The International Society of Offshore and Polar Engineers. 2011.

[18] E. Hansen. “A discrete element model to study marginal ice zone dynamics and the behaviour of vessels moored in broken ice”. Dr. Ing. Thesis. Norwegian Univeristy of Science and Technology, 1998.

[19] G. Howell and A. Duggal. “The Terra Nova FPSO Turret Mooring System”. OTC paper no. 13020. Offshore Tehcnology Conference. 2001.

[20] IMVPA. *Arctic Offshore Technology Assessment of Exploration and Production Options for Cold Regions of the US Outer Continental Shelf. Prepared for United States Minerals Management Service*. Tech. rep. IMV Projects Atlantic Project No. C-0506-15, Technical Report No. TR-001. United States Minerals Management Service, 2008.

[21] ISO. *Petroleum and natural gas industries - Arctic offshore structures*. International Standard ISO 19906. 2010.

[22] Keinonen. "Ice Management for Ice Offshore operations". OTC paper no. 19275. Offshore Tehcnology Conference. 2008.

[23] E. Kreyszig. *Advanced Engineering Mathematics*. 9th. John Wiley & Sons, INC., 2006. ISBN: 0471728977.

[24] T. Kärnä and E. Nykänen. "An Approach for Ridge Load Determination in Probabilistic Design". IAHR. 2004, pp. 42–50.

[25] G. Lever and J. Kean. "Harsh Environments FPSO Development for Terra Nova". International Offshore and Polar Engineering Conference. 2000.

[26] S. Løset, K. N. Shkhinek, O. T. Gudmestad, and K. V. Høyland. *Actions from Ice on Arctic Offshore and Coastal Structures*. St. Petersburg: LAN, 2006. ISBN: 5811407033.

[27] R. McLendon. *Types of Offshore Oil Rigs*. May 19, 2010. URL: http://www.mnn.com/earth-matters/energy/stories/types-of-offshore-oil-rigs (visited on 05/20/2012).

[28] Merco Press. *Second oil rig to join Falklands' oil exploration round next year*. Nov. 12, 2010. URL: http://en.mercopress.com/2010/11/12/second-oil-rig-to-join-falklands-oil-exploration-round-next-year (visited on 05/20/2012).

[29] D. E. Nevel. "Wang's Equation for Ice Forces From a Pressure Ridge". Cold Regions Engineering. 1991, pp. 666–672.

[30] Offshore Magazine. *Technip grabs Red Hawk cell Spar*. URL: http://www.offshore-mag.com/articles/print/volume-62/issue-10/departments/gulf-of-mexico/gulf-of-mexico.html (visited on 05/20/2012).

[31] offshoretechnology.com. *Glider, Gulf of Mexico, United States of America*. URL: http://www.offshore-technology.com/projects/glider/glider1.html (visited on 05/20/2012).

[32] T. D. Ralston. "Ice Force Design Considerations For Conical Offshore Structures". Ed. by D. Muggeridge. Vol. II. International Conference on Port and Ocean Engineering Under Arctic Conditions. 1977, pp. 741–752.

[33] K. Riska. *Oil Export from Varandey Terminal*. Presentation, NSR 75 years anniversary. Feb. 21, 2008.

[34] B. F. Ronalds. “Deepwater Facility Selection”. OTC paper no. 14259. Offshore Technology Conference. 2002.

[35] A. Sablok and S. Barras. “The Internationalization of the Spar Platform”. OTC paper no. 20234. Offshore Technology Conference. 2009.

[36] B. Sand and G. Horrigmoe. “Simulations of IceRidge Forces on Conical Structures”. International Offshore and Polar Engineering Conference. 2001, pp. 754–760.

[37] Sevan Marine. *FPSO Sevan Voyageur*. URL: http://sevanmarine.com/index.php/projects/16-fpso-sevan-voyageur (visited on 05/20/2012).

[38] Sevan Marine. *Sevan 1000 FPSO for Goliat*. 2012. URL: http://sevanmarine.com/index.php/projects/582-sevan-1000-fpso-for-goliat (visited on 05/20/2012).

[39] K. Shkhinek, A. Bolshev, S. Frolov, A. Malyutin, and B. Chernetsov. “Modelling of Level Ice Action on Floating Anchored Structure Concepts for the Shtokman Field”. International Association of Hydraulic Engineering and Research. 2004, pp. 84–94.

[40] L. G. Spedding. *Landfast and shear zone ice conditions in the southern Beaufort Sea - Winter 1977/78*. Esso Resources IPRT-16ME-79, 1979.

[41] H. van der Ster. *Western Towboat recently completed towing the MODU Kulluk.* Oct. 19, 2011. URL: www.towingline.com/archives/1143 (visited on 05/22/2012).

[42] G. Timco and R. Burden. “An analysis of the shapes of sea ice ridges”. *Cold Regions Science and Technology* 25 (1997), pp. 65–77.

[43] G. Timco and A. Cornett. “The influence of variable-thickness ice on the loads exerted on sloping structures”. *Cold Regions Science and Technology* 26 (1997), pp. 39–53.

[44] G. Timco, R. Frederking, K. Kamesaki, and H. Tada. “Comparison of Ice Load Calculation Algorithms for First-year Ridges”. REIFS99. International Workshop on Rational Evalulation of Ice Forces on Structures. 1999, pp. 88–102.

[45] Vryhof Anchors. *Anchor Manual 2010, The Guide to Anchoring*. 2010. URL: www.vryhof.com/pdf/anchor_manual.pdf (visited on 05/29/2012).

[46] Y. S. Wang. “Analysis and Model Tests of Pressure Ridges Failing Against Conical Structure”. IAHR. 1984.

[47] B. Wright. *Evaluation of Full Scale Data for Moored Vessel Stationkeeping in Pack Ice.* Tech. rep. PERD/CHC Report 26-200. Ottawa, Canada: The National Research Council of Canada, 1999.

[48] B. Wright. *Full Scale Experience with Kulluk Stationkeeping Operations in Pack Ice.* Tech. rep. PERD/CHC Report 25-44. Ottawa, Canada: The National Research Council of Canada, July 2000.

[49] B. D. Wright and D. L. Schwab. *Beaufort Sea ice stereo photo analysis 1973-1978.* Gulf Canada Resources Inc., 1979.

Appendix A

Ice Forces from Ralston's Equations

This appendix gives the equations for calculating level ice loads on conical structures based on the method developed by Ralston.

This section is entirely based on Ralston [32]. Some equations have been rewritten. The basis for Ralston's solution is a plastic limit analysis. A velocity field of the ice is constructed, and it is assumed that the rate of work done by the boundary forces is equal to the rate of energy dissipation that results from the assumed motion. Upstream of the structure, directly outside the cone radius, a deforming region is given by:

$$r_{wl} \leq r \leq A \tag{A.1}$$

$$-\frac{\pi}{2} \leq \theta \leq \frac{\pi}{2} \tag{A.2}$$

where r_{wl} is the waterline radius of the cone, A the distance to the end of the deforming region and (r, θ) are cylindrical coordinates.

The ice is assumed to follow a uniform rigid motion defined as:

$$\vec{V} = -V\vec{e_x} \tag{A.3}$$

where $\vec{V}$ is the velocity in x-direction, V is the absolute drift speed of ice and $\vec{e_x}$ is the unity vector in x-direction. Inside the deforming region a vertical velocity is induced:

$$\vec{w} = -V \tan(\alpha) \frac{A - r}{A - r_{wl}} \cos(\theta \vec{e_z}) \tag{A.4}$$

where $\vec{w}$ is the velocity in z-direction, α is the slope angle of the cone and $\vec{e_z}$ is the unity vector in z-direction.

Ice blocks sliding on the surface of the cone has a velocity field defined as

$$\vec{V} = -V\vec{e_x} + V \tan(\alpha) \cos(\theta)\vec{e_z} \tag{A.5}$$

The horizontal force is computed by setting the external work, $F_H V$, equal to energy dissipation due to the deformation of the ice sheet. To determine the vertical component, force balance is used.

To determine the coefficients in Ralston's equations, the parameter $\rho = A/r_{wl}$ must be determined. The correct value of ρ is the one that solves the equation

$$\rho - \ln(\rho) + 0.0830(2\rho + 1)(\rho - 1)^2 \left(\frac{\rho_w g D^2}{\sigma_f h} \right) = 1.369 \tag{A.6}$$

where D is the diameter of the structure, σ_f the flexural strength of ice, ρ_w the density of water and h is the ice thickness.

To solve this equation the Newton-Raphson [23] method is appropriate, as the derivative of Equation A.6 with respect to ρ is given as

$$\frac{df}{d\rho} = 1 - \frac{1}{\rho} + 0.498(\rho^2 - \rho) \left(\frac{\rho_w g D^2}{\sigma_f h} \right) \tag{A.7}$$

The Newton-Raphson procedure is included in the MATLAB program.

There are two solutions of Equation A.6, under one and above one. Based on the deforming region defined in Equation A.1, it is the solution above one that is of interest.

Once ρ is determined the two first coefficients are found as

$$A_1 = \frac{1 + 2.711\rho \ln(\rho)}{3(\rho - 1)} \tag{A.8}$$

$$A_2 = 0.075(\rho^2 + \rho - 2) \tag{A.9}$$

To determine the rest of the coefficients, the complete elliptical integrals of the first and second kind must be found. There are two different definitions of these integrals, where the first is

$$K(k) = \int_0^{\pi/2} (1 - k^2 \sin(\theta))^{-1/2} d\theta \tag{A.10}$$

$$E(k) = \int_0^{\pi/2} (1 - k^2 \sin(\theta))^{1/2} d\theta \tag{A.11}$$

This is the definition that Ralston uses, while MATLAB uses the second definition given as

$$K(m) = \int_0^{\pi/2} (1 - m\sin(\theta))^{-1/2} d\theta \tag{A.12}$$

$$E(m) = \int_0^{\pi/2} (1 - m\sin(\theta))^{1/2} d\theta \tag{A.13}$$

The difference is that the first definition uses the elliptical modulus k, while the second uses the parameter m. They are thus related as $k^2 = m$. Since MATLAB is used for computations the second definition will be used, and input values used by Ralston must be squared.

Some intermediate functions are defined by Ralston to simplify the calculations.

$$h(\alpha, \mu) = \cos(\alpha) - \frac{\mu}{\sin(\alpha)} \left(E[\sin^2(\alpha)] - \cos^2(\alpha) K(\sin^2(\alpha)) \right) \tag{A.14}$$

$$f(\alpha, \mu) = \sin(\alpha) + \mu \cos(\alpha) K(\sin^2(\alpha)) \tag{A.15}$$

$$g(\alpha, \mu) = \frac{\frac{1}{2} + \frac{\alpha}{\sin(2\alpha)}}{\frac{\pi \sin(\alpha)}{4} + \frac{\mu \sin(\alpha)}{\tan(\alpha)}} \tag{A.16}$$

where μ is the coefficient of friction between ice and structure. The remaining coefficients are then given as

$$A_3 = \frac{0.9}{4\cos(\alpha)}\left[\left(1+\mu\frac{E[\sin^2(\alpha)]}{\tan(\alpha)}\right)-\mu\sin(\alpha)f(\alpha,\mu)g(\alpha,\mu)\right] \tag{A.17}$$

$$A_4 = \frac{\tan(\alpha)}{1-\mu g(\alpha,\mu)} \tag{A.18}$$

$$B_1 = \frac{h(\alpha,\mu)}{\frac{\pi}{4}\sin(\alpha)+\frac{\mu\alpha}{\tan(\alpha)}} \tag{A.19}$$

$$B_2 = \frac{0.9}{4}\left[\frac{\pi}{2}\cos(alpha)-\mu\alpha-\frac{f(\alpha,\mu)h(\alpha,\mu)}{\frac{\pi}{4}\sin(\alpha)+\frac{\mu\alpha}{\tan(\alpha)}}\right] \tag{A.20}$$

All necessary coefficients have now been established. These are used in Equations A.21 and A.22 to calculate horizontal and vertical loads on the cone.

$$F_H = \left[A_1\sigma_f h^2 + A_2\left(\rho_w\rho_i\right)ghD^2 + A_3\left(\rho_w-\rho_i\right)gh\left(D^2-D_r^2\right)\right]A_4 \tag{A.21}$$

$$F_V = B_1F_H + B_2\left(\rho_W\rho_i\right)gh\left(D^2-D_r^2\right) \tag{A.22}$$

Appendix B

Multi-year Ridge Model by Wang

This appendix gives the equations for determining loads from multi-year ridges on conical structures, using the method by Wang.

The geometric specifications of the multi-year ridge is given in Figure B.1. Wang defined a velocity field for different ridge types, where the main difference was ridge length. Only the Long Ridge Type I is analysed further. Before proceeding the following notation is introduced.

$$A = a/B_t \qquad B = b/B_t \qquad D = d/B_t$$

$$R = B_b/B_t \qquad S = \sigma_s/\sigma_r \qquad T = t/H$$

$$Q = R, 1^* \qquad U = \gamma_w - \gamma_i, \gamma_i^* \qquad u = gB_t^2/\sigma_r H$$

$$\gamma_i = \rho_i g \qquad \gamma_w = \rho_w g$$

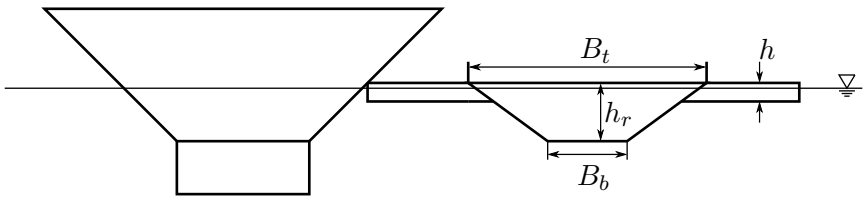

Figure B.1: Ridge cross-section with dimensions as defined by Wang. The ridge is interacting with a cone-shaped structure.

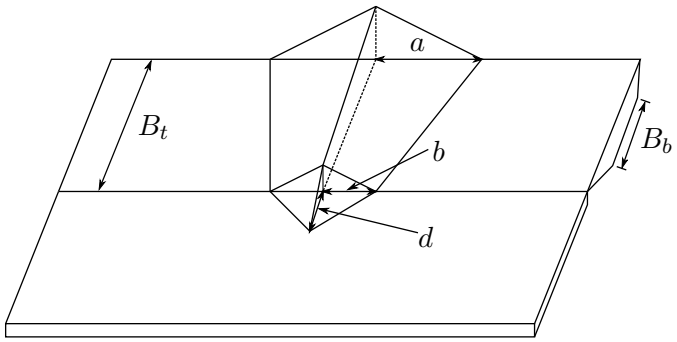

Figure B.2: Deformation of Long Ridge Type I. This figure shows the ridge breaking upwards, and is thus for an upward breaking cone. For a downward breaking cone the deformation is similar, but directed downwards instead.

For the functions marked with *, the first value should be used for downward cones, while the second value should be used for upward cones.

Further, the following functions are defined

$$F_a = \frac{U\left(7 + 7R + R^2 + R^3\right)}{8} + \frac{1 + 4R + R^2}{1 + R + Q} \tag{B.1}$$

$$F_b = F_a + ST^2 - 1.5U\left(1 + R\right) \tag{B.2}$$

$$F_r = \frac{3\left(1 + 4R + R^2\right)}{\left(1 + 2R\right)\left(2 + R\right)} \tag{B.3}$$

$$F_d = 2ST^2 + 2UTD + \frac{4ST^2}{D} \tag{B.4}$$

The distances A, B and D are determined by minimizing the following equation for the vertical force (given by Nevel [29])

$$\frac{6V}{\sigma_r H^2} = F_a A - 2F_b B + \left(F_a + F_d\right)\frac{B^2}{A} + \frac{F_r + 4ST^2 D}{A} \tag{B.5}$$

This is done by setting the derivative of Equation B.5 with respect to A, B and D equal to zero. This gives the following

$$F_a A^2 - \left(F_a + F_d\right) B^2 = F_r + 4ST^2 D \tag{B.6}$$

$$F_b A - \left(F_a + F_d\right) B = 0 \tag{B.7}$$

$$\frac{1}{D^2} = \frac{1}{B^2} + \frac{UT}{2ST^2} \tag{B.8}$$

From Equation B.8 it can be concluded that B is greater than D. From Equation B.7 it can be concluded that F_b is greater than zero since F_a, F_d, A and B are greater than zero. Using Equation B.7, Equation B.6 is solved for $1/B^2$. This is again used in Equation B.8 to give

$$C_0 + C_1 D + C_2 D^2 + C_3 D^3 + C_4 D^4 = 0 \tag{B.9}$$

where the coefficients are given as

$$C_0 = 4F_a\left(2ST^2\right)^2 - F_rF_b^2 \tag{B.10}$$

$$C_1 = 8ST^2\left[F_a(F_a + 2ST^2) - F_b^2\right] \tag{B.11}$$

$$C_2 = \left(F_a + 2ST^2\right)\left[F_a(F_a + 2ST^2) - F_b^2\right] + 16F_aST^2UT + \frac{F_rF_b^2UT}{2ST^2} \tag{B.12}$$

$$C_3 = 4F_aUT\left(F_a + 2ST^2\right) \tag{B.13}$$

$$C_4 = F_a\left(2UT\right)^2 \tag{B.14}$$

C_2, C_3 and C_4 are positive, and C_1 is positive if

$$U \geq 4\left(1 + ST^2\right)\left(-1 + \sqrt{1 + \frac{S^2T^4}{6\left(1 + ST^2\right)^2}}\right) \tag{B.15}$$

The value of ST^2 ranges between 0 and 1, which means that the expression in Equation B.15 ranges between 0 and 0.165. Any practical value of U will be larger than 0.165 (see expression for U above), which means that C_1 can be considered positive.

C_1, C_2, C_3 and C_4 are thus positive, which means that C_0 has to be negative to ensure that Equation B.9 has one positive root. This is fulfilled if

$$F_b > 4ST^2\sqrt{\frac{F_a}{F_r}} \tag{B.16}$$

If this is true, Equation B.9 is solved using the root function in MATLAB. Then, B and A are found using Equations B.8 and B.7. All distances needed to determine the vertical breaking force are now known. By using Equation B.7, Equation B.6 becomes

$$A\left(F_aA - F_bB\right) = F_r + 4ST^2D \tag{B.17}$$

Using this with Equation B.3, and rearranging, the vertical and horizontal forces are determined as

$$F_v = \frac{\sigma_r H^2 \left(AF_a - BF_b\right)}{3} \tag{B.18}$$

$$F_h = \xi_1 F_v \tag{B.19}$$

If Equation B.16 is not true, all hinge cracks occur within the ridge. Equations B.7 and B.8 are not valid, but a conservative estimate of the forces can be found by setting the distances B and D equal to zero. This gives

$$A = \sqrt{\frac{F_r}{F_a}} \tag{B.20}$$

which is used in Equation B.18 to determine the force.

Appendix C

Matlab Program

This appendix explains the MATLAB program developed that calculates all ice loads and restoring coefficients. A result file is included that shows input and output from the program. Further, the program is checked against numerical examples in literature to ensure that it gives correct results. The MATLAB program is available electronically.

All calculations are performed in MATLAB. The program developed is capable of calculating ice loading on any circular structure, using well known methods presented in the thesis. Stationkeeping in form of mooring is also handled, with the assumption of inelastic catenary mooring lines.

Object-oriented programming has been used. In conventional procedural programming data is passed to function, which perform the necessary operations on the data. In object-oriented programming the data and operations are encapsulated in objects that interact with each other.

The program is executed using the *Main.m* file. This file has two main parts. In the first part objects are defined using the input parameters in the *Input.m* file. The user may alter the input parameter in *Input.m* located in the @Input-folder, which is self explanatory. The second part of the *Main.m* file contains calls to methods. Methods are functions that implement the operations performed on objects of a class. The different classes and scripts of the program are shown in figure C.1.

Output from the calculations can be accessed in the *Workspace* in MATLAB, but it is also available in the text file *results.txt* which follows on page XVI. The MATLAB code is not included in a printed version, but can be accessed electronically.

It should be noted that figures in section 7.1.1 are produced by using *RangeCalculations.m* instead of *Main.m*. In order to do this the input file must be modified.

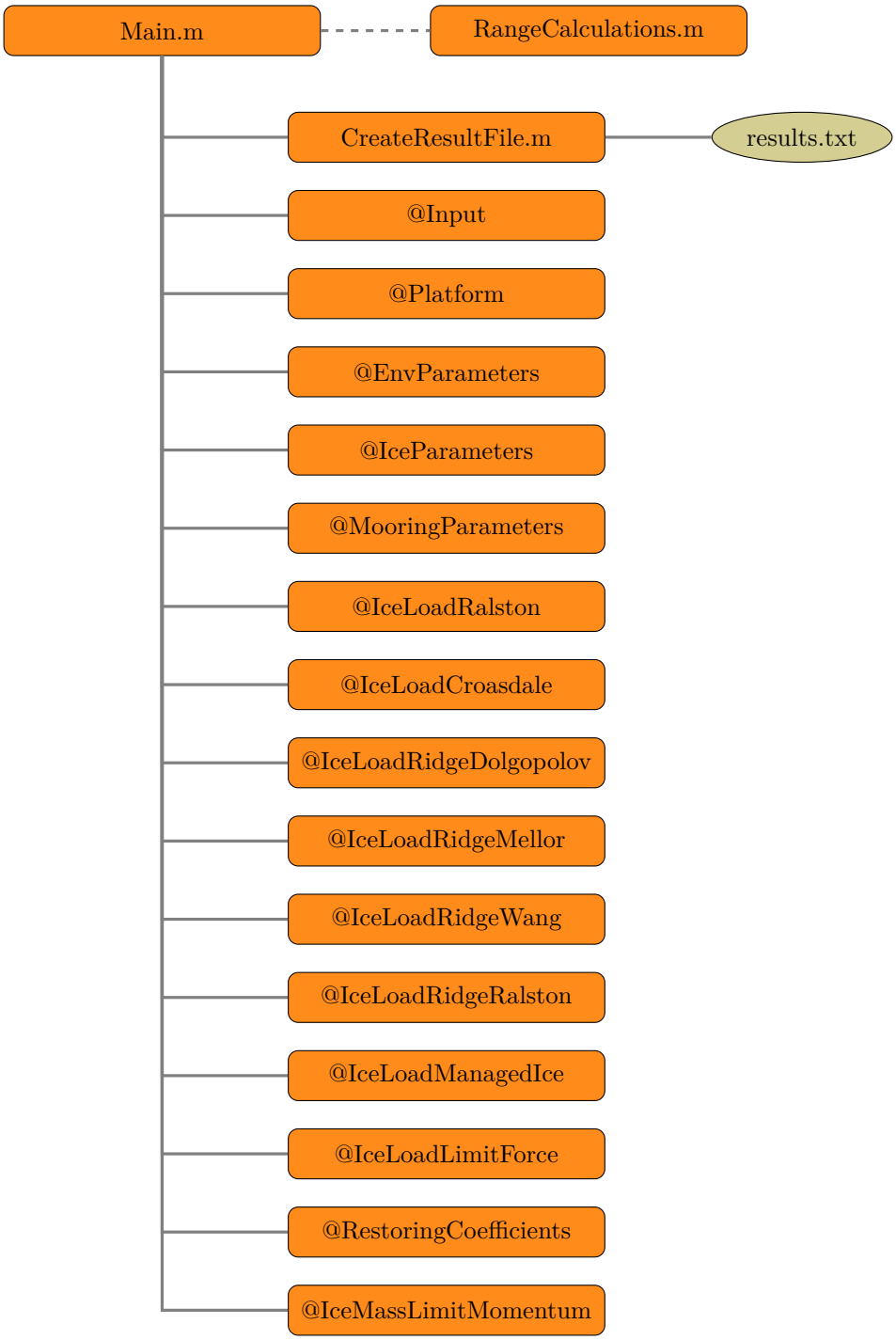

Figure C.1: Flowchart of MATLAB program. All main classes are shown. To produce the plots in Figures 7.2, 7.3, 7.4, 7.5, and 7.6 the RangeCalculations.m is used instead of Main.m. This requires some modifications of the Input.m file in the @Input folder, which is explained in the file itself.

results.txt

```
=====================================================
########################-INPUT-########################
=====================================================
=--------------Environmental parameters--------------=
=====================================================
* Acceleration of gravity       =     9.81 [m/s^2]
* Density of water              =  1025.00 [kg/m^3]
* Density of air                =     1.23 [kg/m^3]
* Maximum wind speed            =    39.00 [m/s]
* Water depth                   =   500.00 [m]
=====================================================
=-----------------------Platform--------------------=
=====================================================
* Waterline diameter            =   100.00 [m]
* Rubble ridedown diameter      =    70.00 [m]
* Slope angle                   =   -45.00 [deg]
* Depth of sloping part         =    15.00 [m]
=====================================================
=-------------------Ice parameters------------------=
=====================================================
* Friction coefficient          =     0.10 [-]
* Density                       =   917.00 [kg/m^3]
* Flexural strength,level ice   = 5.00E+05 [N/m^2]
* Elastic modulus               = 5.00E+09 [N/m^2]
* Poisson ratio                 =     0.30 [-]
* Level ice thickness           =     2.00 [m]
* Keel depth, first-year ridge  =    25.00 [m]
* Sail height, first-year ridge =     5.00 [m]
* Angle of internal friciton    =    45.00 [deg]
* Void ratio of rubble          =     0.30 [-]
* Thickness, MY-ridge           =    20.00 [m]
* Top width, MY-ridge           =   110.00 [m]
* Bottom width, MY-ridge        =    40.00 [m]
* Flexural strength, ridge ice  = 5.00E+05 [N/m^2]
* Floe thickness, managed ice   =     2.00 [m]
* Porosity of rubble            =     0.30 [-]
* Ice rubble friction           =     0.00 [-]
* Ice rubble cohesion           =  1500.00 [Pa]
* Bearing capacity              =     6.00 [-]
* Rubble pressure ratio         =     1.00 [-]
* Ice pressure                  = 15000.00 [Pa]
* Angle of rubble block         =     0.79 [rad]
* Length and width of ice floe  = 10000.00 [m]
* Average ridge building force  =   100000 [N/m]
* Wind drag coefficient of floe = 2.00E-03 [-]
* Ice drift speed               =     0.08 [m/s]
=====================================================
```

```
=----------------------Mooring----------------------=
=======================================================
* Water depth                    =   500.00 [m]
* Lenght of line                 =  3000.00 [m]
* Weight in water                =  4500.00 [N/m]
* MBS                            = 3.10E+07 [N]
* Horizontal pretension          = 9.30E+06 [N]
* Number of lines                =    24.00 [-]
* Diameter of turret             =    20.00 [m]
=======================================================

=======================================================
#######################-RESULTS-#######################
=======================================================
=-----------------Level ice--Ralston----------------=
=======================================================
* Horizontal force              = 1.470E+07 [N]
* Vertical force                = 1.544E+07 [N]
=======================================================
=-----------------Level ice--Croasdale--------------=
=======================================================
* Horizontal force              = 1.147E+07 [N]
* Vertical force                = 9.386E+06 [N]
=======================================================
=------------First-year Ridge--Dolgopolov------------=
=======================================================
* Horizontal force              = 2.009E+08 [N]
* Vertical force                = 1.737E+08 [N]
=======================================================
=--------------First-year Ridge--Mellor--------------=
=======================================================
* Horizontal force              = 2.441E+08 [N]
* Vertical force                = 2.089E+08 [N]
=======================================================
=--------------Multi-year Ridge--Wang----------------=
=======================================================
* Horizontal force              = 2.274E+08 [N]
* Vertical force                = 1.860E+08 [N]
=======================================================
=--------------Multi-year Ridge--Ralston-------------=
=======================================================
* Vertical force, initial       = 7.686E+07 [N]
* Vertical force, hinge         = 1.191E+08 [N]
* Horizontal force, initial     = 9.394E+07 [N]
* Horizontal force, hinge       = 1.456E+08 [N]
=======================================================
=---------------------Managed ice-------------------=
=======================================================
* Horizontal force, Scenario 1 = 3.957E+07 [N]
```

```
* Horizontal force, Scenario 2 = 1.800E+06 [N]
* Horizontal force, Scenario 3 = 3.900E+06 [N]
* Vertical force, Scenario 1   = 3.237E+07 [N]
* Vertical force, Scenario 2   = 1.473E+06 [N]
* Vertical force, Scenario 3   = 3.191E+06 [N]
=====================================================
=-----------------Limiting ice force-----------------=
=====================================================
* Horizontal driving force     = 1.373E+09 [N]
=====================================================
=--------------------Mooring system-------------------=
=====================================================
* Individual stiffness         = 1.779E+05 [N/m]
* C11                          = 2.135E+06 [N/m]
* C22                          = 2.135E+06 [N/m]
* C66                          = 5.693E+08 [N/m]
* X                            = 2.888E+03 [N/m]
=====================================================
```

C.1 Verification of Code

As several different procedures have been implemented in the MATLAB program, it is important to verify that the program performs correct calculations. The API RP-2N [2] standard has numerical examples of level ice calculations based on Ralston's method and multi-year ridges based on Wang's method. Ralston [32] also has a numerical example for his method. Sand and Horrigmoe [36] performed calculations using Wang's method. The ice loads in managed ice are calculated using rather easy equations, and results compare well with examples by Croasdale, Bruce, and Liferov [9]. These are not compared any further. For limit driving force examples in literature is limited to those by Croasdale [8].

Level ice calculations by Ralston's method are first checked. Ralston [32] uses different dimensions of the platform (cone) and other ice conditions. The *Input.m* file is therefore changed to match the conditions. The following results are obtained

Table C.1: Input to example in Ralston [32] for calculation of level ice loads using Ralston's method. The cone is upward breaking.

Parameter	**Value**	**Unit**
Level ice thickness	0.914	m
Flexural strength	6.89×10^5	N/m^2
Waterline diameter	18.3	m
Rubble diameter	6.1	m
Friction coefficient	0.15	
Angle of inclination	45	deg

Table C.2: Results from MATLAB program and example in Ralston [32], for level ice loads using Ralston's method.

Parameter	**Matlab program**	**Ralston**
Horizontal force, [MN]	3.21	3.16
Vertical force, [MN]	3.05	3.01

Ralston's method is also presented in section 5.4.8.c of API RP 2N [2]. Although the equations are presented different, the result from the example should match the results from the MATLAB program.

Table C.3: Input to example in section 5.4.8.c of API RP 2N [2] for calculation of level ice loads using Ralston's method. The cone is upward breaking.

Parameter	**Value**	**Unit**
Level ice thicknes	2	m
Flexural strength	5×10^5	N/m^2
Ice density	909.3	kg/m^3
Waterline diameter	100	m
Rubble diameter	70	m
Friction coefficient	0.15	
Angle of inclination	45	[deg]

Table C.4: Results from MATLAB program and example in section 5.4.8.c of API RP 2N [2], for level ice loads using Ralston's method.

Parameter	**Matlab program**	**API**
Horizontal force, [MN]	65.26	64.23
Vertical force, [MN]	63.49	62.69

To verify the ridge breaking load calculated in the MATLAB program using Wang's method, the example in section 5.4.11.c of API RP 2N [2] is used.

Table C.5: Input to example in section 5.4.11.c of API RP 2N [2] for calculation of ridge breaking load using Wang's method.

Parameter	**Value**	**Unit**
Level ice thickness	2	m
Flexural strength	5×10^5	N/m^2
Ice density	909.3	kg/m^3
Water density	1030	kg/m^3
Ridge thickness	10	m
Ridge width top	30	m
Ridge width bottom	20	m

Table C.6: Results from example in section 5.4.11.c of API RP 2N [2] and calculations by MATLAB program, for ridge breaking loads using Wang's method.

Parameter	**Matlab program**	**API**
Vertical force, [MN]	31.53	31.52

Ralston [32] also presents a short example where he calculates initial and hinge crack loads using the method be presents. Input parameters are given in Table C.7, and results in Table C.8. This method assumes a rectangular ridge. In the MATLAB program the width of the ridge is set to B_t.

Table C.7: Input to example in Ralston [32] for calculation of ridge breaking loads using method by Ralston.

Paramter	**Value**	**Unit**
Flexural strength	6.89×10^5	N/m^2
Elastic Modulus of ice	5.52×10^9	N/m^2
Water density	1030	kg/m^3
Ridge thickness	15.2	m
Ridge width	30.5	m

Table C.8: Results from example in Ralston [32] and calculations by MATLAB for ridge loads based on method by Ralston.

Parameter	**Matlab program**	**API**
Vertical force, initial crack, [MN]	20.4	20.5
Vertical force, hinge crack, [MN]	31.5	31.6

Comparison of limit driving forces is also not performed in detail as the equations are straight forward.

All results from the MATLAB program are very close to the results found in literature. The small discrepancies are most likely due to small differences in physical parameters, and the accuracy of MATLAB compared to accuracy of calculations in literature. This suggests that the MATLAB program gives correct values for the ice loads.